

ROUGH DRAFT

SAND85-0598
Unlimited Release
Printed 1987

Distribution
Category UC-70

ANALYSES TO EVALUATE THE EFFECT OF THE EXPLORATORY SHAFT ON REPOSITORY PERFORMANCE OF YUCCA MOUNTAIN

Joseph A. Fernandez
Thomas E. Hinkebein
NNWSI Geotechnical Design Division
Sandia National Laboratories
Albuquerque, NM 87185

John B. Case
IT Corporation
2340 Alamo SE
Albuquerque, NM 87106

ABSTRACT

This report presents preliminary analyses to determine whether the construction of two shafts associated with the Exploratory Shaft Facility could influence the long-term isolation capabilities of a high-level nuclear waste repository at Yucca Mountain, on and adjacent to the Nevada Test Site. The calculational effort, using analytical solutions, focuses primarily on the influence of the shaft liner and the zone of increased rock damage around the shaft (due to shaft construction). The impact of the shaft penetrating into the Calico Hills unit on the sorptivity of zeolites of this unit is also evaluated. Two mechanisms are considered in determining whether the rock damage zone (or the modified permeability zone, MPZ) can significantly enhance radionuclide releases. These mechanisms include water flow down the shaft fill and MPZ from an unanticipated scenario occurring at the surface, and air flow up the shaft due to convective and barometric forces. The influence of the liner on the performance of the repository is determined by evaluating the potential chemical interaction between ground water and the concrete liner and the subsequent potential for precipitates to deposit within the MPZ and the shaft fill. The sorption capability of the Calico Hills unit is evaluated by calculating the changes in ground-water temperature as water migrates down the shaft and MPZ. It is concluded from these calculations that the presence of the shafts and the associated MPZ and shaft liner does not significantly impact the long-term isolation capability of the repository. This conclusion is reached because (1) water entering the shaft can be dissipated effectively at the base of the shaft, (2) air flow out of the shaft can be controlled effectively by emplacement of shaft fill, (3) deposition of solids from the interaction of the shaft liner with the ground water will be a localized phenomenon and should not decrease the drainage capability of the rock at the base of the shaft, and (4) the elevation of ground-water temperature reaching the base of the shaft will not significantly impact the sorptivity of the Calico Hills zeolites. This report also describes methods to remove the liner, to restore the MPZ and to emplace a seal, in the event that future analyses suggest that these actions are necessary.

Received w/ Ltr Dated 4/17/88
8804110003

8804110006 880401
PDR WASTE PDR
WMA-II

ROUGH DRAFT

CONTENTS

	<u>PAGE</u>
EXECUTIVE SUMMARY	viii
1.0 PURPOSE OF REPORT	1-1
2.0 SHAFT DESIGN INFORMATION	2-1
2.1 Location of the Exploratory and Escape Shafts	2-1
2.2 Construction of the Exploratory Shafts	2-4
2.3 Shaft Sealing Concepts	2-5
2.4 Preferred Options for Shaft Seals	2-6
3.0 INFLUENCE OF THE MODIFIED PERMEABILITY ZONE ON THE PERFORMANCE OF THE YMMGDS	3-1
3.1 Modified Permeability Zone Characteristics	3-1
3.2 Potential for Enhancing Radionuclide Release Due to Water Entering the Exploratory Shaft	3-8
3.2.1 Model Used for Water Flow into Shaft	3-9
3.2.1.1 Model Description	3-10
3.2.1.2 Input Values Used	3-17
3.2.1.3 Inflow Volumes	3-18
3.2.1.4 Duration and Rate of Flow into Shaft	3-20
3.2.2 Model Used for Water Flow out of the Shaft	3-26
3.2.2.1 Model Description	3-26
3.2.2.2 Input Values Used	3-31
3.2.3 Water Balance in the Exploratory Shaft	3-32
3.2.4 Impact of Relocating the Exploratory Shafts	3-37
3.2.5 Conclusions	3-41
3.3 Potential for Enhancing Radionuclide Release From Air Movement Due to Convective Forces	3-41
3.3.1 Air Flow Mechanism	3-42
3.3.2 Method of Analysis	3-44
3.3.3 Model Description	3-44
3.3.3.1 Temperature and Pressure Distributions	3-45
3.3.3.2 Flow Path Resistances	3-46

CONTENTS

	<u>PAGE</u>
3.3.4 Influences of MPZ on Air Flow	3-48
3.3.5 Conclusions	3-54
3.4 Potential for Enhancing Radionuclide Release from Air Movement Due to Barometric Forces	3-55
3.4.1 Air Flow Mechanism	3-55
3.4.2 Model Description	3-55
3.4.2.1 Physical Model	3-56
3.4.2.2 Mathematical Model and Assumption	3-56
3.4.3 Input to the Mathematical Model	3-60
3.4.4 Model Results	3-63
3.4.5 Conclusions	3-72
3.5 Remedial Measures to Restore the Modified Permeability Zone	3-72
3.5.1 Restoration of the MPZ Using Expansive Concrete	3-74
3.5.2 Restoration of the MPZ by Grouting	3-75
3.5.3 Conclusions	3-78
4.0 INFLUENCE OF THE SHAFT LINER ON THE PERFORMANCE OF YMMGDS	4-1
4.1 Changes in the Hydraulic Conductivity of the Liner	4-1
4.1.1 Conclusions	4-2
4.2 Effect of Ground-Water Chemistry on the Hydraulic Conductivity of the Exploratory Shaft Fill and Modified Permeability Zone	4-3
4.2.1 Leaching of Alkaline Species From the Concrete Liner	4-4
4.2.2 Chemical Equilibrium Model of Ground- Water Reactions	4-7
4.2.2.1 Migration of Precipitates	4-10
4.2.2.2 Model for Precipitate Deposition	4-13
4.2.3 Results and Conclusions	4-13
4.3 Remedial Measures to Remove the Liners From the Exploratory and Escape Shafts	4-14
4.3.1 Conclusions	4-22

CONTENTS

	<u>PAGE</u>
5.0 INFLUENCE OF THE ES PENETRATION INTO THE CALICO HILLS UNIT . .	5-1
5.1 Changes in the Sorptivity of the Calico Hills Unit Due to Elevated Ground-Water Temperature	5-1
5.1.1 Temperature Elevation of Water Entering the Shaft	5-1
5.1.2 Impact of Increased Ground-Water Temperature on the Sorptivity of the Calico Hills Unit	5-2
5.2 Changes in the Thickness of the Tuffaceous Beds of Calico Hills Above the Ground-Water Table	5-3
5.3 Conclusions	5-4
6.0 CONCLUSIONS AND RECOMMENDATIONS	6-1

APPENDICES

A.	Perspective into Radionuclide Transport	A-1
B.	Explanation of Water Inflows to ES-1	B-1
C.	The Density Method as Applied to Flow through a Porous Media	C-1
D.	Estimated Construction Schedule and Costs	D-1
E.	Calculation of Temperature of Water From the Base of the Exploratory Shafts	E-1
F.	Comparison of Data Used in This Report With the Reference Information Base (RIB)	F-1
G.	Data Recommended for Inclusion into the Site and Engineering Properties Data Base (SEPDB) and Information Proposed for the Inclusion into the Reference Information Base (RIB)	G-1

REFERENCES	R-1
-------------------	-----------	------------

FIGURES

	<u>Page</u>
2-1. Schematic of Exploratory Shafts and Corresponding Geologic Stratigraphy	2-2
2-2. Geology of Exploratory Shaft and Environs	2-3
2-3. General Arrangement for Shaft Seals Showing Optional Components	2-7
3-1. Cross Section Through a Shaft in Welded Tuff Showing Fracture Spacing Relative to Shaft Radius	3-3
3-2. Modified Permeability Zone Model for Topopah Spring Welded Tuff for Expected Conditions at 310-m Depth	3-7
3-3. Geometry of Model Used to Estimate Flow into a Shaft from Saturated Alluvium	3-11
3-4. Phases of Flow for Flow into a Shaft from Saturated Alluvium	3-12
3-5. Types of Flow Considered in Estimating Flow into a Shaft	3-14
3-6. Capture Zone Near a Shaft	3-15
3-7. Estimated Volumes of Water Entering ES-1 (PMF, Shaft Fill Conductivity = 10^{-2} cm/s, Excavated Shaft Diameter = 4.42 m)	3-19
3-8. Estimated Duration of Flows into ES-1 (PMF, Hydraulic Conductivity of Alluvium - 100 and 10 cm/s)	3-21
3-9. Estimated Duration of Flows into ES-1 (PMF, Hydraulic Conductivity of Alluvium - 1 to 0.1 cm/s)	3-22
3-10. Estimated Duration of Flow into ES-1 (PMF, Hydraulic Conductivity of Alluvium - 10^{-2} cm/s and 10^{-3} cm/s)	3-23
3-11. Estimated Duration of Flow into ES-1 (PMF, Hydraulic Conductivity of Alluvium - 10^{-4} to 10^{-5} cm/s)	3-24
3-12. Schematic of Model Used to Compute Water Balance in the Exploratory Shaft	3-27
3-13. Comparison of Methods Used to Compute Drainage from Shaft	3-30
3-14. Estimated Buildup of Water in Sump of ES-1 (Hydraulic Conductivity of Alluvium - 100 cm/s and 10 cm/s)	3-34

FIGURES

	<u>Page</u>
3-15. Estimated Buildup of Water in Sump of ES-1 (Hydraulic Conductivity of Alluvium - 1 cm/s and 0.1 cm/s)	3-35
3-16. Estimated Buildup of Water in Sump of ES-1 (Hydraulic Conductivity of Alluvium - 10^{-2} cm/s and 10^{-3} cm/s)	3-36
3-17. Estimated High-Water Locations Associated with a PMF in the Exploratory Shaft Area	3-38
3-18. Topographic Cross Section in the Vicinity of the New ES-1 and ES-2 locations	3-40
3-19. Mechanisms for Convective Air Flow	3-43
3-20 Total Flow Rate as a Function of Shaft Fill, Air Conductivity (Vertical Emplacement and Low Conductivity MPZ Model)	3-50
3-21 Total Flow Rate as a Function of Shaft Fill, Air Conductivity (Vertical Emplacement and High Conductivity MPZ Model)	3-50
3-22 Total Flow Rate as a Function of Shaft Fill, Air Conductivity (Horizontal Emplacement and Low Conductivity MPZ Model)	3-51
3-23 Total Flow Rate as a Function of Shaft Fill, Air Conductivity (Horizontal Emplacement and High Conductivity MPZ Model)	3-51
3-24 Air Flow Through ES-1 and ES-2 (Shaft Fill and MPZ Flows Included) as a Percentage of Flow Through the Rock over Repository Air (Vertical Emplacement and Low Conductivity MPZ Model)	3-52
3-25 Air Flow Through ES-1 and ES-2 (Shaft Fill and MPZ Flows Included) as a Percentage of Flow Through the Rock over Repository Air (Vertical Emplacement and High Conductivity MPZ Model)	3-52
3-26 Air Flow Through ES-1 and ES-2 (Shaft Fill and MPZ Flows Included) as a Percentage of Flow Through the Rock over Repository Air (Horizontal Emplacement and Low Conductivity MPZ Model)	3-53

FIGURES

	<u>Page</u>
3-27 Air Flow Through ES-1 and ES-2 (Shaft Fill and MPZ Flows Included) as a Percentage of Flow Through the Rock over Repository Air (Horizontal Emplacement and High Conductivity MPZ Model)	3-53
3-28 Schematic of Repository use in Barometric Pressure Model . .	3-57
3-29 Barometric Pressure Events	3-62
3-30 Ratio of Displaced Air Volume to Void Volume for ES-1 (Vertical Emplacement and Low Conductivity MPZ Model) for a Severe Thunderstorm Event	3-64
3-31 Ratio of Displaced Air Volume to Void Volume for ES-1 (Vertical Emplacement and High Conductivity MPZ Model) for a Severe Thunderstorm Event	3-64
3-32 Ratio of Displaced Air Volume to Void Volume for ES-1 (Vertical Emplacement and Low Conductivity MPZ Model) for a Tornado Event	3-65
3-33 Ratio of Displaced Air Volume to Void Volume for ES-1 (Vertical Emplacement and High Conductivity MPZ Model) for a Tornado Event	3-65
3-34 Ratio of Displaced Air Volume to Void Volume for ES-1 (Vertical Emplacement and Low Conductivity MPZ Model) for a Seasonal Event	3-66
3-35 Ratio of Displaced Air Volume to Void Volume for ES-1 (Vertical Emplacement and High Conductivity MPZ Model) for a Seasonal Event	3-66
3-36 Ratio of Displaced Air Volume to Void Volume for ES-1 (Horizontal Emplacement and Low Conductivity MPZ Model) for a Severe Thunderstorm Event	3-67
3-37 Ratio of Displaced Air Volume to Void Volume for ES-1 (Horizontal Emplacement and High Conductivity MPZ Model) for a Severe Thunderstorm Event	3-67
3-38 Ratio of Displaced Air Volume to Void Volume for ES-1 (Horizontal Emplacement and Low Conductivity MPZ Model) for a Tornado Event	3-68
3-39 Ratio of Displaced Air Volume to Void Volume for ES-1 (Horizontal Emplacement and High Conductivity MPZ Model) for a Tornado Event	3-68

FIGURES

	<u>Page</u>
3-40 Ratio of Displaced Air Volume to Void Volume for ES-1 (Horizontal Emplacement and Low Conductivity MPZ Model) for a Seasonal Event	3-69
3-41 Ratio of Displaced Air Volume to Void Volume for ES-1 (Horizontal Emplacement and High Conductivity MPZ Model) for a Seasonal Event	3-69
3-42. Schematic of MPZ Restoration and Shaft Seal Emplacement . .	3-73
3-43. Minimum Conductivity for Grouting	3-77
4-1. Plot of pH of Water from Below the Shaft Liner as a Function of the Volumetric Flow Rate of Water Through the Shaft or MPZ	4-8
4-2. Schematic of Deposition of Precipitate	4-12
4-3. Frontal Advance of the Precipitation Front in the MPZ . . .	4-15
4-4. Production Cycle for Breaking and Removing the Liner and Placement of Backfill	4-17
4-5. Liner Breakage by the Roadheader Method	4-18
4-6. Removal of Concrete Using the Orange Peel Grab	4-21
5-1 Contours of the Thickness of the Unsaturated Portion of the Calico Hills Unit Beneath the Repository	5-4

TABLES

	<u>Page</u>
3-1 Relative Permeability Factors Associated with the Modified Permeability Zone	3-8
3-2 Summary of Areas and Lengths-Vertical Emplacement	3-47
3-3 Summary of Areas and Lengths-Horizontal Emplacement	3-47
4-1 Chemical Analysis of Water Before and After Contact with PSU 82-022 Cement	4-6
4-2 Summary of Advantages, Disadvantages, and Cost of Liner Removal Methods	4-23
4-3 Comparison of Production Cycle Times for Various Methods Used to Remove Concrete Liners	4-25
4-4 Comparison of Costs for Breaking Out the Concrete Lining and Rock	4-26

ROUGH DRAFT

Executive Summary

One aspect of the Nevada Nuclear Waste Storage Investigations (NNWSI) Project is the development of the Exploratory Shaft (ES) testing program. The purpose of the ES testing program is to obtain at-depth site information on the hydrology and geology at the site. The results from these tests will be used to determine the effectiveness of the geologic setting at Yucca Mountain to isolate high-level radioactive waste. Before initiating the construction of the exploratory shafts (ES-1 and ES-2), it is necessary to determine the quality assurance levels to be applied to the ES design and construction. The purpose of this report is to provide a technical basis in establishing the appropriate quality assurance levels to the design and construction of the exploratory shafts. (The Department of Energy, Nevada Operations Office (DOE-NVO) will establish the quality assurance levels.) This technical basis is developed through the use of analytical solutions that address the primary concern in this report: Do the shaft liner, the shaft internals, and the increased rock damage around the shaft (due to shaft construction) significantly influence the release of radionuclides from the repository? Because the shaft internals will be removed to accommodate emplacement of shaft fill, there is no impact of the shaft internals on the long-term performance of the repository. Therefore, only the significance of the rock damage zone or the modified permeability zone (MPZ)* and the shaft liner on the long-term performance of the repository are considered. A secondary concern addressed in this report is the effect of one shaft penetrating the Calico Hills unit. Because the shaft penetrates the zeolitic portion of the Calico Hills unit, the effect of elevated temperature of ground waters on the zeolites at the base of the shaft is of concern. The decreased thickness of the Calico Hills unit at the ES-1 is also of concern and is discussed in this report.

Because release and transport of radionuclides from the underground facility can be due to several mechanisms, scoping calculations are

*The modified permeability zone is the zone immediately surrounding an underground excavation in which the permeability of the rock mass has been altered due to stress redistribution and blast damage effects.

ROUGH DRAFT

presented in the beginning of the report to provide a perspective on the more important mechanisms that should be considered when assessing the significance of the MPZ. From these calculations, release of radionuclides due to downward water transport is considered to be the most realistic and dominant mechanism. Convective air transport of gases through the drifts and shaft was also determined as important to evaluate because of the thermal energy differences within the repository. The calculations, therefore, focus primarily on conditions that would enhance the downward transport of radionuclides in the aqueous phase and air transport of gases due to convection.

In the first mechanism, it is assumed that water can enter the upper portion of the shaft, infiltrate to the base of the shaft, and potentially build up at the base of the ES and drain into the surrounding rock mass. The calculation presented in this report first defined a broad range of inflows into the shaft. These inflows are dependent on the hydrologic conditions assumed at the surface. Of particular concern is the influence of the MPZ on the inflow into the shaft. These inflows, in turn, are assumed to be transported to the base of the shaft where buildup of waters can occur as well as drainage.

Because, in general, water entering the shaft is contained within the exploratory shaft sump and subsequently drained, it is concluded that the MPZ does not influence the radionuclide release performance of the Yucca Mountain Mined Geologic Disposal System (YMMGDS). In two cases where limited water entry through seals at the repository station* does occur, the transport of radionuclides is not influenced. This is because the maximum computed flow through the repository station seals is 21 m^3 per event, which can easily be isolated from the waste disposal drift by repository design features. These features can include constructing a sump capable of storing and draining this volume of water near the exploratory shaft or within the Exploratory Shaft Facility (ESF).** In addition,

*The repository station is a location in the underground facility that corresponds to the drift area that is adjacent to a repository shaft at the repository level.

**The ESF is the exploratory shaft, any associated surface structure and underground openings constructed for the purpose of site characterization.

ROUGH DRAFT

with proper repository drift grading, the water can be directed to the low point in the repository and the water does not enter the waste disposal area.

The authors conclude that for water inflow the MPZ does not influence the performance of the YMMGDS because (1) the probability of the scenario selected to develop a source of water that could enter the shaft is extremely low or incredible and (2) both the ES-1 and ES-2 have been relocated to more favorable locations outside the flood plain of existing arroyos (where the water inflow scenario presented in the report would clearly provide a realistic upper bound of water flow into the shaft).

An additional concern about the water inflow in the MPZ and out of the base of the shaft is the potential to form precipitates in the MPZ and the shaft fill. Precipitation could occur because the concrete liner will cause some modifications to the ground water. These water chemistry changes may cause the ground water to become supersaturated with respect to some minerals and precipitation could then occur. If precipitation occurs above the repository station, lower water flows would enter the base of the shaft. If precipitates form at the base of the shaft, the drainage capacity at the base of the shaft could be decreased.

From the models of precipitate deposition in this report, precipitates form and immediately deposit in void spaces. As this process continues, a buildup of precipitates occurs in a frontal advance. It is concluded that if anticipated volumes of water ($\sim 44 \text{ m}^3/\text{year}$) enter the shafts, no significant formation of precipitates occurs. If unanticipated volumes ($\sim 20,000 \text{ m}^3/\text{event}$) enter the shaft, precipitates could advance as much as 60 m behind the liner in the MPZ where fracture porosity is small. However, once the flow advances beyond the base of the liner, the maximum frontal advance will be 0.016 m/event due to the increased porosity of the shaft fill. Hence, the deposition of solids from the interaction of the shaft liner with ground water will be a localized phenomenon. We can, therefore, conclude that the fractures in the MPZ above the repository horizon may fill, thereby reducing the permeability of the MPZ where

ROUGH DRAFT

deposition occurs. Because deposition is a localized phenomenon, the drainage capacity of the rock at the base of the shaft should not be detrimentally reduced, assuming that the shaft liner in the base of the shaft is removed.

As mentioned earlier, the MPZ may be significant because it can potentially enhance the release of gaseous radionuclides by increasing the air flow through the MPZ. Because the emplaced waste in the repository will release heat, temperature gradients will develop in the rock mass. The temperature differential will tend to cause air to rise in the exploratory shafts. The analyses presented in this report also consider flow through the rock above the waste disposal areas.

For several combinations of host rock air conductivity above the repository, the percentage of flow through the shaft fill and the MPZ to the total flow through the rock mass above the waste disposal areas as well as through the shaft fill and the MPZ, was plotted as a function of shaft fill conductivity. It was concluded from the analysis that shafts and ramps are not preferential pathways for gaseous radionuclide releases if the air conductivity of the shaft fill is less than about 3×10^{-4} m/min or an equivalent hydraulic conductivity of 10^{-2} cm/s. When the air conductivity of the shaft fill is greater than 3×10^{-4} m/min the air flow through the shaft fill and MPZ is predominantly through the shaft fill. It is only when the conductivity of the shaft fill is low that flow through the MPZ is proportionally greater than flow through the shaft fill. However, when flow through the MPZ is proportionally greater than flow through the shaft fill, the total air flow through the MPZ and shaft fill, as compared to the flow through the rock over the repository, is extremely low, i.e., less than 2.5%. Therefore, it can also be concluded that the MPZ does not detrimentally influence the performance of the YMMGDS by enhancing the release of gaseous radionuclides. However, it is also prudent to emplace a shaft fill having a hydraulic conductivity of less than 10^{-2} cm/s.

A final area of concern mentioned above was the penetration of the ES into the Calico Hills unit. From the analyses presented in this report,

ROUGH DRAFT

the impact of this penetration on the sorptivity of the Calico Hills unit was found to be negligible. This conclusion was reached for the following reasons:

- (1) Water passing through the ES will be completely separated from waste stored in the repository and will not constitute a preferred pathway.
- (2) The minimum thickness (70 m) of the Calico Hills unit at the eastern edge of the repository will be preserved while allowing much valuable information to be gained by sinking the ES into the upper margin of the Calico Hills.
- (3) The elevation of ground-water temperature caused by global temperature field of the repository will be less than that required to have any significant impact on the sorptivity of the Calico Hills zeolites. Therefore if any radionuclides do reach the base of ES-1, radionuclides would still be effectively retained at the base of the shaft.
- (4) The temperature of water passing through the ES was calculated to closely approach the global formation temperature for all considered water flow rates, including the maximum flooding event defined in this report.

The discussion and results presented above were focused on determining that the design and construction of the ESs should not influence the performance of the YMMGDS. Should future analyses indicate that either the shaft liner or the MPZ could influence the performance of the YMMGDS, we have provided a description of the preferred methods for restoration of the MPZ, liner removal, and seal emplacement. In this report, the following conclusions were reached on the preferred methods for restoration of the MPZ, liner removal and seal emplacement.

ROUGH DRAFT

o Grouting in the welded tuff is feasible and is the preferred method for restoring the MPZ because drilling grout holes allows a direct examination of the modified permeability zone and provides a direct method for locating discrete fracture zones. Also, at present, it is not certain how large an interface stress can be developed through the use of only an expansive concrete (one of the alternatives) or how effective such stress development would be in closing fractures. Grouting the MPZ, however, does incur a greater cost than constructing an expansive concrete plug.

o Evaluation of the advantages and disadvantages suggests that the hydraulic splitter method is the favored approach for liner removal. Conventional equipment with the slight modification of suspending the splitters from chains may be used. The costs are somewhat less than for other methods evaluated. It is possible that drilling and splitting patterns could be optimized through analysis of superpositions effects from an array of splitters. The method does not leave any undesirable chemical residue. While supplemental hand methods may be required, this is not considered a significant disadvantage.

o The construction sequence for emplacing a shaft plug entails making saw cuts at the top and bottom of the plug, removing the liner, excavating the keyway, backfilling to the underside of the plug, placement of concrete, and contact grouting.

1.0 PURPOSE OF REPORT

The Nevada Nuclear Waste Storage Investigations (NNWSI) Project, managed by the Nevada Operations Office of the U. S. Department of Energy (U.S. DOE-NVO), is examining the feasibility of developing a nuclear waste repository in an unsaturated tuff formation beneath Yucca Mountain. Yucca Mountain is located on and adjacent to the Nevada Test Site, Nye County, Nevada. One aspect of the NNWSI Project is the development of the Exploratory Shaft (ES) testing program. The purpose of the ES testing program is to obtain at-depth site information on the hydrology and geology of the site. The testing will be performed in the unsaturated tuff at Yucca Mountain. The results from these tests will be used to determine the effectiveness of the geologic setting at Yucca Mountain to isolate high-level radioactive waste.

Before initiating the construction of the exploratory shafts (ES-1 and ES-2), it is necessary to determine the quality assurance levels to be applied to the ES design and construction. The U.S. DOE-NVO is responsible for assigning the quality assurance levels. This report provides analyses to establish the basis for the appropriate quality assurance levels. This basis is established by evaluating whether the design and construction of ES-1 and ES-2 could compromise long-term isolation capabilities of the repository. The concern raised was: Do the shaft liner, the shaft internals, and the increased rock damage around the shaft (due to shaft construction) significantly influence the release of radionuclides from the repository? Because the shaft internals, including instrument conduits, utility piping, ventilation ducts, and conveyances hardware, will be removed to accommodate emplacement of shaft fill, shaft internals will have no impact on the long-term performance of the repository. Therefore, only the significance of the rock damage zone or the modified permeability zone (MPZ) and the shaft liner on the long-term performance of the repository is considered. An integral part of the overall repository system in the long-term performance of the repository is the closure of the Exploratory Shafts (ES-1 and ES-2). Therefore, it is necessary to determine the desired performance of these sealed shafts and, for completeness, the entire

DRAFT

DRAFT

DRAFT

sealing system. Additionally, the development of a model for the MPZ is required.

In Fernandez et al. (1987), performance goals and design requirements for the sealing system are presented. The need for sealing is also assessed by evaluating the water flow into and out of the underground facility, shafts, and ramps for anticipated conditions. In Case and Kelsall (1987), a model for the MPZ in welded tuff is presented. Development of the MPZ is due to the blast damage effects and stress relaxation. In this report, selected results from both of the previous reports are restated. These results are supplemented by additional analyses that establish a perspective into the mechanisms of most concern to radionuclide release, and geochemical modification to ground-water chemistry due to the presence of the liner. This report also describes contingency plans to remove the liner, to restore the MPZ, and to emplace a seal. This information is presented in case future analyses suggest that removal of the liner and restoration of the MPZ are required. It is not the intent of this report to present a total systems analysis. Such an analysis will be provided as part of the Safety Analyses Report, which will be submitted as part of the License Application.

DRAFT

Appendix A presents analyses used to establish a perspective on the most likely mechanism for radionuclide transport. Reference conditions considered in this report are given in Chapter 2. Chapter 3 presents the analyses used to assess the influence of the MPZ on the performance of the Yucca Mountain Mined Geologic Disposal System (YMMGDS). The analyses described in Chapter 3 assess the potential of water to enter the waste disposal area after entering the shaft and the potential for air flow (and indirectly radionuclide release) out of the repository due to convective and barometric forces. The assessment of the amount of water that could enter waste disposal areas from shafts is made by considering a range of shaft inflows that vary in time as well as in total flow. These inflows are then coupled with the drainage capacity of the ES sump to determine water buildup in the sump. Where the buildup of water exceeds the sump storage capacity, water flow into the underground facility and duration of flow are noted. Both water flow volumes and duration of flow contribute to

determining the potential for enhancing radionuclide releases. The assessment of air flow out of the repository is made by considering the convective circulation of air in response to thermal gradients and the movement of air in response to changes in barometric pressures. The significance of this air movement is determined by considering how much air flows preferentially through the shafts and ramps. For the barometric analysis the volume of air that can exit from shafts and ramps due to several, surface, weather conditions is also evaluated.

The influence of the liner on the performance of the YMMGDS is evaluated in Chapter 4, and the interaction of water entering the shaft with the shaft liner is evaluated. Once the changes in water chemistry are noted, the potential and location of mineral precipitation is assessed. Remedial measures to restore the MPZ and remove the liner are presented in Chapters 3 and 4, respectively. Also, in Chapter 4 the procedure for emplacing a shaft seal is presented together with the schedule and cost estimate for removing the shaft liner, emplacing backfill and emplacing a shaft seal if this becomes necessary. Chapter 5 addresses the influence of ES-1 penetration into the Tuffaceous Beds of Calico Hills. The issue of concern is the potential change of the sorptivity of the Calico Hills unit. This potential sorptivity change may result from elevating the temperature of water passing through the ES. The thickness of the Calico Hills unit following shaft sinking is also discussed.

DRAFT

DRAFT

2.0 SHAFT DESIGN INFORMATION

The repository in the underground facility is comprised of drifts that are connected to form a nearly horizontal plane. The underground facility will be located in the unsaturated portion of the Topopah Spring Member approximately 200 to 400 m above the ground-water table. The Topopah Spring Member is predominantly a densely welded, highly fractured tuff having a low matrix hydraulic conductivity.

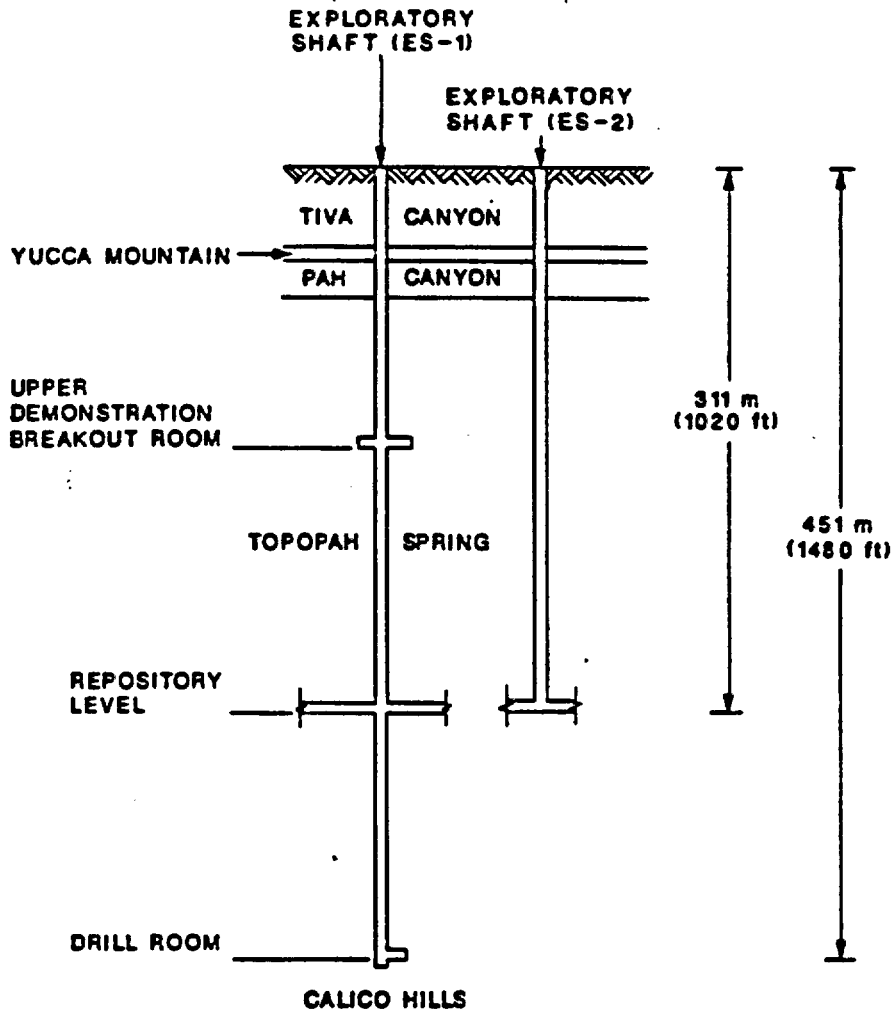
Access to the underground facility is provided by ramps and shafts. The current, repository design incorporates six openings to the underground facility, including four vertical shafts and two inclined ramps. Both types of excavation will penetrate several stratigraphic units, including the alluvium and welded and nonwelded tuff units. The ramps connect directly into the main access drifts at the northern end of the repository. The shafts are located in the northeastern portion of the repository. The men-and-materials and emplacement exhaust shafts have shallow sumps extending 24 and 3 m below the repository, respectively. The bottoms of both of these shafts are within the Topopah Spring Member. The sump for the ES-1 is 140 m below the repository. ES-1 will penetrate the unsaturated portion of the Tuffaceous Beds of Calico Hills. The bottom of the ES-2, associated with ES-1, will only slightly extend below the repository level. Figure 2-1 shows profiles of the shafts superimposed on the geologic stratigraphy at each location.

2.1 Location of the Exploratory and Escape Shafts

ES-1 and ES-2 are located in a wide valley through which the north and south forks of Coyote Wash flow at the northern and southern margins (Figure 2-2). The valley floor is underlain by coarse alluvium and mud/debris flow deposits, with surficial fine-grained sand, probably of eolian origin. Bedrock (Tiva Canyon Member) is exposed in the steep valley walls to the north and south and headward in the valley to the west. Bedrock is exposed in the washes upstream of the ES-1 location.

DRAFT

DRAFT



References: SNL Drwg. No. R07001
Geology Estimated from Bentley (1984)

DRAFT

Figure 2-1. Schematic of Exploratory Shafts and Corresponding Geologic Stratigraphy

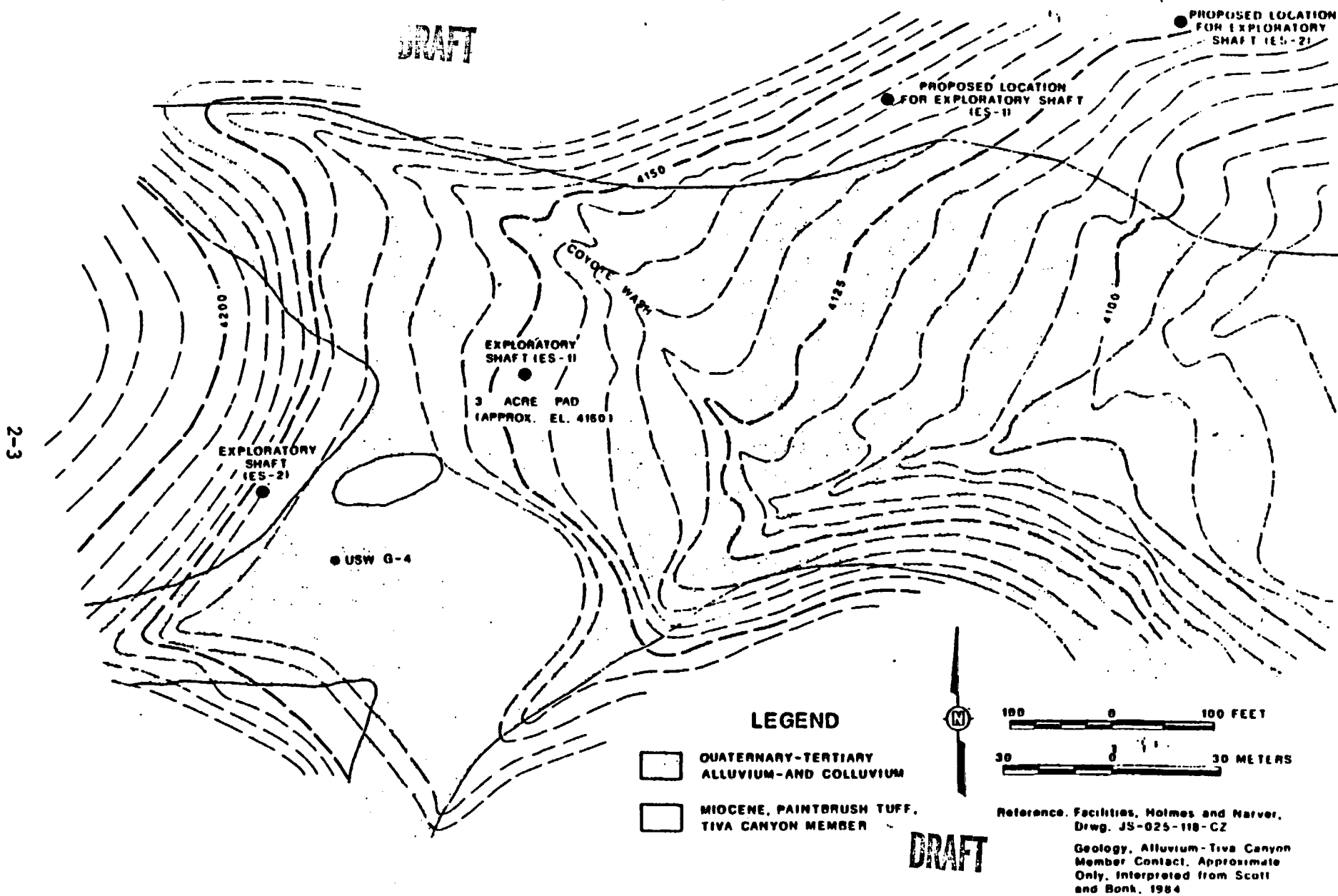


Figure 2-2. Geology of Exploratory Shaft and Environs

DRAFT

Downstream, the washes lie on alluvium. At boreholes USW G-4, near the shaft location, and UE 25a-6, near the mouth of Coyote Wash, alluvium is 6.5 to 10 m thick (Fernandez and Freshley 1984, pp. 60, 69).

The originally proposed location of ES-1 is within the alluvial-filled valley. The ES-2 site is located out of the alluvium and in a southwest direction from ES-1. At the conclusion of this study, new locations for ES-1 and ES-2 were proposed. These proposed locations are also shown on Figure 2-2. These new locations for ES-1 and ES-2 will be approximately 107 m and 93 m north of and above the confluence of two small ephemeral streams that are tributaries of the Coyote Wash drainage system. The new locations for both shafts will be out of the alluvium.

2.2 Construction of the Exploratory Shafts

Before the underground facility is constructed, an exploratory shaft facility will be developed. The exploratory shaft facility primarily includes (1) the main shaft (ES-1), which will transport people, materials, and equipment from the surface to the subsurface test area and will provide additional ventilation capacity to the long exploratory drifts, (2) an underground testing area, and (3) a secondary shaft (ES-2) which will be used for ventilation, materials handling, and emergency egress. It is the current intent of the NNWSI Project to incorporate ES-1 and ES-2 into the underground facility design.

If Yucca Mountain is selected as the disposal site for radioactive waste operations, ES-1 will be used as the primary source of intake air during waste emplacement. All shaft internals will be removed prior to these operations, but the concrete liner will be left in place. The 3.66-m diameter, emergency-exit shaft will be used as an air supply during repository operations to ventilate the repository shop facilities that support the waste emplacement operations. Because the volume of air supplied by ES-2 will be minimal, the external features and the hoist hardware can be left in place without hindering its intended function during repository operations. Also, if the shaft internals for ES-2 remain in place, then the shaft could continue as an emergency exit.

DRAFT

DRAFT

The current design details for ES-1 and ES-2 follow. The excavated diameter for ES-1 and ES-2 will be approximately 4.3 m with a finished diameter of 3.7 m. Both shafts will be lined with an unreinforced concrete liner at least 0.3 m thick and having an unconfined compressive strength of 35 MPa after 28 days. A reinforced liner will be emplaced in the shaft collar and in the brow* at each breakout. The collars for the new locations of ES-1 and ES-2 will be in bedrock. The bottom of the shaft will be lined with a 0.30 m layer of concrete that has a design, unconfined compressive strength of 24 MPa. Most of the concrete liner will not be reinforced but will contain some steel rods to hold the forms used to construct the liner.

Both shafts will be mined using a conventional drill-blast-muck mining sequence. During the mucking operation, minimal amounts of water will be used to suppress the dust in the shaft so that tests characterizing the unsaturated zone will not be affected. Because the excavation of the shafts involves blasting, some additional fracturing of the rock mass into the shaft wall may occur. The blasting will be controlled (i.e., to enhance the vertical advance, limit damage in the rock surrounding the shaft, and produce acceptable-sized rock fragments (U.S. DOE, 1987, Section 8.4.2.1.1)).

2.3 Shaft Sealing Concepts

The primary functions of shaft seals are to:

- o Reduce the potential for surface water or ground water to enter the waste emplacement areas via the shafts
- o Deter human entry to the repository via the shafts.

*The portion of the shaft liner that is located at the upper portion of the shaft and is generally reinforced concrete is the shaft collar. The shaft brow refers to the roof rock in the shaft station where the shaft opens up into the shaft station. The shaft station refers to the location where the drift intersects the shaft.

DRAFT

DRAFT

These functional requirements may be satisfied by one or more seal components. For example, human entry will be discouraged by backfill or seals placed below the ground surface.

Flow through the shaft can be reduced by backfill placed along the length of the shaft or by one or more seals (plugs) placed at intervals. Backfill alone may not be a satisfactory option if there is the potential for flow through an MPZ adjacent to the shaft wall. In such a case, it would be necessary to form a cutoff through the damaged zone, possibly by keying a plug into the walls. Another alternative to reducing the potential of water flow into the waste disposal area is the emplacement of a repository station seal in the drift connected to the exploratory shaft. Figure 2-3 illustrates the general arrangement for shaft seals.

2.4 Preferred Options for Shaft Seals

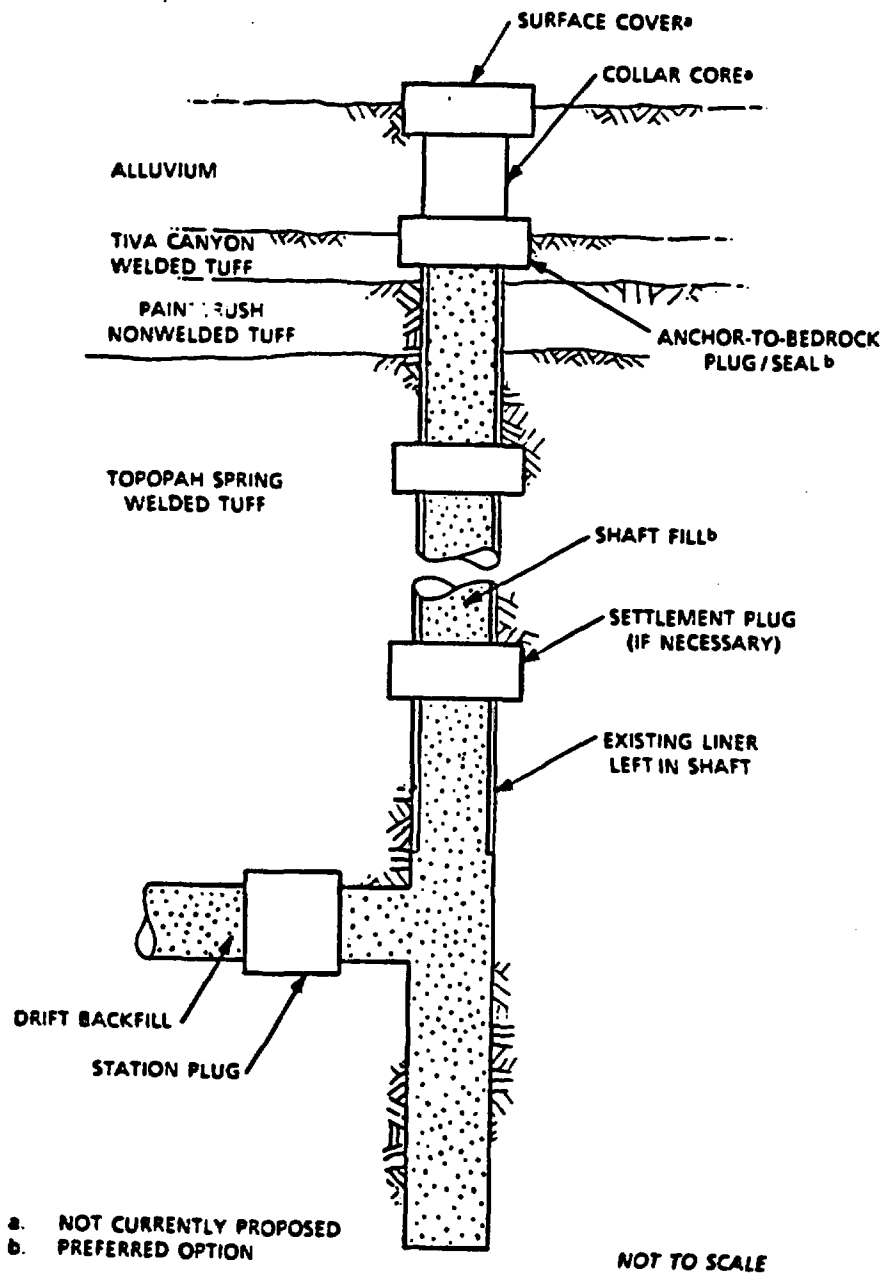
Currently, the preferred option for reducing water flow and deterring human entry is the anchor-to-bedrock plug/seal because:

- o The anchor-to-bedrock plug/seal can be located in a relatively benign environment protected from surficial temperature extremes, surficial geologic processes, and heat generated by the waste. Station plugs, located at the intersection of the shafts and repository station drifts, are isolated from the waste emplacement areas by barrier pillars*, but the maximum temperatures at the repository horizon could potentially reach or exceed 100°C. The in situ stress would also be greater than that associated with a plug/seal closer to the surface.
- o The design requirement for the anchor-to-bedrock plug/seal is less stringent than that for a seal at the base of the shaft because of the lower maximum head (Fernandez et al., 1987).

*The barrier pillar refers to the rock zone surrounding the shaft that isolates the shaft from subsidence effects of underground rooms. For a nuclear waste repository, the barrier pillar also isolates the shaft from a high temperature environment.

DRAFT

DRAFT



DRAFT

Figure 2-3. General Arrangement for Shaft Seals Showing Optional Components

DRAFT

- o Only one seal is required for each shaft, making a total of four, whereas eight total seals might be required if seals are placed in the shaft stations.

- o Construction of a seal at shallow depth in a shaft (about 10 m) should be easier and cheaper than construction at the base of the shaft. If necessary, the alluvium can be stripped away to facilitate construction of the anchor-to-bedrock plug/seal.

- o The anchor-to-bedrock plug can be designed to reduce the potential for flow through the MPZ, whereas simple placement of shaft backfill would have no influence on the MPZ. Moreover, development of the MPZ at the shallow depth of the anchor-to-bedrock plug should be less than that at the station plug location where inelastic deformation is more likely to occur (Case and Kelsall, 1987).

DRAFT

DRAFT

3.0 INFLUENCE OF THE MODIFIED PERMEABILITY ZONE ON THE PERFORMANCE OF THE YMMGDS

Shafts represent potential pathways that could compromise the ability of the geologic repository to meet the performance objectives for the period following permanent closure. Performance can be compromised in two ways. First, water could enter the underground facility through the shafts and contact waste packages in waste disposal areas, potentially accelerating the radionuclide release. Second, release of gaseous radionuclides could occur through the shafts.

Two zones associated with shafts can affect the water entry and airborne release--the shaft interior and the MPZ behind the shaft liner. The intent of this chapter is to determine how the MPZ and the shafts in general affect repository performance. This is accomplished by assuming that the shaft is filled by a simple granular material and by using an MPZ model. Using this information, water flow into underground facility from the shafts and air flow out of the shafts is computed.

3.1 Modified Permeability Zone Characteristics

This section presents a brief description of a model of the MPZ that considers modification due to stress redistribution and blasting. A more complete description of the model and the site-specific parameters at Yucca Mountain that were used in the development of the model is presented by Case and Kelsall (1987) and is described briefly below.

It is postulated that the significant mechanisms for modifying permeability in fractured, welded tuff are 1) the opening or closing of fractures in response to stress changes, and 2) creating new fractures or the opening of old fractures by blasting. The approach for developing the modified permeability zone model includes the following five steps which are described in detail in Case and Kelsall:

DRAFT

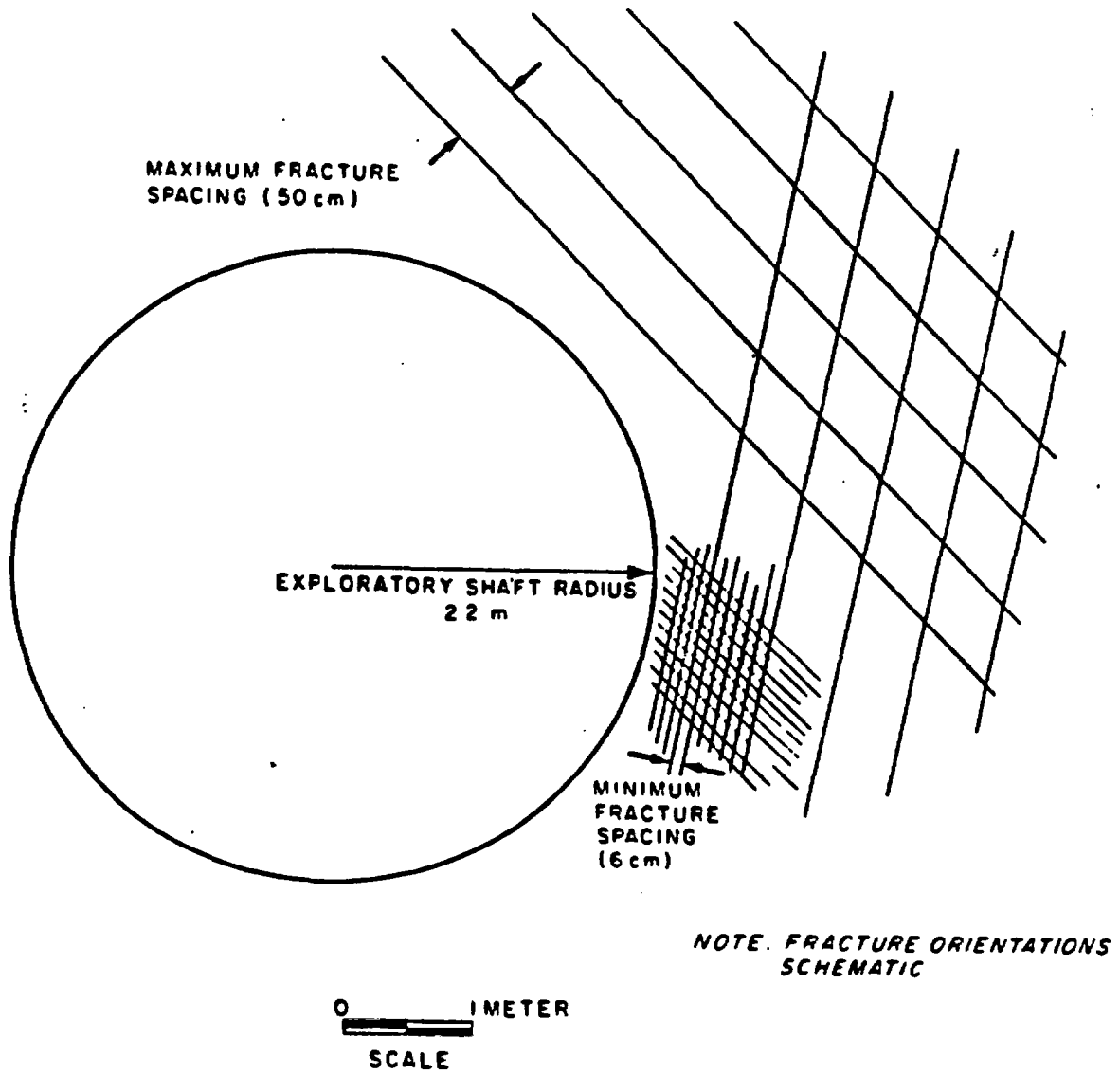
DRAFT

1. Calculate stress changes around a shaft by using an appropriate closed-form solution for elastic or elastoplastic analysis of a circular shaft located in a uniform stress field.
2. Obtain relationships from published laboratory and field testing results which describe the effects of stress on the permeability of single fractures and fractured rock.
3. Calculate rock mass permeability as a function of radius away from the shaft based on the calculated stresses and the stress-permeability relationships obtained from testing.
4. Estimate permeability changes due to blasting from evaluation of case histories which indicate the depth of damage and estimate the probable increase in fracture frequency in the damaged zone.
5. Combine the results derived from performing steps 3 and 4 to obtain the combined effects of stress redistribution and blasting.

As excavation occurs, stresses are relieved and possibly blast induced fracturing may occur. Considering a representative volume of rock adjacent to the shaft, it is to be expected that the geomechanical response to excavation will be influenced by rock mass properties (which take into account the effect of fractures) rather than by the properties of the intact rock since the range of fracture spacing is small relative to the shaft diameter (Figure 3-1). Similarly, the permeability of the rock mass will be influenced by fractures as well as by the rock matrix. [This discussion applies specifically to welded tuff and may be less applicable to nonwelded units in which the typical fracture spacing is 80 cm to 200 cm (Langkopf and Gnirk, 1986, p. 66).] The fracture orientations shown in Figure 3-1 are schematic; actual fracture patterns in welded tuff are expected to range from two oriented sets plus a random set to three oriented sets plus a random set (Langkopf and Gnirk, 1986, p. 48).

DRAFT

DRAFT



DRAFT

Figure 3-1. Cross Section Through a Shaft in Welded Tuff Showing Fracture Spacing Relative to Shaft Radius

DRAFT

The redistribution of stresses around an opening in fractured tuff might affect the permeability of the rock mass in two ways; (1) by the fracturing of originally intact rock due to excessive compressive or tensile stresses and (2) by the opening or closing of preexisting fractures due to changes in the normal stresses acting across the fractures or shearing along the fractures. The potential for fracturing of intact rock was evaluated by simple elastic analysis by Case and Kelsall (1987) for the case of a circular shaft excavated in a homogeneous, isotropic and linearly elastic medium. This analysis showed that the maximum tensile or compressive stresses at the shaft wall at repository depth are approximately 10 % of the reported mean values for tensile and unconfined compressive strength of intact rock. The analysis showed that fracturing of intact rock due to stress concentrations around a repository depth is unlikely, even allowing for variation from the mean reported strength values and potential anisotropy in the stress field.

Whereas stress redistribution around a shaft is unlikely to lead to fracturing of intact rock (which could in turn lead to increased permeability), the effects of stress changes across fractures may have a significant effect on permeability. This arises because the rock mass is densely fractured and because the aperture of the fractured is sensitive to the stress applied across the fractures. Therefore, as the stress changes the permeability changes.

Elastic and elastoplastic stress analysis for a shaft excavated in tuff were performed by Case and Kelsall (1987). Their results indicate that a wide variation in rock mass behavior might be observed, depending on depth, in situ stress, and rock properties. Because rock mass strength* may vary with depth (due to variations in porosity and fracture spacing), rock mass behavior may vary even within a lithologic unit. For the welded units, the expected response is elastic in nonlithophysal zones, but plastic response may occur in lithophysal zones or in intensely fractured

*Rock mass strength is defined as the maximum stress that can be carried by the rock mass (Hoek and Brown, p. 150). The maximum stress level is found to be dependent on the strength properties of intact rock, and discontinuities, and is dependent on confining stress.

DRAFT

DRAFT

zones where strength is lower. Plastic behavior is expected for the nonwelded Calico Hills tuff near the base of the shaft because of the low strength (which is similar to the lower bound for welded tuff) and the higher in situ stresses due to depth. For the nonwelded Paintbrush unit overlying the Topopah Spring the behavior may be elastic or plastic depending on rock mass strength and in situ stresses. Formation of a plastic zone surrounding the shaft may be limited to less than one shaft radius from the shaft boundary, however, if the shaft liner is placed as quickly as possible after excavation. The effects of rock support in limiting inelastic deformation were not considered in this analysis.

Fractures may also be introduced by blasting. Several investigators have described the mechanics of blasting in rock (Langefors and Kihlstrom, 1978, Chapter 1; Hoek and Brown, 1980, Chapter 10; Brady and Brown, 1985, Chapter 17). Fracturing may occur in several ways after blast detonation. Fracturing may be induced near the blasthole due to quasi-static gas pressure that sets up tensile tangential stress or by crack propagation where gas pressure enters existing fractures and extends them. Fracturing may also occur further from blast detonation holes as seismic compressive waves are partially reflected off free surfaces (voids or open joints).

In actual rock masses, the extent and pattern of fracturing will be influenced by rock properties such as strength, anisotropy, pre-existing fractures in the rock mass and in situ stress. Fracturing is also influenced by the blasting method and by the charge weight of explosives, which are expected to be reduced near the excavation perimeter. Because relatively low charge weights can be used in the perimeter holes, the damage to the rock beyond the perimeter can be limited.

In this report, the blast-damaged zone is a zone extending from either 0.5 m to 1.0 m from the shaft wall where blast-induced fracturing may occur. The extent of the zone is derived from a general relationship between blast damage and charge density for tunnel blasting conditions (Holmberg and Persson, 1980) where some measures for controlling blasting are utilized. Blasting is assumed to increase the fracture frequency by a

DRAFT

DRAFT

factor of three in the blast-damaged zone. It is further assumed that the newly created fractures have similar characteristics to existing fractures. In this preliminary model, the permeability in the blast-damaged zone would increase by a factor of three due to an increase in fracture frequency over the increase that occurs due to stress relief.

The increase in permeability due to stress relief and blast effects for the exploratory shaft for the expected case is illustrated in Figure 3-2 and summarized for expected and upper bound cases at two depths in Table 3-1. The analyses were conducted for depths of 100 m and 310 m, corresponding to depths near the top of the Topopah Spring and at the repository horizon. The results in Table 3-1 are reported as a relative rock mass permeability factor, which is expressed as a ratio of increased permeability to undisturbed permeability in the modified permeability zone, and which is expressed for convenience in subsequent calculations as a uniform factor over an annulus extending one radius from the shaft wall.*

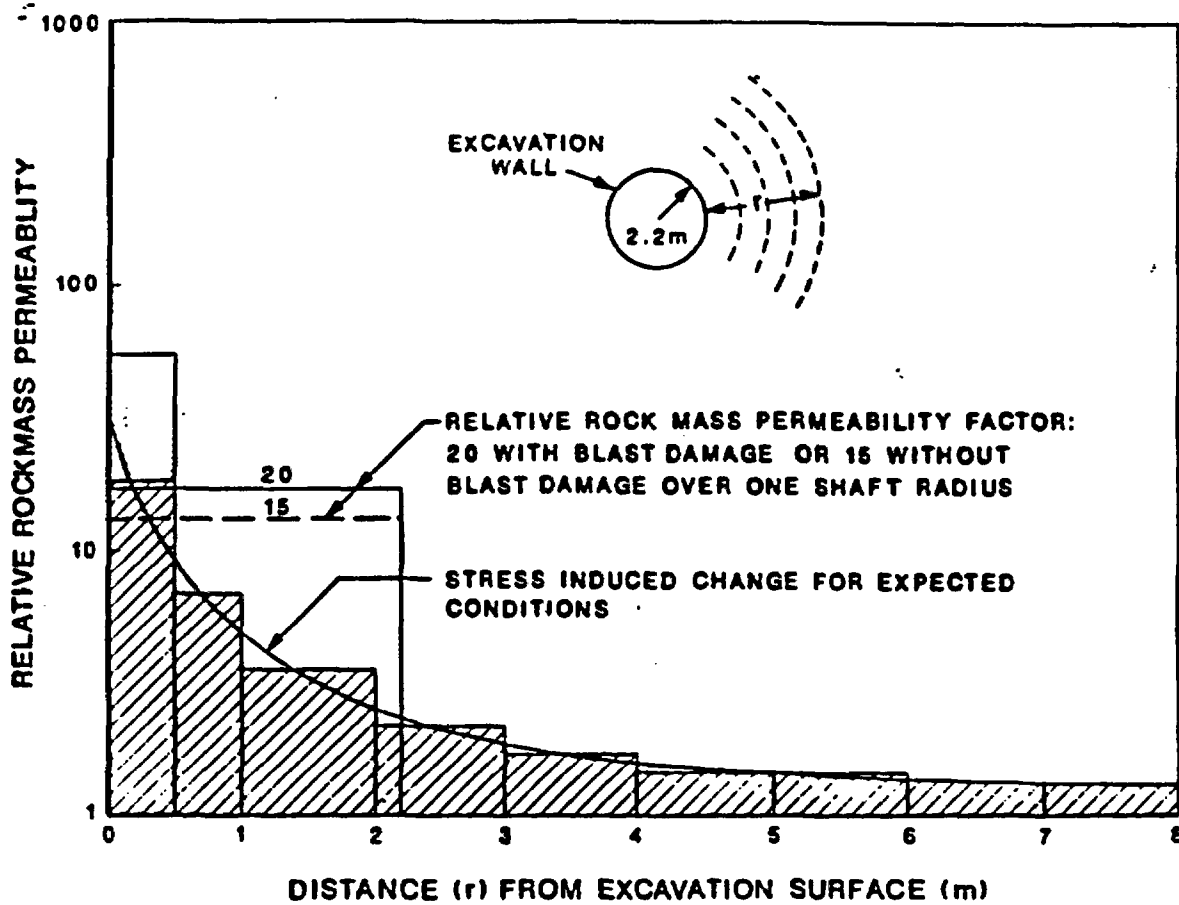
The expected case is based upon an elastic analysis with expected strength, in situ stress, sensitivity of permeability to stress, and a 0.5 m-wide blast-damaged zone. The upper bound case is based upon an elastoplastic analysis with lower bound strength, upper bound in situ stress, greatest sensitivity of permeability to stress, and a 1.0-m-wide blast-damaged zone.

For the expected conditions at 310 m depth (i.e., considering mean values for rock mass strength, in situ stress, and stress permeability sensitivity, and a 0.5-m-wide blast-damaged zone), the relative rock mass permeability factor is 20 times the permeability of the undamaged rock mass. For the upper bound condition at 310-m depth, the relative rock mass permeability factor is 80 times the undisturbed permeability.

*The relative rock mass permeability factor for the expected case is calculated by first performing the radial integration of relative rock mass permeability from the shaft radius (2.2 m) to approximately a radius of 10 m and then calculating a factor by dividing by the area of the annulus extending from 2.2 m to 10 m from the shaft.

DRAFT

DRAFT



LEGEND

- PRELIMINARY ESTIMATE
BLAST INDUCED DAMAGE
- STRESS INDUCED CHANGE
IN PERMEABILITY

DRAFT

Figure 3-2. Modified Permeability Zone Model for Topopah Spring Welded Tuff for Expected Conditions at 310-m Depth

DRAFT

TABLE 3-1

RELATIVE PERMEABILITY FACTORS ASSOCIATED WITH THE MODIFIED
PERMEABILITY ZONE^(a)
(After Case and Kelsall, 1987)

Depth	Stress Redistribution Without Blast Damage		Expected ^(b) Case	Upper Bound ^(c) Case
	Elastic	Elastoplastic		
100	15	20	20	40
310	15	40	20	80

(a) Relative permeability factors are averaged over an annulus one radius wide around the 4.4-m diameter ES.

(b) This is based upon an elastic analysis with expected strength, in situ stress, sensitivity of permeability to stress, and a 0.5-m wide blast damage zone.

(c) This is based upon an elastoplastic analysis with lower bound strength, upper bound in situ stress, greatest sensitivity of permeability to stress, and a 1.0-m-wide blast damage zone.

3.2 Potential for Enhancing Radionuclide Releases Due to Water Entering the Exploratory Shaft

The purpose of this section is to determine whether rock damage surrounding a shaft, caused by excavation of the shaft, can significantly enhance the release of radionuclides. The release mechanism for is water entering the waste disposal areas through the ES and contacting the waste. Therefore, it is necessary to establish the hydrologic properties of the zone through which water can be transmitted to the base of the shaft. This zone includes the shaft interior and the MPZ. It is also important to establish a scenario of water entry into the waste disposal area.

Relative permeability factors for the MPZ are given for the expected and the upper bound cases (Section 3.1). Both MPZ models include a blast-damaged zone and are evaluated to provide a range of water flows through the MPZ. The scenario of water entry into the waste disposal area is the following. Surface water from a major flood enters the shaft (see Section 3.2.1). This water migrates to the base of the shaft where buildup of the water occurs if water entry into the shaft is greater than water

DRAFT

DRAFT

drainage. If the water height in the shaft is greater than the floor of the repository station, water entry into the underground facility through the connecting repository drift is possible. This scenario is described in more detail below.

3.2.1 Model Used for Water Flow into the Shaft

In Figure 3-2 the upper portion of the ES-1* is located in the alluvial-filled portion of the drainage basin; whereas, the upper portion of the ES-2 is located in bedrock upgradient from the location of ES-1. Because the upper portion of the ES-1 is located in alluvium and at the confluence of two washes, Coyote Wash and the wash to the south, a greater potential exists for surface-water entry into ES-1 than into ES-2. The mechanism modelled in this section is water flow from saturated alluvium to the shaft. Because the upper portion of ES-2 is not surrounded by alluvium, this mechanism does not exist. It is, therefore, assumed that the bulk of the water from a major flooding event that saturates the alluvium enters the ES-1. Using this logic, a hydrologic flow model was developed (Fernandez et al., 1987) to estimate the amount of water that could enter the upper portion of the ES. This model, discussed below, assumes that the alluvium surrounding the ES becomes saturated and can enter the shaft. This scenario is evaluated to arrive at a realistic, upper bound of water flow into ES-1. In reality, alluvium in an initially, unsaturated state can provide an effective barrier to downward water infiltration, thereby limiting flow into the shaft.

At the conclusion of this study, new locations of ES-1 and ES-2 were proposed by U.S. DOE/NVO (Figure 2-2) further north and east of the original locations. Because the proposed locations are both out of the alluvial-filled portion of the drainage basin, the potential for surface-water entry has been reduced substantially. Therefore, we feel that the estimates of water flow entering the shaft provided in this chapter do

DRAFT

*The ES-1 and ES-2 locations used in the analysis are the locations presented in the final EA (U.S. DOE, 1986, p. 4-11).

represent conservative, upper-bound values to water flow into the exploratory shafts.

DRAFT

3.2.1.1 Model Description

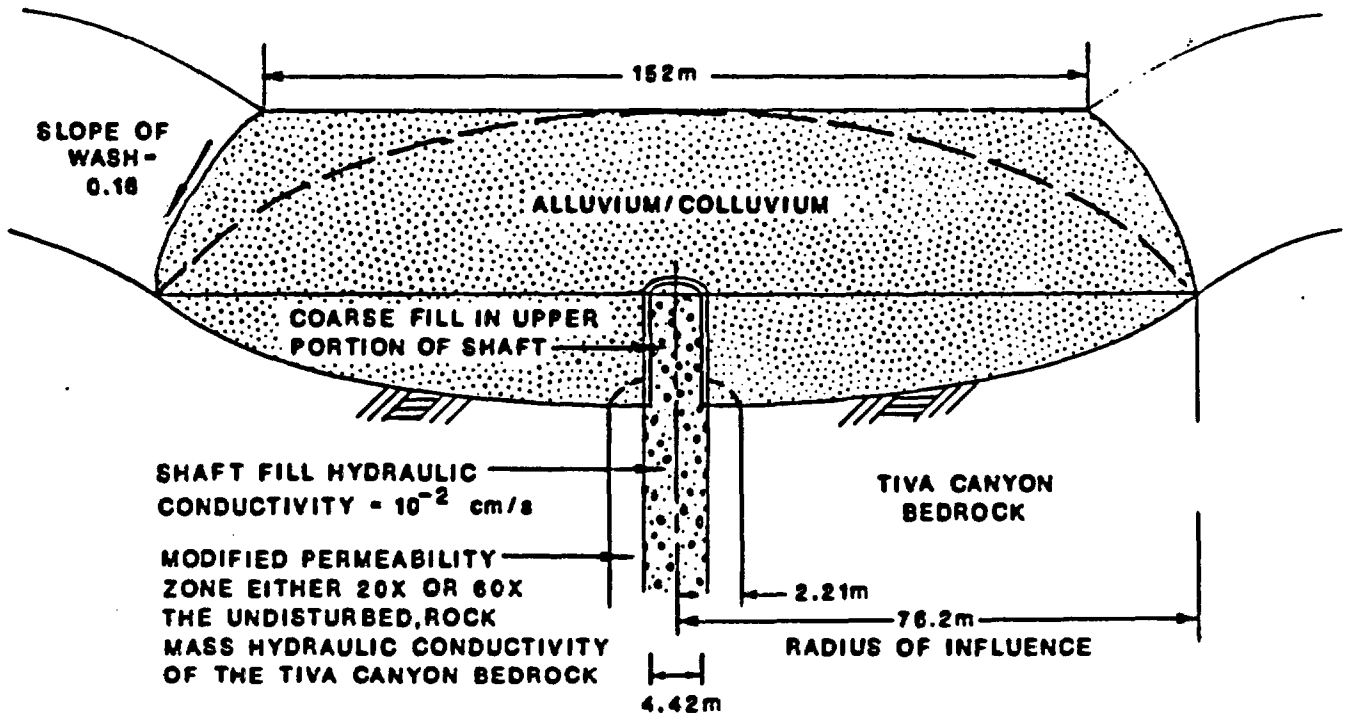
In arriving at a reasonable, upper-bound estimate of water flow into the ES-1 from a major flooding event, it is assumed that a probable maximum flood (PMF) would occur at the ES locations. The model used to compute the flow into the upper portion of the shaft is illustrated by Figure 3-3. Alluvium overlies the welded, highly fractured Tiva Canyon Member. The upper portion of the shaft through the alluvium is filled with a coarse fill to minimize restriction of flow into the shaft. The lower portion of the shaft contains a fill having a saturated hydraulic conductivity of 10^{-2} cm/s, extending to the outside diameter of the shaft. (In reality, a shaft liner, having a lower hydraulic conductivity than the shaft fill, remains in place. By ignoring the presence of the shaft liner, a higher flow through the shaft is computed.) The MPZ extends one radius from the shaft wall. Two cases for the MPZ are considered in which the MPZ is either 20 or 60 times the undisturbed, rock mass hydraulic conductivity. This value of 60 is the average of two values, 40 and 80, associated with MPZ models at 100- and 310-m depths.

Flow progresses in three phases: an initial desaturation phase, a steady-state phase, and a final desaturation phase (Figure 3-4). Before initiation of Phase I, it is assumed that the alluvium becomes fully saturated, and the water in the shaft above the alluvium-Tiva Canyon contact enters the upper portion of the shaft. Desaturation of the alluvium occurs first at curve "1" and progressively to curve "n" (Figure 3-4a). As the radius of influence is changed in response to desaturation, the radius of influence associated with curve "n" represents quasi-steady-state conditions that are held constant until the supply of water replenishing the alluvium no longer exists (Figure 3-4b). As

*The Probable Maximum Flood (PMF) is the greatest flood that may reasonably be expected taking into account all pertinent conditions of location, meteorology, hydrology and terrain (Chow, V. T., 1964, p. 25 to 72).

DRAFT

DRAFT

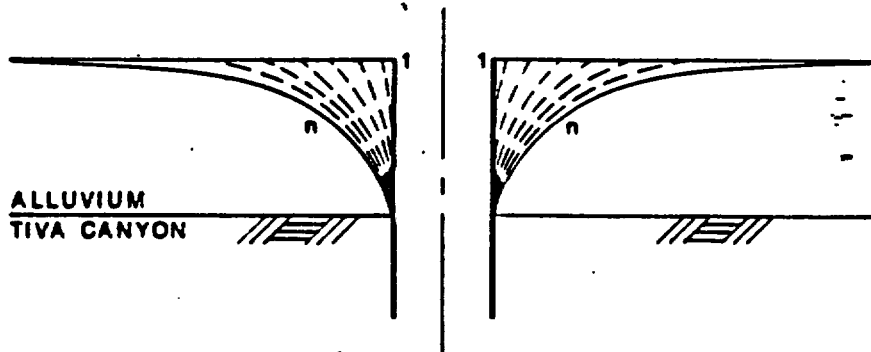


DRAFT

Figure 3-3. Geometry of Model Used to Estimate Flow into a Shaft from Saturated Alluvium

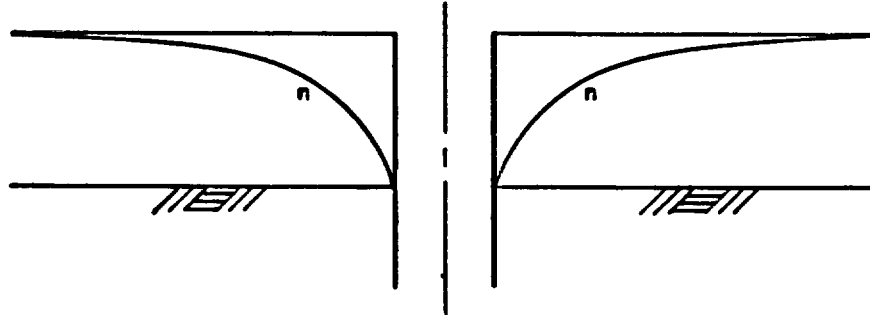
DRAFT

A. PHASE I: INITIAL DESATURATION



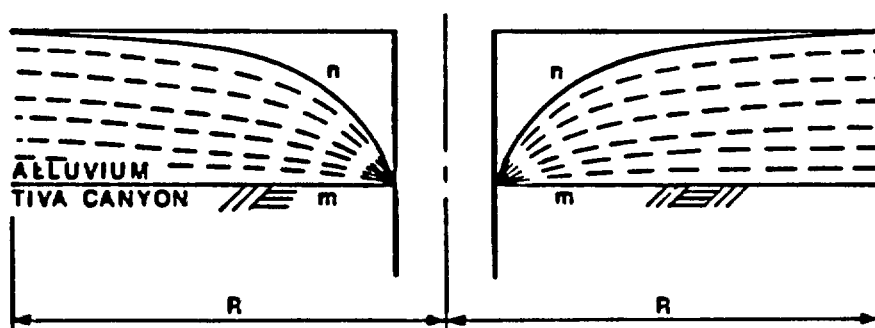
Radius of influence moves to outer radius of models under full saturation height.

B. PHASE II: STEADY-STATE DRAINAGE



Radius of influence is maintained at outer radius, and under full saturation height during the steady state period.

C. PHASE III: DESATURATION OF ALLUVIUM



R - RADIUS OF INFLUENCE

Saturation height declines with time.

DRAFT

Figure 3-4. Phases of Flow for Flow into a Shaft from Saturated Alluvium

Phase III begins, the only water remaining is that contained under curve "n." Desaturation then proceeds from curve "n" to curve "m."

During each phase of drainage, four types of flow are considered: unconfined radial flow under the Dupuit flow assumption, alluvial flow, Tiva Canyon flow, and flow through the MPZ and the shaft fill. Each of the flow are discussed below.

Radial flow is computed using the following equation:

$$Q_s = \frac{\pi K (H^2 - H_o^2)}{\ln\left(\frac{R}{r_o}\right)} \quad (4-1)$$

Where R = radius of influence,

Q_s = flow rate into the shaft,

K = hydraulic conductivity,

H = piezometric level at radius R,

H_o = piezometric level at radius r_o , and

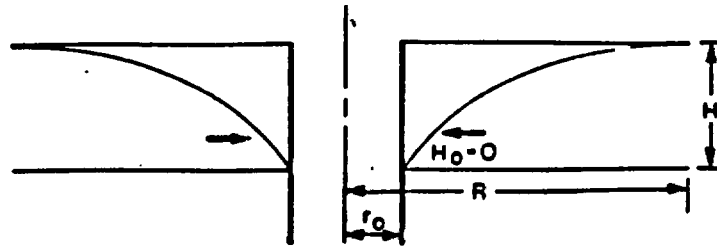
r_o = shaft radius.

This equation, taken from Terzaghi and Peck (1967, p. 167), assumes steady-state flow in the horizontal direction under unconfined conditions. Radial flow is illustrated in Figure 3-5a.

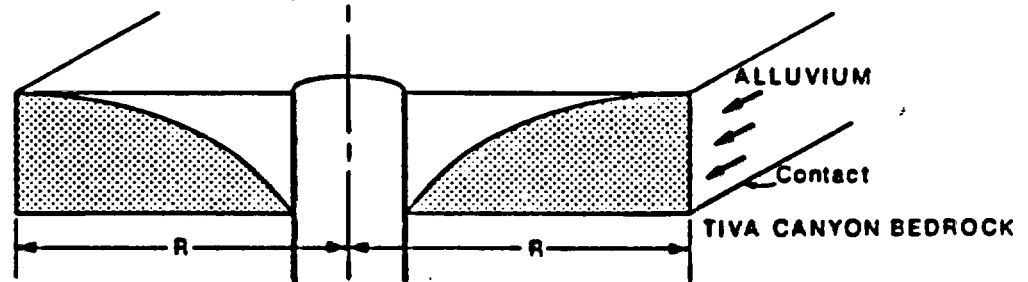
Alluvial flow is assumed to occur through the crosshatched area as shown in Figure 3-5b, under a hydraulic gradient that coincides with the average alluvial grade. This approach was adopted to simplify the calculations and was compared to an alternate calculation that involved uniform flow above the shaft and a "zone of capture" near the shaft (Fernandez et al., 1987, Appendix A-4). In the "zone of capture" calculation (Figure 3-6), all water flowing down the wash that lies within the capture zone will eventually flow down the shaft. In this zone, the radial flow velocity induced by the drawdown of the water surface near the shaft is sufficiently strong to overcome the tendency for flow to occur laterally down the alluvium in the wash. The more detailed calculation

DRAFT

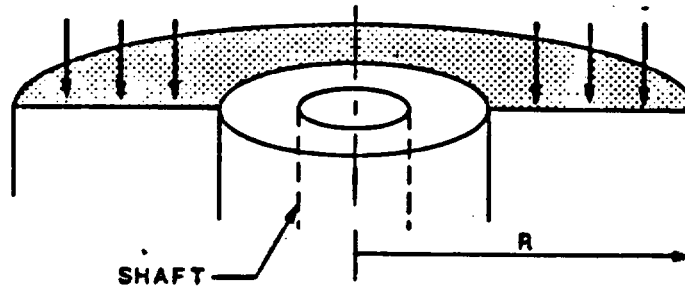
A. DUPUIT (RADIAL) FLOW



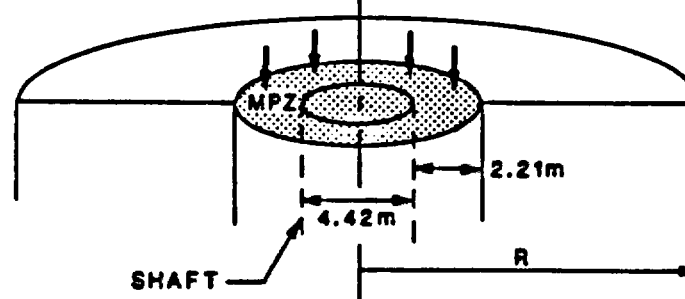
B. ALLUVIAL FLOW



C. TIVA CANYON FLOW



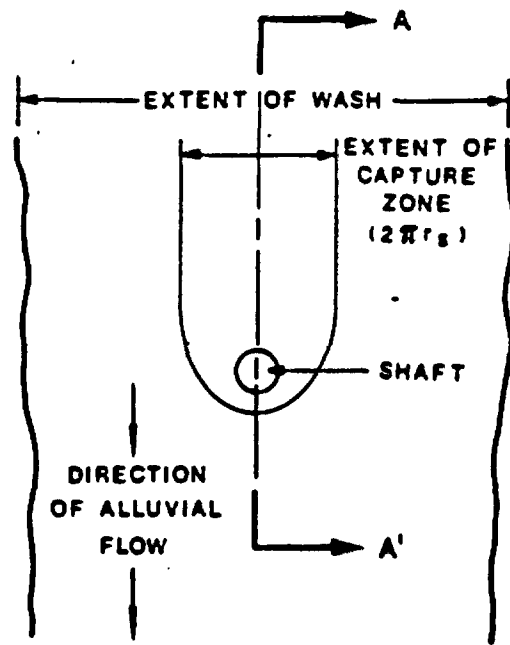
D. MPZ AND SHAFT FLOW



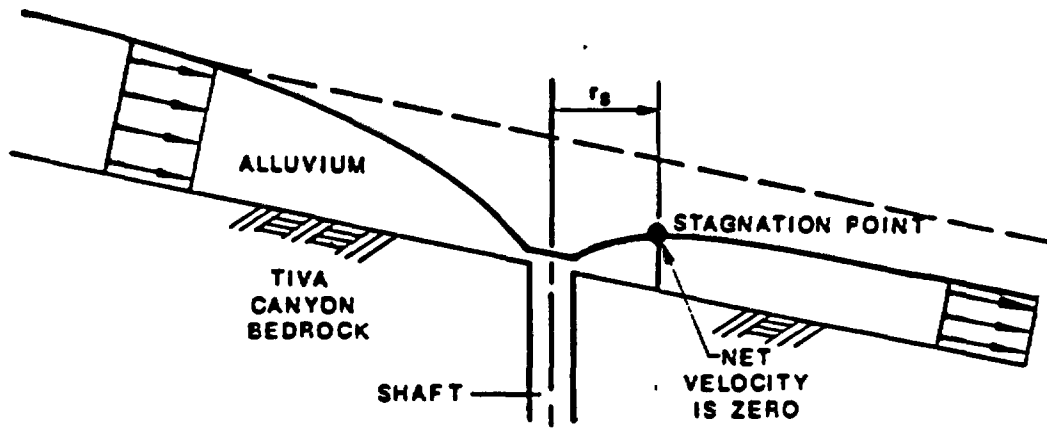
DRAFT

Figure 3-5. Types of Flow Considered in Estimating Flow into a Shaft

DRAFT



(a) PLAN VIEW
(Not to Scale)



(b) ELEVATION VIEW A-A'

DRAFT

Figure 3-6. Capture Zone Near a Shaft

indicated that the simplified approach of computing the alluvial flow as the product of the crosshatched area times the alluvial grade was reasonable. The vertical infiltration through the Tiva Canyon unit is assumed to occur through the crosshatched area under a unit gradient as might occur for fractured rock that is nearly saturated. It is recognized that the bedrock is unsaturated and that infiltration rates are likely to be higher; nevertheless, the flow calculation is conservative in underestimating this component of flow (greater proportion of flow is directed to the shaft).

In this analysis, it is assumed that the shaft fill is near saturation and that flow occurs under unit gradient conditions. It is noted that the degree to which infiltration would occur at unit gradient depends on the level of saturation and that initially the hydraulic gradient could exceed unity. These high infiltration rates would be associated with the saturation of voids and not transmission of water to the base of the shaft. As the infiltration front reaches the base of the shaft at which point water could potentially enter the repository, the hydraulic gradient would be approximately one.*

These flows are superimposed such that flow can occur as Tiva Canyon flow, alluvial flow, or shaft flow. Therefore, as a volume of water is computed for each portion of each phase, flow occurs proportionately through the Tiva Canyon Member, alluvium, and the shaft, as determined by the flow rate computed for each. Flow through the shaft is either the amount computed using the radial formula or the amount computed by the MPZ and shaft fill model, whichever amount is lower. The entire process of

*This can be shown by the Green and Ampt solution for vertical infiltration (Hillel, 1971, p. 142). At the base of the shaft, the hydraulic gradient

is given by $1 + \frac{H_o - H_f}{L_f}$ where H_o equals the pressure head at the surface,

H_f equals suction head at wetting front, and L_f equals the length over which the wetting front has moved. If we assume the pressure head at the surface is 9.1 m (height of saturated alluvium above bedrock), the suction head for the backfill is -1.0 m (a typical value for coarse material) and the length over which the wetting front has moved (311 m), then the calculated hydraulic gradient is nearly one.

DRAFT

desaturation continues until the water supply is depleted. The potential water supply is assumed to be the waters associated with specific flooding events. The input values and assumptions used for this model are discussed below in Section 3.2.1.2.

To arrive at the maximum inflow to the shaft, it is assumed that retainment of all the water associated with a flooding event occurs above each shaft location. This implies that the alluvium has a sufficient storage volume to retain all the water from the flood event, an overly conservative assumption that involves no losses by evapotranspiration or sheet flow downgradient from the shaft locations. In reality, a high percentage of the precipitation will exit the drainage basin, with only a small part percolating into the alluvium or exposed bedrock. Further, it is assumed that water flow is directed vertically downward inside the shaft liner or in the shaft fill as the water percolates to the base of the shaft. It is further assumed that flow occurs through fractures within the MPZ and that water is not absorbed within the tuff matrix.

3.2.1.2 Input Values Used

In applying this model, it was necessary to develop assumptions and evaluate specific conditions for water flow. The following assumptions were used in applying the model.

- o PMF occurs at the ES location. The volume of water used for the PMF is $159,000 \text{ m}^3$ (Fernandez et al., 1987).
- o No sheet flow or evapotranspiration occurs and all of the flood waters are retained in the alluvium upgradient from the shaft location.
- o ES-1 has an inside diameter of 3.7 m.
- o Both ES-1 and ES-2 shafts in the Tiva Canyon have an outside diameter of 4.3 m. In this analysis an overbreak of 0.08 m on each side of the shaft is assumed giving an excavated diameter of 4.4 m.
- o MPZ in Tiva Canyon Member extends from shaft wall to a radius of 4.4 m from the centerline of the shaft.
- o Hydraulic conductivity of the alluvium varies from 10^{-5} to 100 cm/s (Freeze and Cherry, 1979, pp. 29, 147).

DRAFT

DRAFT

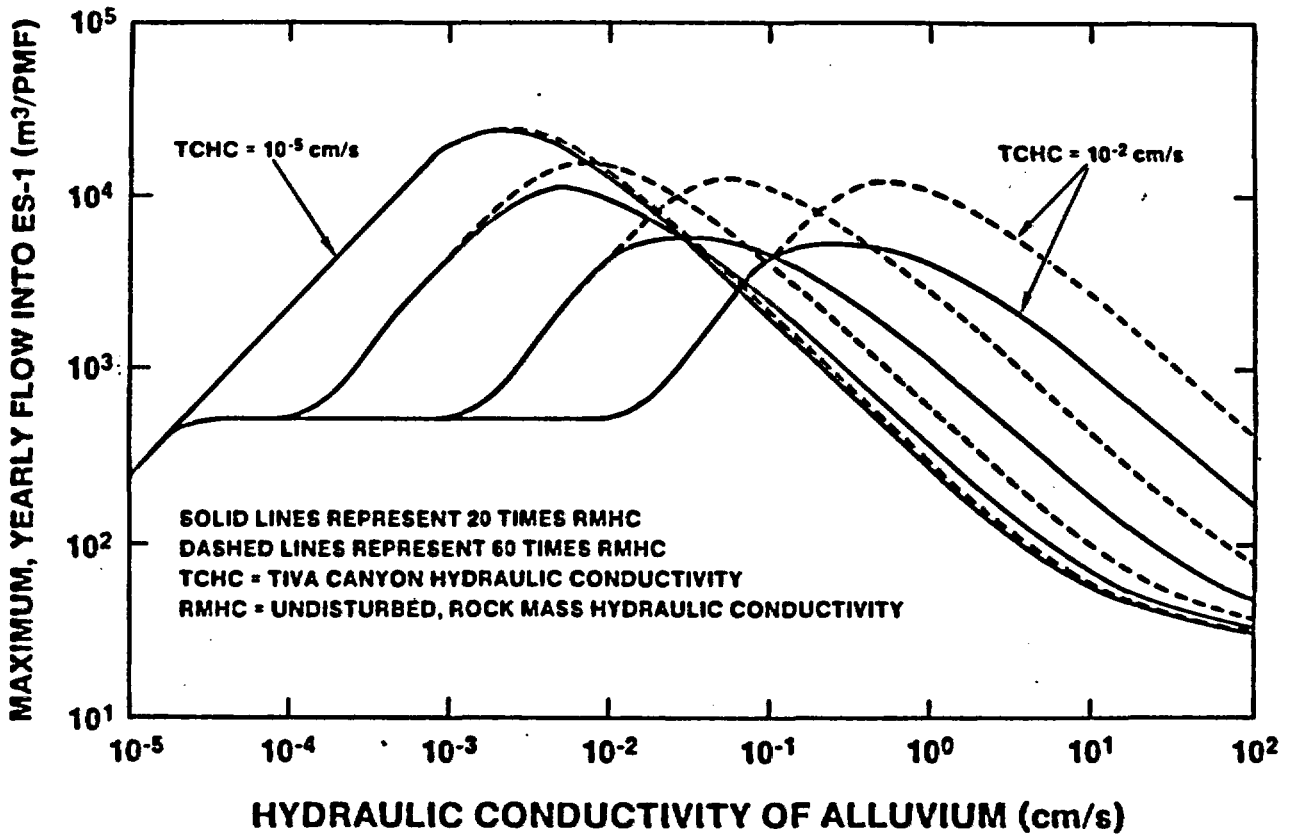
- o Hydraulic conductivity of the Tiva Canyon Member varies from 10^{-5} to 10^{-2} cm/s (Fernandez et al., 1987).
- o Alluvial grade of the water course at each site is 0.16 (based on average water course grade in Coyote Wash).
- o Radius of influence is 76.2 m (based on the approximate width of alluvium at ES-1 location).
- o Depth of alluvium is 9.1 m (based on depth of alluvium at borehole USW G-4).
- o Porosity of alluvium is 0.30 (Fernandez et al., 1987, Appendix D).

3.2.1.3 Inflow Volumes

Applying the model described above, the maximum, yearly inflow into the ES-1 is computed following a PMF event. Because no evapotranspiration and sheet flow out of the drainage basin are assumed, flow into the shaft will continue until the initial water volume associated with the PMF is depleted. For the majority of cases evaluated, the initial flood volume is depleted within the first year following the flooding event. Figure 3-7 illustrates the flow into the shaft for a broad range of conditions. The flow volumes can range from approximately 30 to 20,640 m³/year. By comparison, for anticipated conditions as defined in Fernandez et al. (1987), the estimated volume of water entering ES-1 was approximately 44 m³/year. In some instances, differences are observed between the two models assumed for the MPZ. Differences occur for two reasons. First, flow occurs through the MPZ and the shaft fill. If the majority of the total flow occurs through the shaft fill, the difference between the flows associated with each MPZ model is negligible or small. Secondly, flow into the MPZ and shaft fill can be no greater than the rate at which the water is released from the alluvium using the Dupuit assumption of radial flow to the shaft. Thus, when the saturated, hydraulic conductivity of the alluvium is low, the volume of water entering the MPZ and shaft fill is less than the full capacity of the MPZ and shaft fill. Therefore, no discrimination between the models is observed. A more complete description of shape of the curves presented in Figure 3-7 is given in Appendix B.

DRAFT

DRAFT



DRAFT

Figure 3-7. Estimated Volumes of Water Entering ES-1 (PMF, Shaft Fill Conductivity = 10⁻² cm/s, Excavated Shaft Diameter = 4.42 m)

DRAFT

3.2.1.4 Duration and Rate of Flow into Shaft

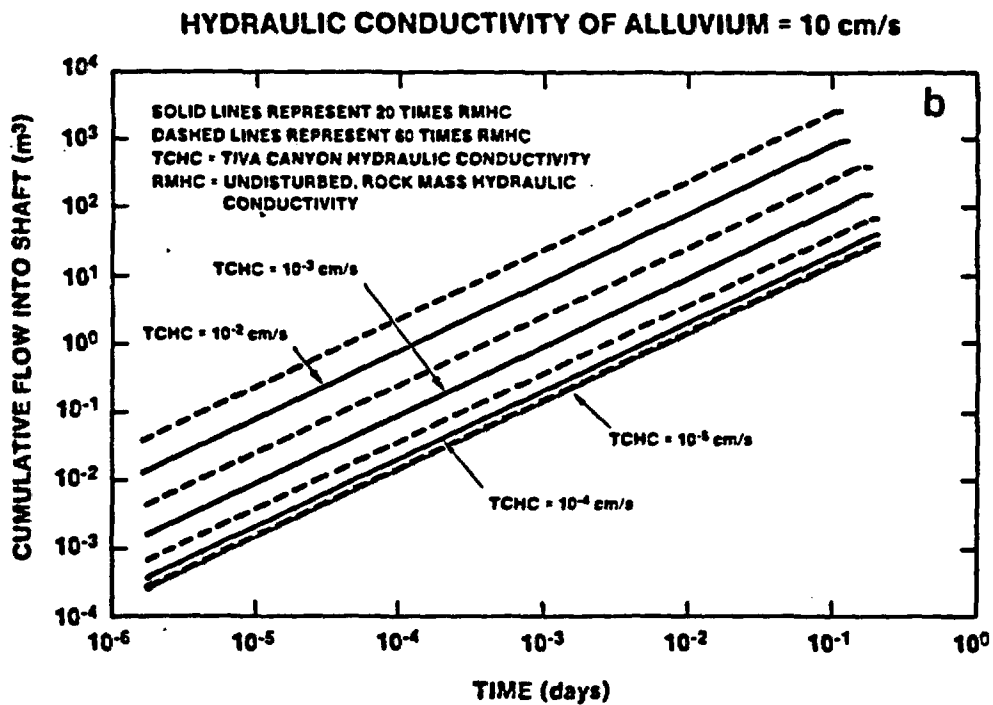
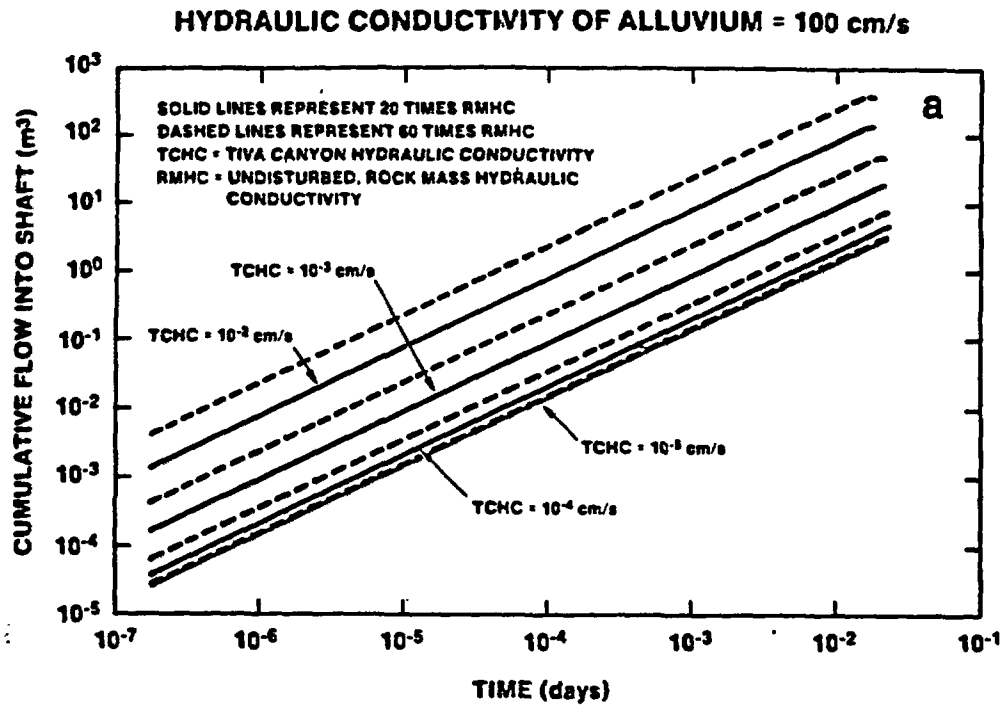
In addition to knowing the total flow down the shaft, it is also important to understand the rate and duration of flow into the shaft. Figures 3-8 to 3-11 illustrate the rate and duration of flow into the upper portion of the shaft. The data presented by these figures are used as the input functions of water flow into shaft to evaluate the potential for water buildup in the sump of the ES.

Each graph in Figures 3-8 through 3-11 illustrates water flows into the ES assuming a constant value of hydraulic conductivity of the alluvium. The range of hydraulic conductivity values for alluvium is 10^{-5} to 100 cm/s. Each graph further illustrates the effect of altering the hydraulic conductivity of the Tiva Canyon Member, located immediately below the alluvium. Because the MPZ models are related to the undisturbed rock mass hydraulic conductivity of the Tiva Canyon, a distinction between the different MPZ models is also displayed.

As indicated earlier, duration of flow and rate of flow (Figures 3-8 to 3-11) are important considerations as to how water can potentially build up at the base of the shaft. Both considerations are discussed below. Duration of flow is dependent on the flow that occurs as described in Section 3.2.1.1, i.e., Tiva Canyon flow, alluvial flow, and radial or shaft flow. These flows are dependent on the selected hydraulic properties of the alluvium and the Tiva Canyon Member. If the selected hydraulic properties are low, the time to drain the waters retained in the alluvium can be long. Conversely, if the hydraulic conductivities are high, the duration of flow into the shaft is limited. This effect is clearly displayed in Figures 3-8 to 3-11. When the hydraulic conductivity of the alluvium is high, 100 cm/s, the duration of flow into the shaft is computed as approximately 10^{-2} days or less than 15 minutes (Figure 3-8a). When the alluvial hydraulic conductivity is low, 10^{-5} cm/s, drainage of flow into the shaft is computed to occur up to 1000 days (Figure 3-11b) following the PMF. The effects of changing duration is also noticed when the hydraulic conductivity of the Tiva Canyon Member changes. As the hydraulic conductivity of the Tiva Canyon Member decreases from 10^{-2} to 10^{-5} cm/s,

DRAFT

DRAFT



DRAFT

Figure 3-8. Estimated Duration of Flow into ES-1 (PMF, Hydraulic Conductivity of Alluvium - 100 and 10 cm/s)

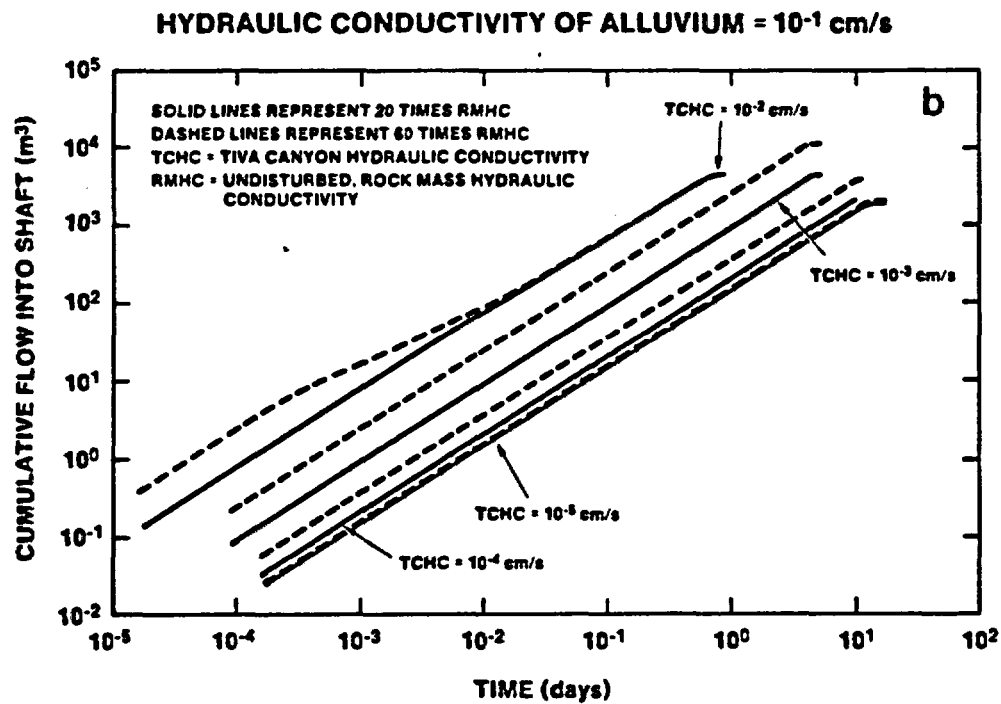
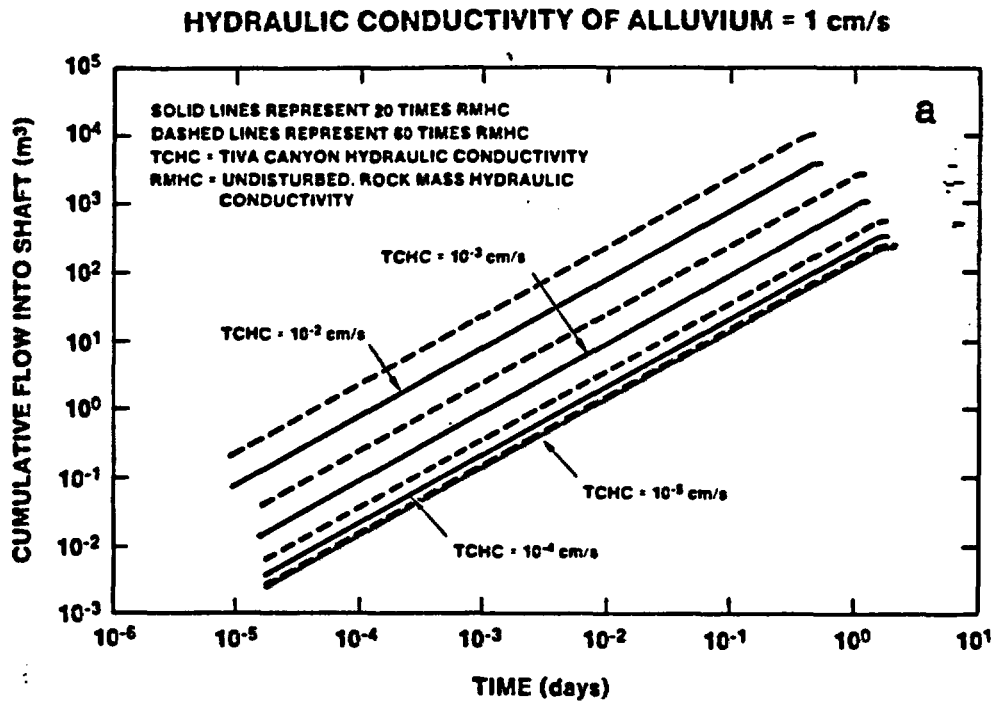


Figure 3-9. Estimated Duration of Flow into ES-1 (PMF, Hydraulic Conductivity of Alluvium - 1 and 0.1 cm/s)

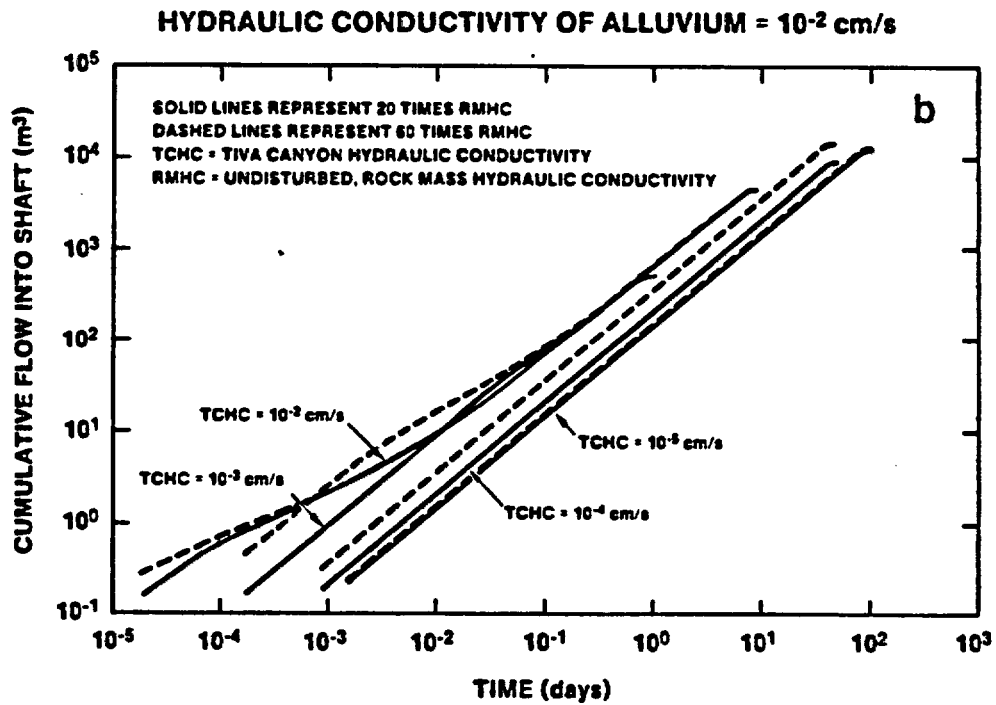
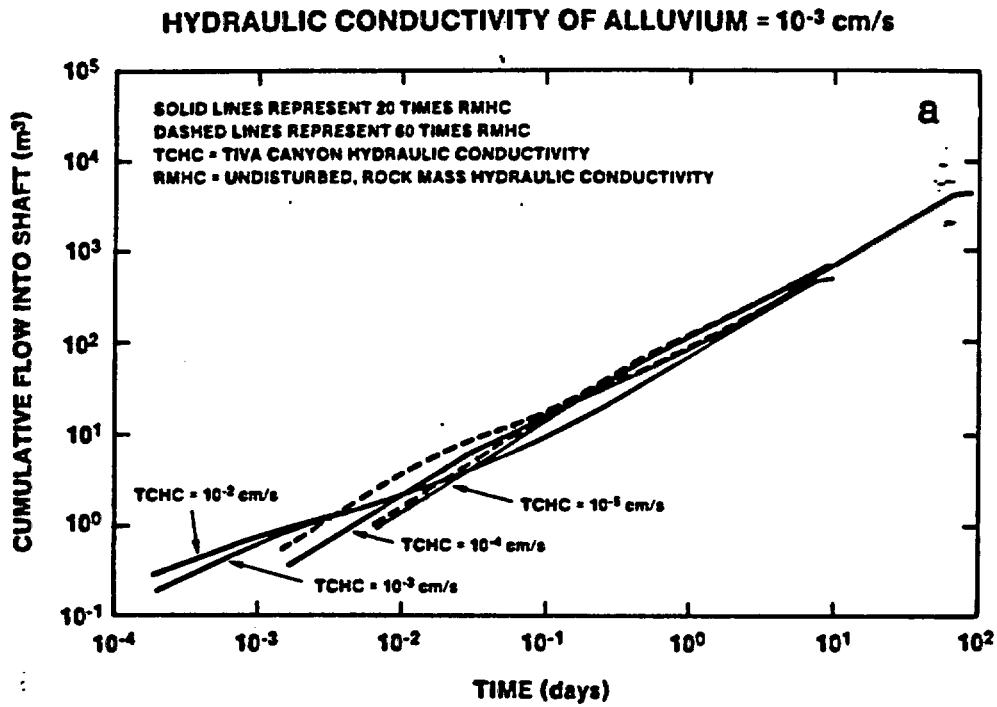
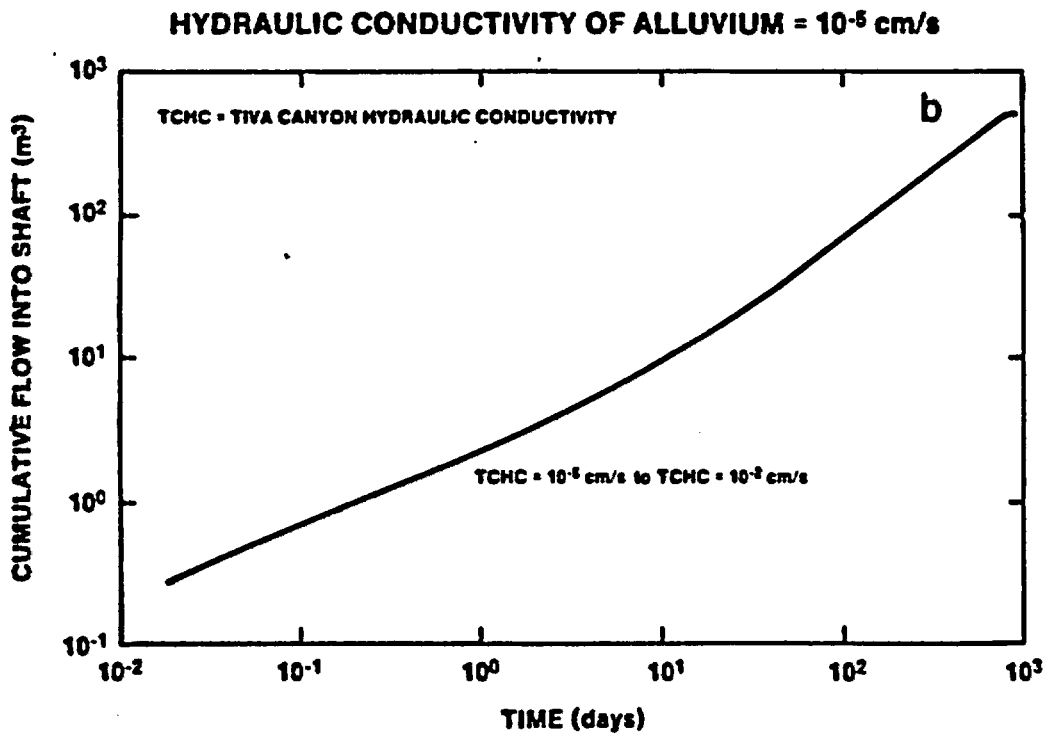
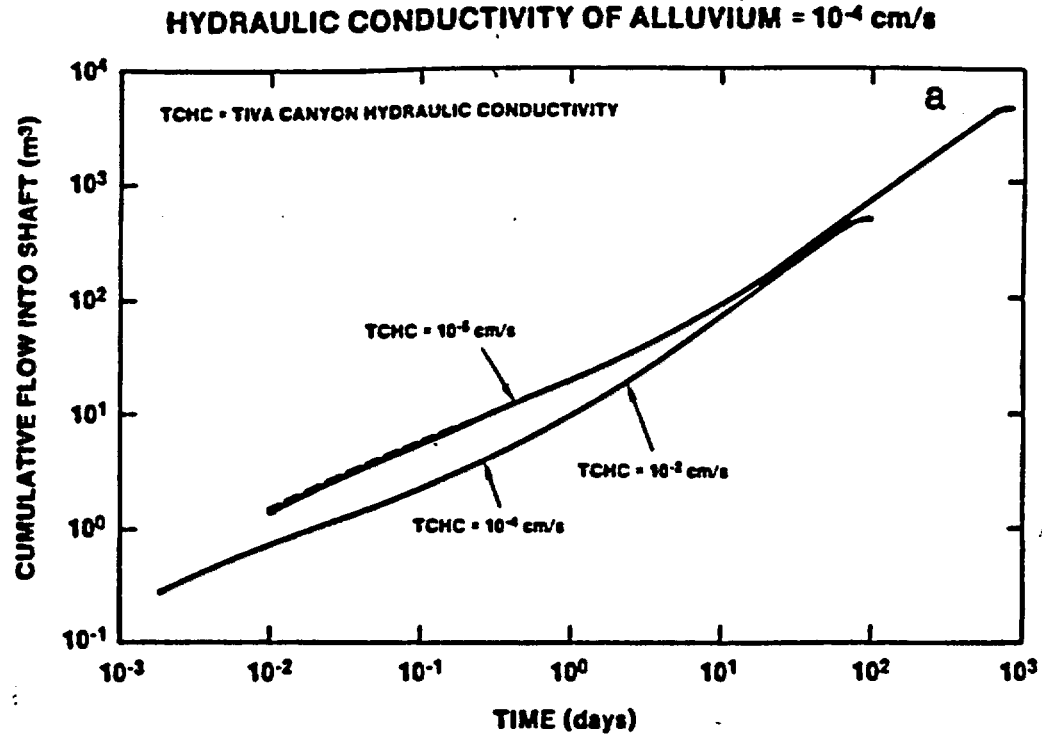


Figure 3-10. Estimated Duration of Flow into ES-1 (PMF, Hydraulic Conductivity of Alluvium - 10^{-2} cm/s and 10^{-3} cm/s)

DRAFT



DRAFT

Figure 3-11. Estimated Duration of Flow into ES-1 (PMF, Hydraulic Conductivity of Alluvium - 10^{-4} to 10^{-5} cm/s)

DRAFT

the duration of flow into the shaft increases. This effect is noticed on all graphs in Figures 3-8 to 3-11. However, the effect is more pronounced when the alluvial hydraulic conductivity decreases.

Another important consideration, aside from the duration of flow, is the rate of flow into the shaft. Flow into the upper portion of the shaft is controlled by the radial flow from the alluvium to the shaft or the flow through the MPZ and the shaft fill. If the radial flow is greater than the potential for flow through the MPZ and shaft fill, the flow entering the MPZ and shaft fill will be controlled by hydrologic properties of the MPZ and shaft fill. This condition suggests that the more water flow that is restricted from entering the shaft and the MPZ due to the properties of the MPZ and the shaft fill, the greater will be the flow down the wash in the alluvium further reducing flow into the shaft. If the radial flow is less than the potential for flow through the MPZ and shaft fill, then the flow entering the MPZ and shaft fill is limited by the radial flow toward the upper portion of the shaft (Figures 3-8 to 3-11). For example, when the alluvial hydraulic conductivity is 100 to 0.1 cm/s, radial flow to the shaft is greater than the capacity of flow through both the MPZ and shaft fill. Therefore, a distinction between the cumulative flows for both MPZ models is noticed. As the alluvial hydraulic conductivity decreases further, the radial flow into the shaft decreases until the radial flow into the upper portion of the shaft is less than full-flow capacity of the MPZ and shaft fill. This effect is first noticed (Figure 3-9b) when the flow model is 60 times the Tiva Canyon hydraulic conductivity of 10^{-2} cm/s. The flow rate into the upper portion of the shaft is further reduced as the alluvial hydraulic conductivity is reduced. When the alluvial hydraulic conductivity is extremely low, i.e., 10^{-5} cm/s, the flow through all MPZ and shaft models is controlled by the radial flow toward the shaft. In this case (Figure 3-11b), no distinction between any of the MPZ models is possible. It is also true that when flow through these MPZ models is less than their full flow capacity, the model is only partially saturated. As mentioned earlier, the data presented in Figures 3-8 to 3-11 are used to estimate the potential for water buildup at the base of the ES.

DRAFT

DRAFT

3.2.2 Model Used for Water Flow out of the Shaft

If water enters the shaft at a rate faster than it can be effectively drained, buildup of water in the shaft is possible. Further, if water buildup is greater than the sump capacity, then lateral migration through the repository station seal, into the underground facility, and ultimately toward the waste disposal areas is possible. The model and input used to determine the potential for water buildup in the sump of the ES are discussed below.

3.2.2.1 Model Description

The purpose of this section is to describe the model used in assessing the potential for water buildup at the base of the ES. It is assumed that the concrete liner at the base of the shaft has been removed. This corresponds to an unlined portion of the shaft approximately 144.5 m from the base of the shaft to the crown of the repository station drift. The actual sump depth is about 140 m, i.e., the distance from the invert* of the repository station drift to the base of the shaft. The excavated diameter of the sump is 4.42 m. The entire shaft is backfilled with a shaft fill having a porosity of 0.3. Figure 3-12 illustrates the physical model described above.

To compute the maximum buildup of water at the base of the shaft the following conservative assumptions are made: (1) the amount of water entering the upper portion of the shaft (see Section 3.2.1.4) is transported immediately to the base of the shaft and (2) no leakage outside of the MPZ occurs above the buildup of water in the base of the shaft. In reality, leakage of water into the rock mass outside of the MPZ can occur as water migrates down the MPZ. The reason for restricting the downward flow of water to the MPZ and shaft fill is not only to maximize the buildup of water at the base of the shaft but also to observe the effect of the MPZ. If water inflow to the shaft is dispersed into the undisturbed rock

*The invert is the lowest point in elevation of the drift.

DRAFT

DRAFT

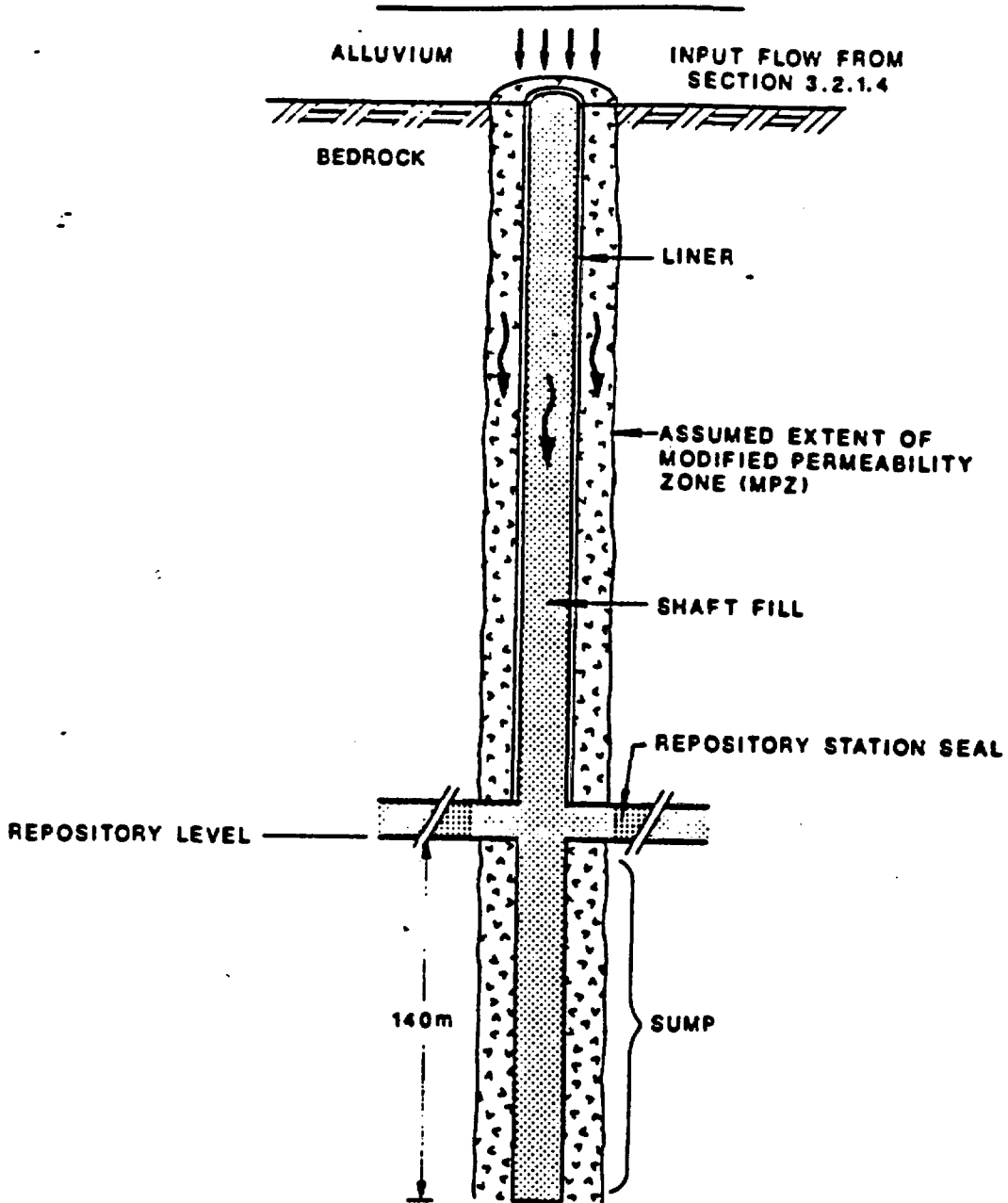


Figure 3-12. Schematic of Model Used to Compute Water Balance in the Exploratory Shaft

DRAFT
3-27

DRAFT

mass, the significance of the presence of the MPZ and shaft fill diminishes.

Once water reaches the base of the shaft, buildup of water occurs increasing the saturation levels in the bulk rock. As water buildup occurs, water can also drain through the bulk rock at the base of the shaft, predominantly through fractures. Only when the height of water in the shaft reaches the invert of the repository station drift does water pass through the repository station seals. (Two repository station drifts extend from the exploratory shaft.)

Flow from the base of the shaft is defined by analytical solutions used for calculating the saturated hydraulic conductivity above the water table using borehole infiltration tests. Flow through the repository station seals is described by Darcy's law.

Several analytical solutions described in Stephens and Neuman (1982, p. 642) were considered in computing the flow through the sump of the shaft. It should be noted that Stephens and Neuman evaluated the suitability of several analytical solutions to predict the saturated hydraulic conductivity of soils. The pressure head in the soils evaluated ranged from 0 to -1.6 m of water. (Stephens and Neuman, 1982, p. 644). The pressure head in the matrix of type can range from 0 to -1000 m of water. However, because we are computing the drainage of water from a shaft sump that is located predominantly in a highly fractured welded tuff, drainage will occur primarily through the fractures. Because these fractures are closely spaced and because the range of pressure heads for fractures (0 to -1 m) is similar to that of coarse sand (Wang and Narasimhan, 1985, p. 24; Klavetter and Peters, 1981, p. 20), we feel that selected analytical solutions presented by Stephens and Neuman can reasonably approximate the drainage from a shaft. Furthermore, a better understanding of the hydrologic characteristics and the drainage properties of fractures tuff will be obtained by field tests associated with the Exploratory Shaft testing.

The analytical solutions considered in this report included those developed by Glover, Nasberg-Terletska, and Zanger. To evaluate the

DRAFT

differences between these analytical solutions, Stephens and Neuman defined two dimensionless quantities, C_u and H_D , defined as

$$C_u = \frac{Q_s}{K_s r H} \quad \text{and}$$

$$H_D = \frac{H}{r}$$

where Q_s = infiltration or drainage rate at steady state, m^3/s

K_s = saturated, hydraulic conductivity, m/s

r = shaft radius, m

H = height of water column in shaft, m

The dimensionless value, C_u , was defined as follows:

$$C_u = \frac{2\pi H_D}{\sinh^{-1}(H_D) - 1} \quad (\text{Glover})$$

$$C_u = \frac{2.364 H_D}{\log_{10}(2 H_D)} \quad (\text{Nasberg-Terletskata})$$

$$C_u = \frac{2\pi \frac{A}{H} H_D^2 - \frac{A}{H}}{\sinh^{-1} \frac{A}{H} H_D - \frac{A}{H}} \quad (\text{Zanger})$$

The value of A in the Zanger equation represents the length of the shaft in hydraulic contact with the rock. Because the drainage rate is directly proportional to C_u , a relative comparison of C_u factors can illustrate a difference in the drainage rate out of the shaft. A comparison of the C_u factor, for the analytical solutions considered, is presented in Figure 3-13a. In Figure 3-13b, the flow rates from the shaft, as computed for each analytical solution, are displayed. To be conservative, the lowest drainage rate is selected in computing the drainage from the shaft sump. This suggests that the Nasberg-Terletskata formula is used for the majority of shaft, i.e., the lower 325 m of the shaft. In the upper part of the shaft, the Zanger formula provides a lower drainage rate. While the current plan for the ESF includes drilling below the repository station, no credit is taken for the storage capacity (approximately $2000 m^3$, backfilled) and drainage capacity offered by the 245 to 300 m

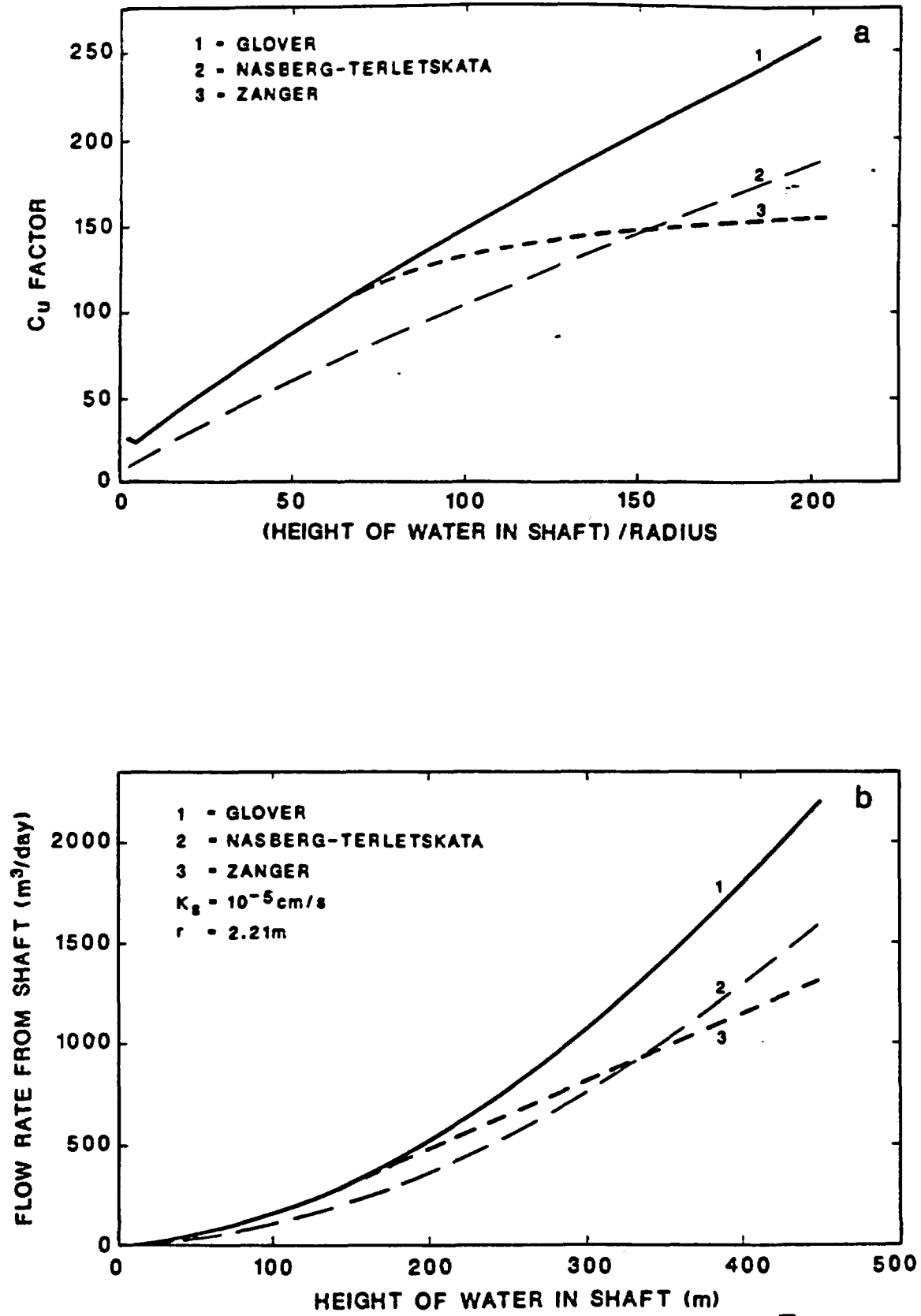


Figure 3-13. Comparison of Methods Used to Compute Drainage from Shaft

DRAFT

drift. This drift is tentatively located at the interface between the Topopah Spring Member and the Tuffaceous Beds of Calico Hills.

When the height of water in the shaft is greater than the sump depth, drainage can also occur through the station seals. Flow through the station seals is defined by the following equation.

$$Q_p = K_s \frac{dh}{dl} A_p$$

where Q_p = drainage rate through the repository station plug

$\frac{dh}{dl}$ = gradient of flow between the two faces of the repository station seal

dh = change in hydraulic potential over the length of the seal

dl = assumed length of the seal, i.e., twice the width of the drift cross-sectional, and

A_p = cross-sectional area of the plug

If it is assumed that the pressure head (equal to the height of water above) is dissipated by vertical flow, than as the height of water builds up in the shaft, the gradient across the plug increases. The following sections describe the input values of K_s used in formulas given above.

3.2.2.2 Input Values Used

The sump of the ES will be constructed predominantly in the densely welded portion of the Topopah Spring Member with approximately 15 m penetrating the nonwelded zeolitic interior of the tuffaceous beds of Calico Hills. The Topopah Spring Member is considered to be freely draining and has a high permeability because of its pervasive and abundant fractures. The nonwelded portion of the tuffaceous beds of Calico Hills, is not as intensely fractured. However, the saturated, bulk rock hydraulic conductivity of either the densely welded portion of the Topopah Spring Member or the nonwelded Calico Hills vitric or zeolitic units is much higher than their matrix hydraulic conductivity. Estimates for the bulk, saturated hydraulic conductivity for the Topopah Spring Member and the tuffaceous beds of Calico Hills are approximately 1.2×10^{-3} cm/s (Sinnock

DRAFT

DRAFT

et al., 1984, pp 11-12) and 2.4×10^{-4} or 10^{-3} cm/s (Scott et al., 1983, p. 299, and Sinnock et al., 1984, pp. 11-12), respectively. In calculating the drainage rate from the sump, the saturated bulk rock hydraulic conductivity is assumed to range from 10^{-5} to 10^{-3} cm/s. The selection of a specific value is dependent and consistent with the undisturbed, rock mass hydraulic conductivity assumed for the MPZ model. For example, if the undisturbed, rock mass hydraulic conductivity is 10^{-4} cm/s for the MPZ model, then the saturated hydraulic conductivity at the base of the shaft is also assumed to be 10^{-4} cm/s. Because the exploratory shaft penetrates slightly (~20 to 25) into the vitric and zeolitic portion of the Calico Hills nonwelded unit, the bulk, saturated hydraulic conductivity of the rock surrounding the sump has been restricted to a value of 10^{-3} cm/s (Scott et al., 1983, p. 299). Therefore, if the undisturbed, rock mass hydraulic conductivity is assumed as 10^{-2} cm/s for the MPZ model, then the saturated, hydraulic conductivity at the base of the shaft is restricted to a value of 10^{-3} cm/s. It is important to note that the total length of the sump is 140 m and the majority of the sump potentially will be surrounded by welded and highly fractured tuff.

A similar logic is used in selecting the saturated, hydraulic conductivity of the repository station seal. In general, the repository station drift seal restores the surrounding rock mass to its original, undisturbed rock mass hydraulic conductivity. The repository station seal if needed will be located in the densely welded portion of the Topopah Spring Member.

3.2.3 Water Balance in the Exploratory Shaft

Using the inflow rates described by Figures 3-8 and 3-11 in Section 3.2.1 and the appropriate drainage rate from Section 4.2.2, the water balance in the ES is computed. In all cases, water buildup of water is observed. However, in two cases, i.e., when the saturated hydraulic conductivity of the alluvium is 10^{-5} and 10^{-4} cm/s the buildup is, in general, limited because the inflow into the shaft and MPZ is very low. Therefore, graphs of height of water in the shaft versus time are displayed for only six cases, i.e., when the hydraulic conductivity of the alluvium is between 100 to 10^{-3} cm/s.

DRAFT

DRAFT

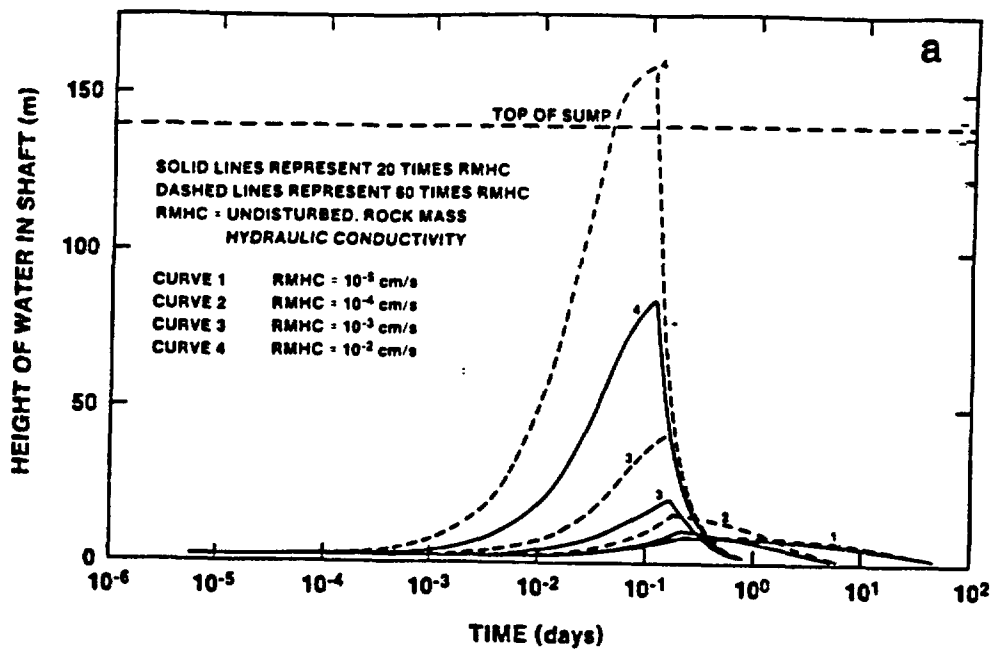
The results displayed in Figures 3-14 to 3-16 show that the height of water build up varies from essentially no water buildup to 159 m. In all cases when the MPZ model is 20 times the undisturbed rock mass hydraulic conductivity, the maximum height of the water reached in the shaft is 118 m, which is below the repository station invert. When the MPZ model is 60 times the undisturbed, rock mass hydraulic conductivity, in only two cases is the height of the water greater than the sump depth. In Figure 3-14b the maximum height is 158 m and in Figure 3-15a the maximum height is 159 m. In the first case, the time over which the height of water in the shaft is greater than the sump depth is approximately 1.6 hours. In the second case, the time is 9 hours. Because the time over which water can pass through the repository station seal is limited, the computed flows through the seals are low. In the first case (Figure 3-14b, Curve 4, dashed line) the volume of water passing the repository station seal is 2.7 m^3 . In the second case, (Figure 3-15a, Curve 4, dashed line), the volume of water passing the repository station seal is 21 m^3 . In all other cases evaluated, no flow through the repository station seal is computed.

Several general features are observed in curves in Figures 3-14, 3-15, and 3-16. The duration of inflow, which corresponds to the time period up to the peak, in all curves is greatest when the Tiva Canyon hydraulic conductivity is the lowest of the assumed range, i.e., 10^{-5} cm/s . This is to be expected as indicated by the duration of flows on Figures 3-8 to 3-11. The portion of the curves to the left of the peaks represent the period during which drainage occurs. The slope of the curves beyond the peak is depended on the hydraulic conductivity of the rock mass through which the water is draining and the height of water in the shaft. The greater rock mass hydraulic conductivity, the greater is the slope. And, the lower the height of water in the shaft the slower is the drainage and the longer it takes for the water in the shaft to fully drain from the shaft. In some cases plateau are observed. These plateau represent the condition when the inflow rate into the shaft is equal to the outflow rate from the base of the shaft. In addition general feature that when the inflows are greater for the 60 times undisturbed rock mass high conductivity, the height of water reached in the shaft is also greater.

DRAFT

DRAFT

HYDRAULIC CONDUCTIVITY OF ALLUVIUM = 10 cm/s



HYDRAULIC CONDUCTIVITY OF ALLUVIUM = 100 cm/s

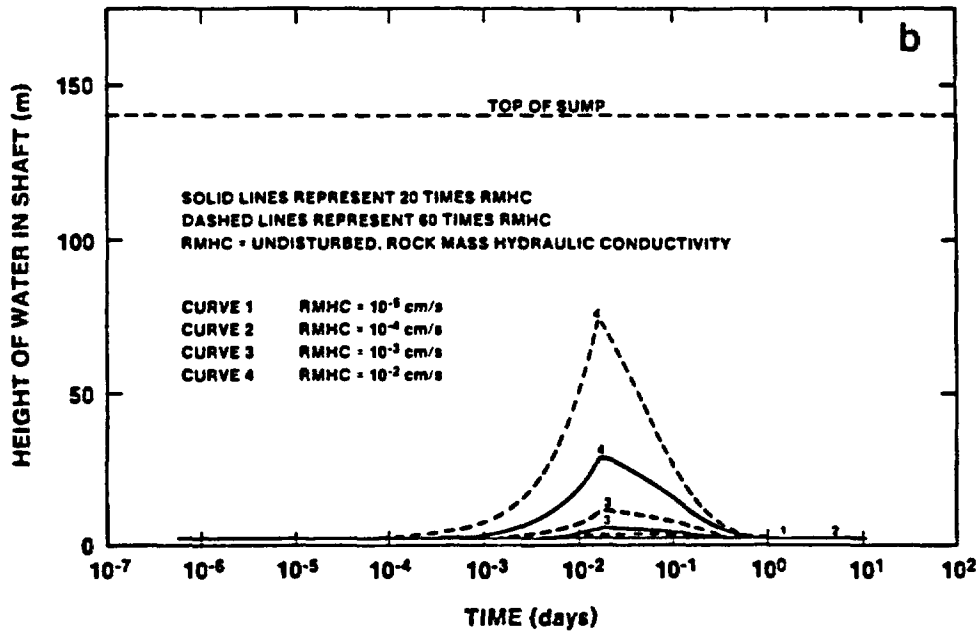
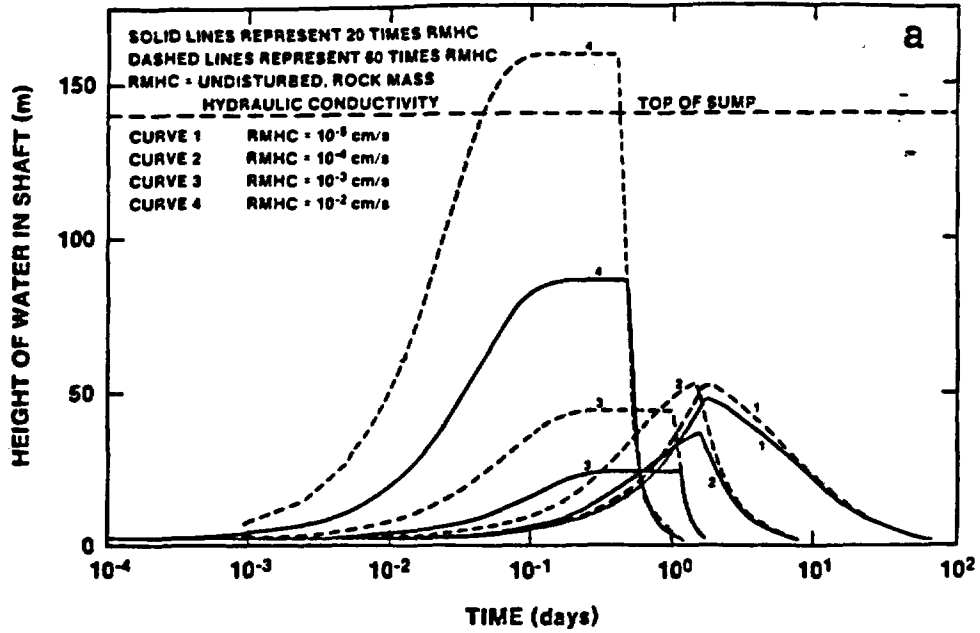


Figure 3-14. Estimated Buildup of Water in Sump of ES-1 (Hydraulic Conductivity of Alluvium - 100 cm/s and 10 cm/s)

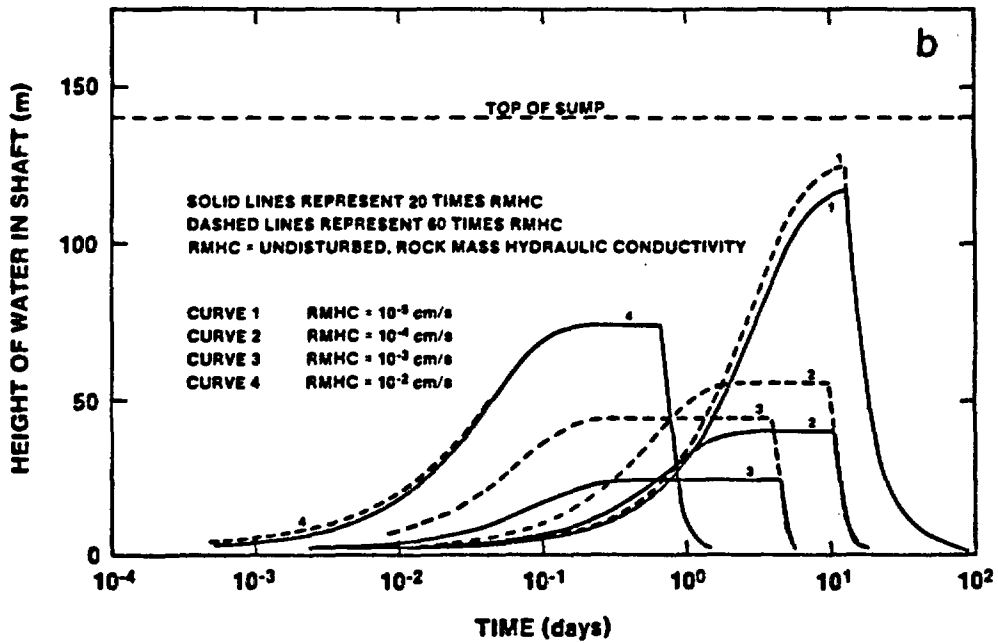
DRAFT

DRAFT

HYDRAULIC CONDUCTIVITY OF ALLUVIUM = 1 cm/s



HYDRAULIC CONDUCTIVITY OF ALLUVIUM = 10^{-1} cm/s

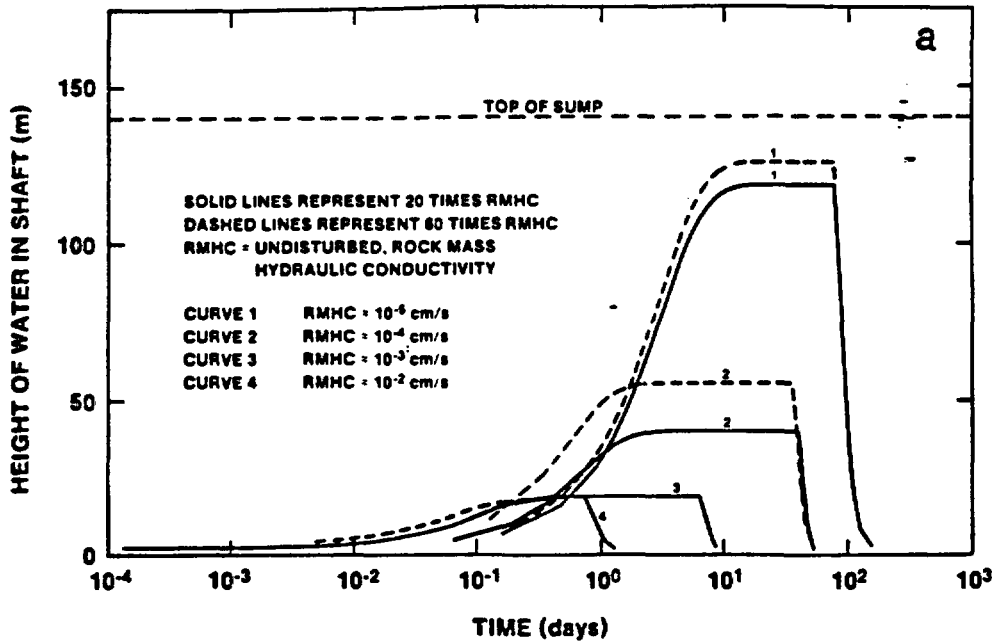


DRAFT

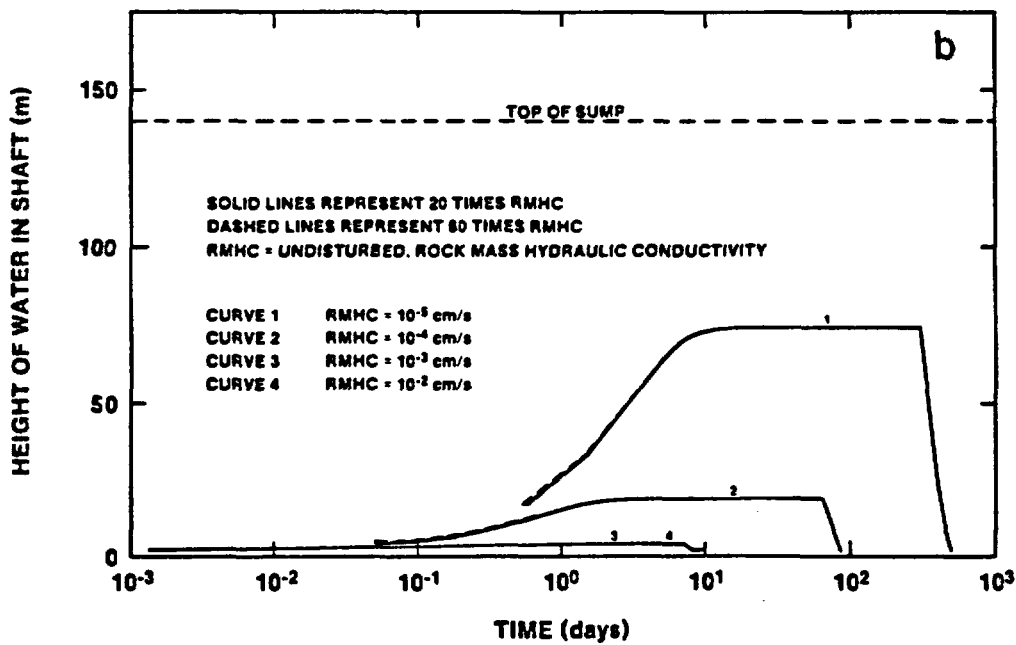
Figure 3-15. Estimated Buildup of Water in Sump of ES-1 (Hydraulic Conductivity of Alluvium - 1 cm/s and 0.1 cm/s)

DRAFT

HYDRAULIC CONDUCTIVITY OF ALLUVIUM = 10^{-2} cm/s



HYDRAULIC CONDUCTIVITY OF ALLUVIUM = 10^{-3} cm/s



DRAFT

DRAFT

Figure 3-16. Estimated Buildup of Water in Sump of ES-1 (Hydraulic Conductivity of Alluvium - 10^{-2} cm/s and 10^{-3} cm/s)

DRAFT

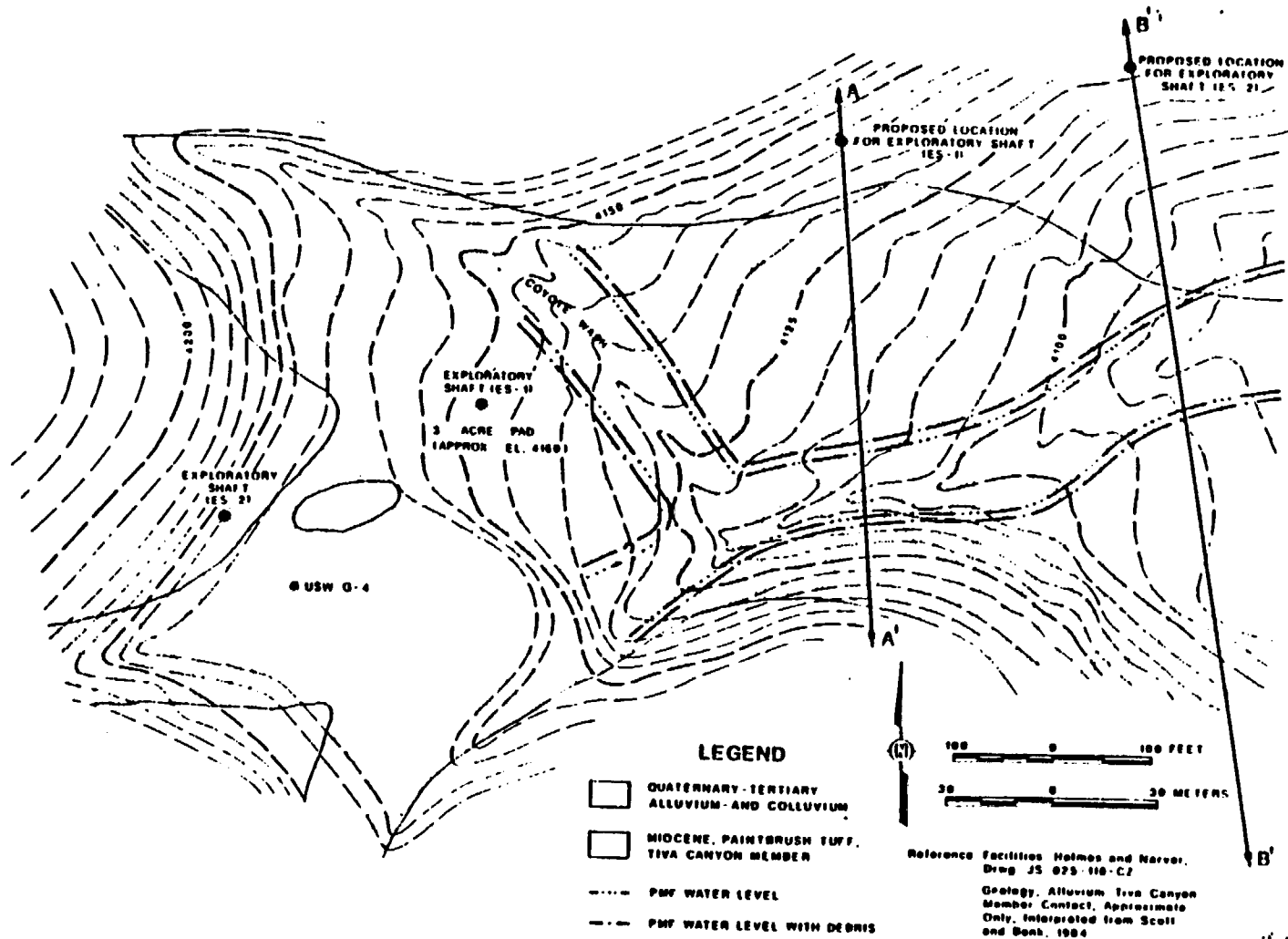
An additional observation is the point at which the peaks occur for a specific, undisturbed rock mass hydraulic conductivity. There are two factors that are important in noting where these peaks occurs, i.e., the magnitude of inflow and the duration of inflow. For example when the alluvial hydraulic conductivity is 100 cm/s. The duration of inflow into the shaft is short. As the time for inflow is extended due to the decreasing hydraulic conductivity of the alluvium, and subsequently the drainage of the total amount of water drainage, the greater is the height reached in the shaft. This high water level is reached approximately when the hydraulic conductivity of alluvium is about 1 cm/s. This point corresponds approximately to the maximum inflow in Figure 3-7. When the hydraulic conductivity of the rock mass is 10^{-5} cm/s, the water in the shaft reaches a high point approximately when the alluvial hydraulic conductivity is 10^{-2} cm/s.

3.2.4 Impact of Relocating the Exploratory Shafts

DRAFT

As indicated in Section 3.2.1.1, the model used to compute flow into the upper portion of the shaft assumed that the upper portion of the shaft penetrates alluvium. This assumption is valid for to the shaft locations given in the final EA. After the analyses presented in this report were completed, the exploratory shaft locations were relocated to the northeast of the final EA locations as shown in Figure 2-2. The concern raised by this relocation was -- does the influence of erosion and flooding at the new shaft locations adversely affect the long-term repository performance?

To address this concern it is important to consider the comparative influence of erosion and flooding at the final EA locations and the relocated positions. Figure 3-17 shows the relocated positions for the ESs relative to potential flood/levels. Because the current ES-1 and ES-2 will be collared in bedrock, this potential for eroding alluvium around the shaft collar is nonexistent. Furthermore, the shaft collars will be located in the Tiva Canyon Member that caps most of Yucca Mountain. In these caprock-protected areas, erosion is relatively slow providing a much greater resistance to downwasting than alluvium. Therefore, the impact



DRAFT

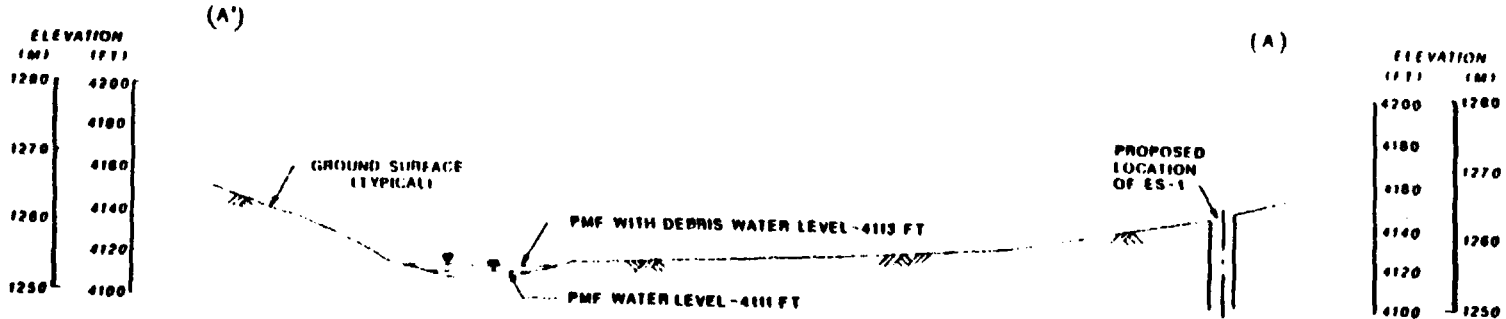
Figure 3-17. Estimated High-Water Locations Associated With a PMF in the Exploratory Shaft Area

DRAFT

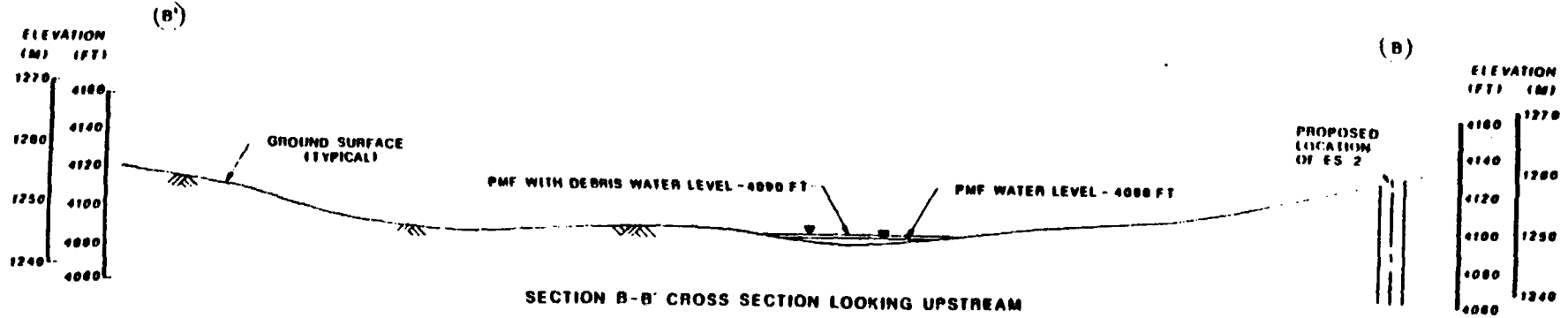
of the erosion of rock at the new exploratory shaft locations is considered to be negligible in comparison to the erosion of alluvium at the old exploratory shaft locations.

To illustrate the comparative influence of flooding, a map defining the extent of the PMF was developed. In developing this map the existing topography and the Manning equation for open channel flow was used. Eight cross sections were used in developing the PMF high water marks shown on Figure 3-17. In applying the Manning equation, the assumptions used were similar to those used by Squires and Young. Specifically, the values for slope of the energy-grade line used in Manning's equation was assumed to be equivalent to the slope of the water surface and the channel bottom (Squires and Young, 1984, p. 24). The value for the roughness coefficient, n , in Manning's equation was assumed to be 0.060. Roughness coefficients used by Squires and Young ranged from 0.030 to 0.055. Because we are estimating the high-level marks for the PMF and because 'n' is proportional to the area of flow, a greater 'n' value suggests a greater area of flow. This greater cross-sectional area of flow corresponds to a higher water-level use during the occurrence of a PMF. Therefore selection of a greater 'n' value (as used in this analysis) conservatively predicts a higher water-level rise.

Figure 3-17 shows the high-water locations for the PMF is the exploratory shaft assuming two peak discharges. The inner lines represent the clear water flow only and the outer lines represent the clear water and debris flows. The peak discharge for the clear water flow is $95 \text{ m}^3/\text{s}$. (U.S. Bureau of Reclamation, 1986). To arrive at the peak discharge for the clear water plus debris flow, the debris flow is assumed to be 50 percent of the clear water flow. Figure 3-17 illustrates that some potential exists for the old ES-1 location to be indicated by a PMF. However, the potential for indicating the shaft entry points of the new ES-1 and ES-2 locations is substantially reduced. The horizontal distance of the high water mark from the ES-1 and ES-2, new locations is 90 m and 70 m, respectively. The ES-1 and ES-2 surface locations are 9 m and 11 m above the highest level of the PMF flows. Figure 3-18 presents the cross-sectional diagrams of the topography and the water elevations of the PMF at



SECTION A-A' CHANNEL CROSS SECTION LOOKING UPSTREAM



SECTION B-B' CROSS SECTION LOOKING UPSTREAM

SCALES FOR CROSS SECTIONS A-A' AND B-B'



DRAFT

Figure 3-18. Topographic Cross Sections in the Vicinity of the New ES-1 and ES-2 Locations

DRAFT

the new locations of the ES-1 and ES-2. These cross-sections are presented to illustrate the distance of the PMF flows from the new ES-1 and ES-2 locations.

From the preceeding discussion, it can be concluded that relocation of the ESs to the northeast from the final EA locations, has substantially reduced the impact that erosion and flooding could have on repository performance.

3.2.5 Conclusions

Because, in general, water entering the shaft, in the postulated PMF scenario, is contained within the ES sump and subsequently drained, it is concluded that the MPZ does not influence the performance of the YMMGDS. In the two cases where limited water entry through the repository station seals does occur, the same conclusion is reached for the following reasons. The flow is limited to a small volume of 21 m^3 , which can easily be isolated by repository design features. These features can include constructing a sump capable of isolating this volume of water. The ESF itself can be graded to develop a sump around the ES. Also, if water enters the underground facility and no sump is provided immediately near the exploratory shaft with proper repository drift grading, water can be diverted to the low point in the repository.

In addition to the rationale given above, we feel that the conclusion reached, i.e., the MPZ does not influence the performance of the YMMGDS, is justified because (1) the probability of the scenario selected to develop a source of water that could enter the shaft is extremely low or incredible and (2) both ES-1 and ES-2 have been relocated to much more favorable locations, where the scenario presented in the report would clearly provide an upper bound of water flow into the shaft.

3.3 Potential for Enhancing Radionuclide Release from Air Movement Due to Convective Forces

For a repository located above the water table, there is the possibility of release of radionuclide by air flow out of the repository through the shafts or through the host rock. This section evaluates the

DRAFT

potential magnitude of air flow rates from the repository and compares the relative influences of the shafts, ramps, and host rock in allowing air flow to occur. More specifically, the calculations examine the influence of the MPZ around the shafts and ramps and the degree to which flow can be limited by backfilling or sealing the shafts.

After emplacement of waste canisters, heat is initially transferred by conduction from the waste canisters to the surrounding rock. Vertical temperature gradients will develop from the repository horizon, and potentially affect air and water density. If sufficient energy in the form of heat is impacted to the air or water vapor, convective transport is established.

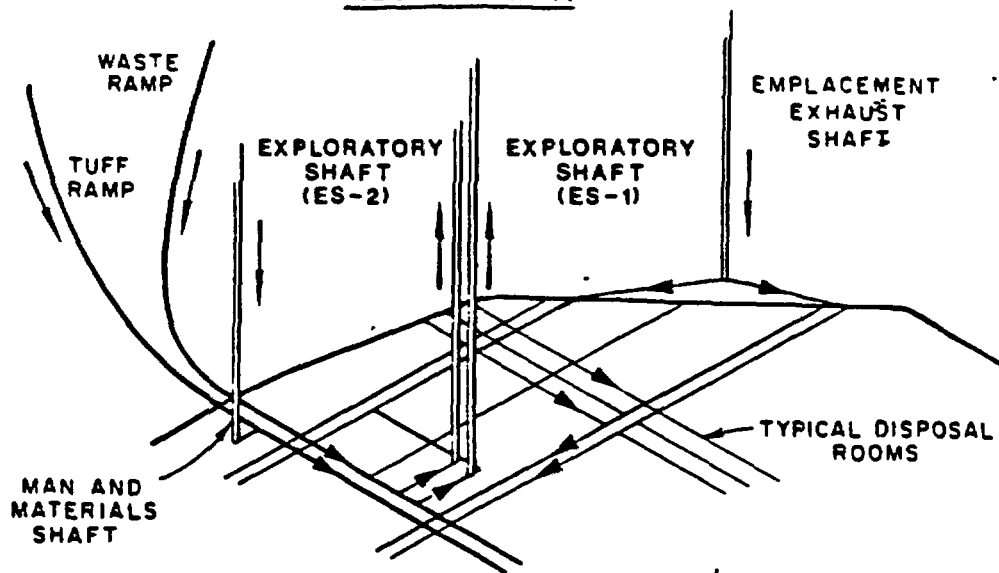
3.3.1 Air Flow Mechanisms

Two potential air flow mechanisms are illustrated in Figure 3-19. Mechanism A assumes that no upward flow occurs through the host rock relative to flow through the shafts, ramps, and drifts. ES-1 and ES-2 are within the repository area, and the temperature gradient is relatively high near the repository horizon due to the emplacement of thermally hot waste packages. The men-and-materials shaft, the emplacement exhaust shaft and the ramps are located outside or just inside the repository perimeter, and the temperature gradients are lower. In response to these temperature gradients, air will tend to rise in ES-1 and ES-2, and will be drawn in through the other entries. The mechanism may occur if the shafts and drifts are open, or if the backfill is relatively permeable so that the resistance to air flow through the backfill is less than that through the rock. In Mechanism B, convective air transport is assumed to occur through the host rock. The waste disposal areas are relatively hot and the heated air tends to rise vertically through the rock as well as through ES-1 and ES-2. Air is drawn in through the peripheral entries to maintain pressure in the rooms.

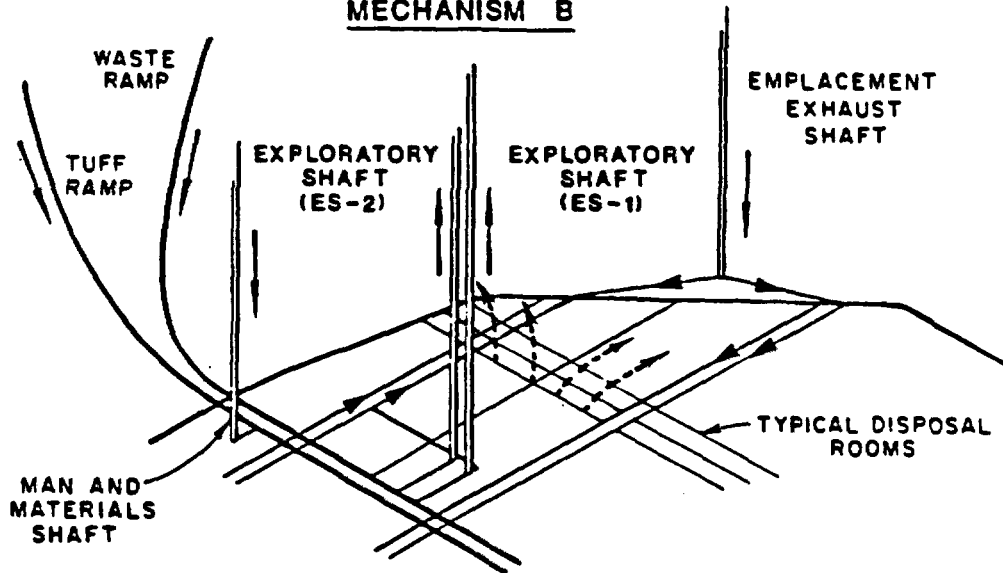
The analyses presented in this report consider Mechanism B in detail. As discussed subsequently for shafts filled with an engineered material

DRAFT

MECHANISM A



MECHANISM B



--- FLOW THROUGH ROCK MASS
— FLOW THROUGH SHAFT

Figure 3-19. Mechanisms for Convective Air Flow (a) flow through shafts only (b) flow through shafts and rock

DRAFT

(hydraulic conductivity less than 10^{-2} cm/s), the flow of air out of the repository would be dominantly through the rock. A detailed discussion of Mechanism A and a comparison between the two mechanisms is presented in Appendix C of Fernandez et al. (1987).

3.3.2 Method of Analysis

The mechanism of convective air flow through a heated repository is considered to be analogous to air flow through an underground mine resulting from natural ventilation. Draft air pressures are calculated by the density method. Air flows are assumed to be induced by the draft air pressure and are calculated using a network resistance model similar to that used in mine ventilation studies (Hartman, 1982, pp. 239-245). Flow is assumed to be governed by Darcy's Law. In Appendix C, a relationship is derived for convective air transport through backfilled shafts and fractured rock from the assumptions mentioned above that is similar in form to a relationship presented by Bear (1976) for convective transport through a porous media. The physical interpretation made is that buoyant forces that evolve from thermal gradients are equal to viscous forces for circulation through filled shafts, surrounding modified permeability zones and rock.

The principal input parameters are the resistance to air flow of the underground openings and the host rock, and the pressure gradient calculated from the difference in pressure between the inlet and outlet points as derived by the air density profiles. A detailed discussion of the assumptions made in the analysis is presented in Appendix C. The assumptions may be summarized as follows: 1) Darcy's Law is valid; 2) air temperatures in the shaft are the same as in the adjacent rock; 3) air flow is incompressible and the air is dry; and 4) air circulation occurs along specified paths.

3.3.3 Model Description

Air flows were calculated by assembling a "network stiffness matrix" (Zienkiewicz, 1977, pp. 12-13) of various resistances, representing the

DRAFT

network of underground openings and the rock mass applying pressure boundary conditions, and solving a system of linear simultaneous equations to calculate nodal pressures. Air flows were then calculated through the network. The following sections describe the temperature and pressure boundary conditions, air conductivities (material properties), and model geometry (networks) used in the analyses.

3.3.3.1 Temperature and Pressure Distributions

Draft pressures were calculated using the accepted mine ventilation practice of computing pressure gradients on the basis of differences in air density at the inlet and outlet points. The first step requires two temperature profiles at the potential repository inlet and outlet points. For purposes of calculating air densities, a peak temperature profile was estimated for the ES-1 based on a peak temperature of 115°C at the repository horizon (The source of this temperature use is the heat liberated from the radioactive waste contained in the waste packages.) At the time at which the peak temperature is attained, the temperature at the other entries outside the repository will be considerably lower. For a conservative analysis (i.e., maximum temperature difference), the temperature profile at the inlet shafts and ramps was assumed to be 13°C.

The calculated draft pressure using the method described above was 0.35 kPa, which corresponds to 1.4 inches of water gage. By comparison, according to Hartman (1982, p. 240) the natural ventilation pressure generated by natural geothermal energy in mines is usually less than 0.5 inches water gage, and seldom exceeds three inches except in extreme cases. The calculated draft pressure falls within this range for this mechanism and would be expected to be higher than 0.5 inches, since the heat generation due to radioactive waste in an underground nuclear waste repository results in larger temperature contrasts than those experienced in a typical underground mine.

3.3.3.2 Flow Path Resistances

The resistance to air flow for incompressible fluid flow through shafts and drifts is dependent on the lengths and cross-sectional areas of the flow regime, and the air conductivities of the backfill, surrounding MPZ, and host rock. In the present analyses, MPZs were modeled around the shafts and ramps accessing the repository, but not around the drifts (see below). The cross-sectional areas and length for the flowpaths for vertical and horizontal emplacement are summarized in Tables 3-2 and 3-3 respectively. The cross sectional areas of the MPZ developed around the shafts were assumed to extend out one radius from the wall. For ramps that which have a noncircular cross section, the MPZ area was calculated from the equivalent radius of a circle with the same area.

For flow through undisturbed rock it is necessary to know the cross-sectional area of the roof of the repository (waste rooms, submains and mains). This area is estimated to be 983,700 m² for vertical emplacement or 486,000 m². In these analyses, the roof areas above the mains and submains were included in the calculation since it is expected thermal convection would develop throughout the underground repository. The equivalent conductivity for flow through the rock to the ground surface was calculated according to the relation for flow in series (Freeze and Cherry, 1979, p. 34). In the present analyses, the thickness of the welded units (Tiva Canyon and Topopah Spring) is 260 m and the thickness of the nonwelded Paintbrush is 40 m. The air conductivity* of the nonwelded Paintbrush was assumed to be either 3×10^{-7} or 3×10^{-5} m/min. This corresponds to a range of hydraulic conductivity from 10^{-5} to 10^{-3} cm/s. The welded tuff units (Tiva Canyon and Topopah Spring) were assumed to have either an air conductivity of 3×10^{-7} or 3×10^{-4} m/min. This corresponds to a range of hydraulic conductivities of from 10^{-5} to 10^{-2} cm/s.

*An conductivity may be derived by calculating an intrinsic permeability from the hydraulic conductivity relationship presented by Freeze and Cherry (1979, p. 27) and then by calculating the air conductivity using the fluid properties of air.

TABLE 3-2

SUMMARY OF AREAS AND LENGTHS - VERTICAL EMPLACEMENT

Flowpath	Backfilled ^(a) Area (A) (m ²)	Modified Permeability Zone ^(b) Area (m ²)	Length (m)
Waste Ramp	34.2	115.8	2012
Tuff Ramp	42.8	136.8	1410
Men-and-Materials Shaft	29.2	105.9	314
EE Shaft	29.2	105.9	314
ES-1	10.5	42.9	311
ES-2	10.5	42.9	311

- (a) Backfilled area is based upon inside dimension of lined shaft or ramp.
 (b) MPZ based upon three times the excavated area of the shaft or ramp which corresponds to an MPZ extending one radius from the edge of the excavated, shaft wall.

TABLE 3-3

SUMMARY OF AREAS AND LENGTHS - HORIZONTAL EMPLACEMENT

Flowpath	Backfilled ^(a) Area (A) (m ²)	Modified Permeability Zone ^(b) Area (m ²)	Length (m)
Waste Ramp	28.3	96.5	2012
Tuff Ramp	30.1	96.5	1410
Men-and-Materials Shaft	29.2	105.9	314
EE Shaft	29.2	105.9	314
ES-1	10.5	42.9	311
ES-2	10.5	42.9	311

- (a) Backfilled area is based upon inside dimension of lined shaft or ramp.
 (b) MPZ based upon three times the excavated area of the shaft or ramp which corresponds to an MPZ extending one radius from the edge of the excavated, shaft wall.

Three combinations of bulk rock hydraulic conductivity were evaluated in the analysis. These combinations were selected to cover a range of conductivities for welded and nonwelded tuff and to examine the influence of a thinner less permeable layer of nonwelded tuff on overall air flow rates if the welded tuff conductivity were high (10^{-2} cm/s).

	Nonwelded Hydraulic Conductivity (cm/s)	Welded Hydraulic Conductivity (cm/s)
Combination 1 (Low)	10^{-5}	10^{-5}
Combination 2 (Intermediate)	10^{-3}	10^{-2}
Combination 3 (High)	10^{-3}	10^{-2}

The equivalent air conductivity of the modified permeability zone was taken to be either 20 or 60 times higher than the conductivity of the undisturbed tuff averaged over an annulus one radius wide extending from the shaft wall. The equivalent conductivity factor of 20 corresponds to expected conditions at depth. The equivalent conductivity factor under worst case assumptions ranged from 40 to 80 times the undisturbed tuff conductivity. The average value of 60 was selected for analysis. The equivalent conductivity factor of the overlying rock was determined, as explained previously to take into account strata with varying conductivities, and the MPZ was assumed to be either 20 or 60 times more permeable than the undamaged rock in each stratigraphic unit.

Air conductivities in the backfill were varied over a range from 3.0×10^{-6} m/min to 3.0 m/min, equivalent to a range of hydraulic conductivity from 10^{-4} to 100 cm/s. The upper bound for air conductivity corresponds to a gravel, while the lower bound corresponds to a silty sand (Freeze and Cherry, 1979, p. 29). The lower bound might also correspond to a compacted backfill engineered for low permeability by adding silt or clay fines.

3.3.4 Model Results

The convective air flow analysis results are presented as a series of plots. The relationship of total flow rate out of the repository to shall fill, air conductivity for vertical and horizontal emplacement modes, and

DRAFT

low and high modified permeability zone models are presented in Figures 3-20 through 3-23. The flow rate through ES-1 and ES-2 expressed as a percentage of the total flow rate out of the repository are presented in Figures 3-24 through 3-27. The three curves on each plot represent the low, intermediate, and high rock conductivity combination presented previously.

The distribution of flow through the shaft fill, the MPZ, and the tuff roof rock was found to be dependent on the shaft fill, air conductivity. With high shaft fill, air conductivity of 1 m/min, the flow into and out of the repository is dominantly through the shaft fill with total flow ranging from approximately 1 to 10 m³/min, depending on the conductivity of the roof rock. With low fill conductivities (less than 10⁻⁵ m/min, flow into the repository is primarily through the modified permeability zone, while flow out of the repository is dominantly through the tuff roof, and total flow rates are less than 10⁻¹ m/min. The high conductivity MPZ model results in somewhat higher flow rate than the low conductivity MPZ model under these circumstances. The conductivity of the tuff units in series influences the total air flow through the repository. For the high conductivity combination, the total flow begins to level off toward a constant value at a shaft fill, air conductivity of about 10⁻³ m/min. For the intermediate and low conductivity combinations, this stabilization of total flow occurs at shaft fill, air conductivity of approximately 10⁻⁵ m/min. At low backfill air conductivity, the total flow rate varies over two orders of magnitude depending on the air conductivity of the rock.

In comparing total flow for the vertical and horizontal emplacement modes, it is apparent that the results are very similar. This is because the geometry of the shafts and ramps accessing the repository are very similar. At high backfill air conductivity, flow is dominantly through the shafts and ramps. At low backfill conductivity, resistance to flow is dominantly through the MPZ of the inlet shafts and ramps. In this analysis, no attempt has been made to distinguish temperature fields between the two emplacement modes although this may have some influence on calculated upper-bound convective air flow rates. It is reiterated that

DRAFT

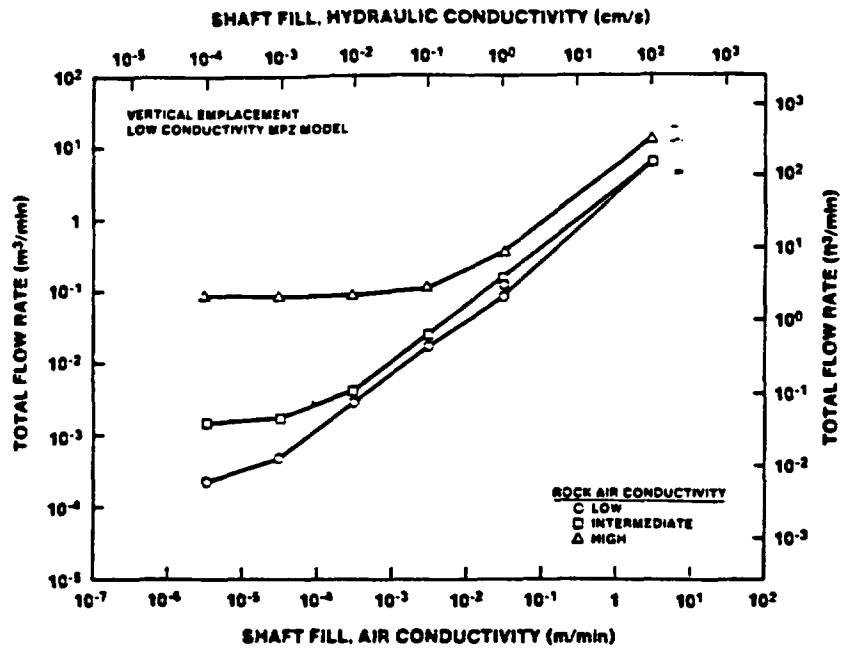


Figure 3-20. Total Flow Rate as a Function of Shaft Fill, Air Conductivity (Vertical Emplacement and Low Conductivity MPZ Model)

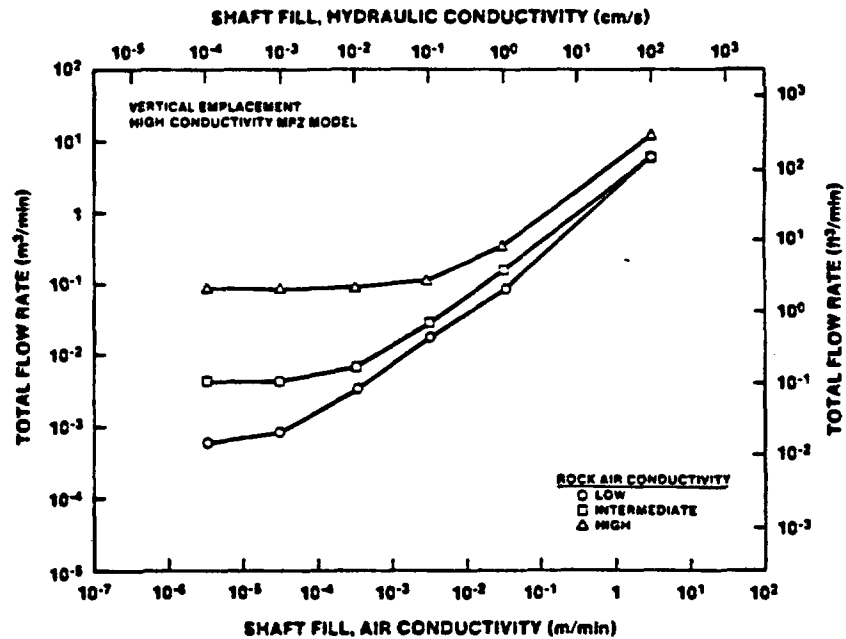


Figure 3-21. Total Flow Rate as a Function of Shaft Fill, Air Conductivity (Vertical Emplacement and High Conductivity MPZ Model)

DRAFT

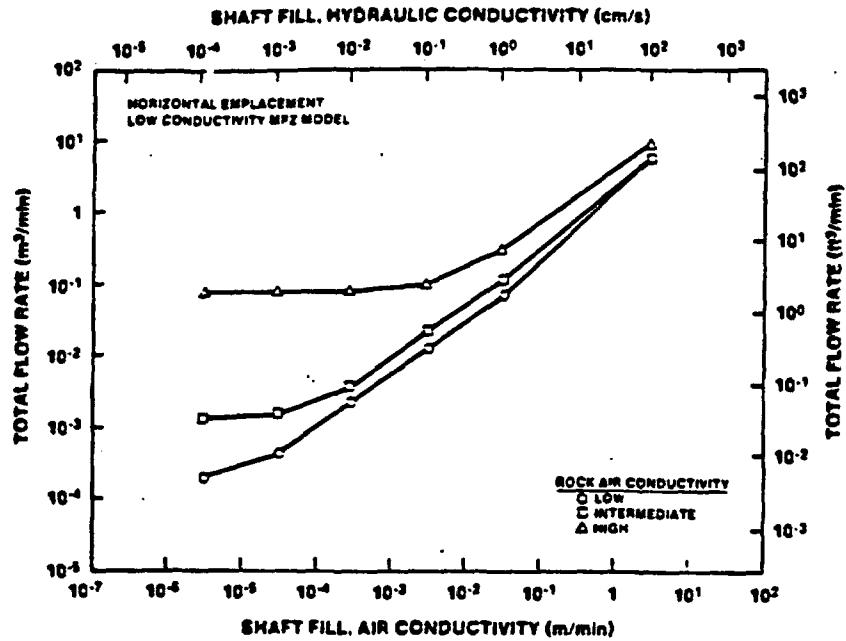


Figure 3-22. Total Flow Rate as a Function of Shaft Fill, Air Conductivity (Horizontal Emplacement and Low Conductivity MPZ Model)

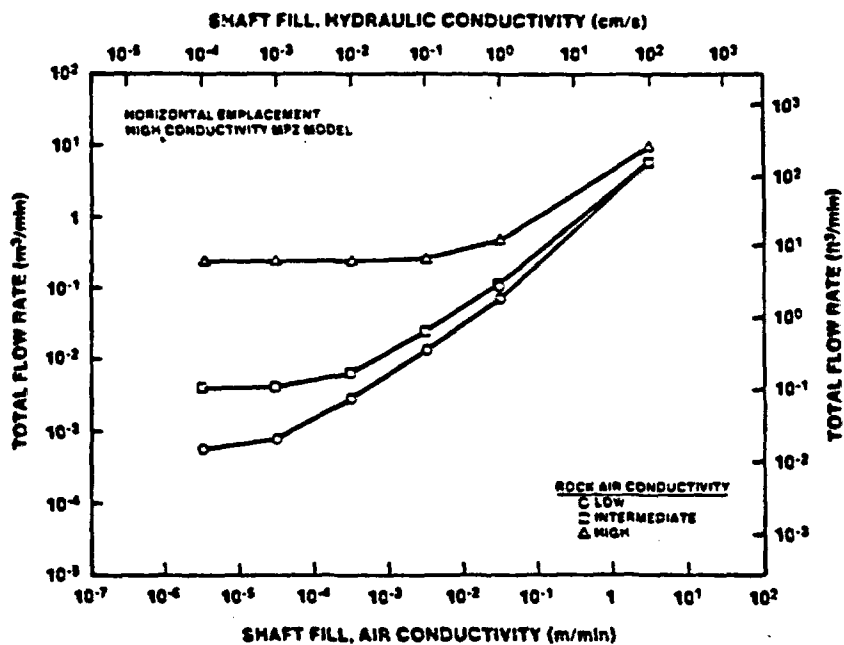


Figure 3-23. Total Flow Rate as a Function of Shaft Fill, Air Conductivity (Horizontal Emplacement and High Conductivity MPZ Model)

DRAFT

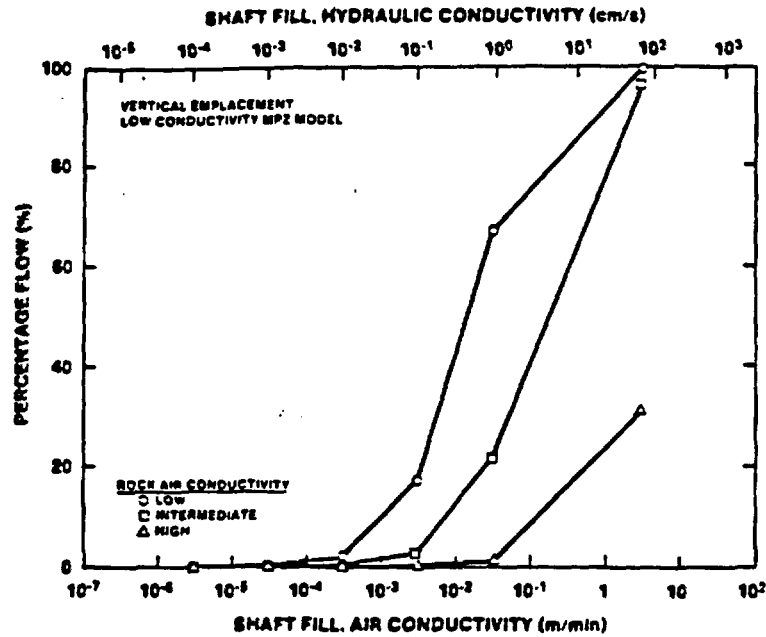


Figure 3-24. Air Flow Through ES-1 and ES-2 (Shaft Fill and MPZ Flows Included) as a Percentage of Flow Through the Rock Over Repository Area (Vertical Emplacement and Low Conductivity MPZ Model)

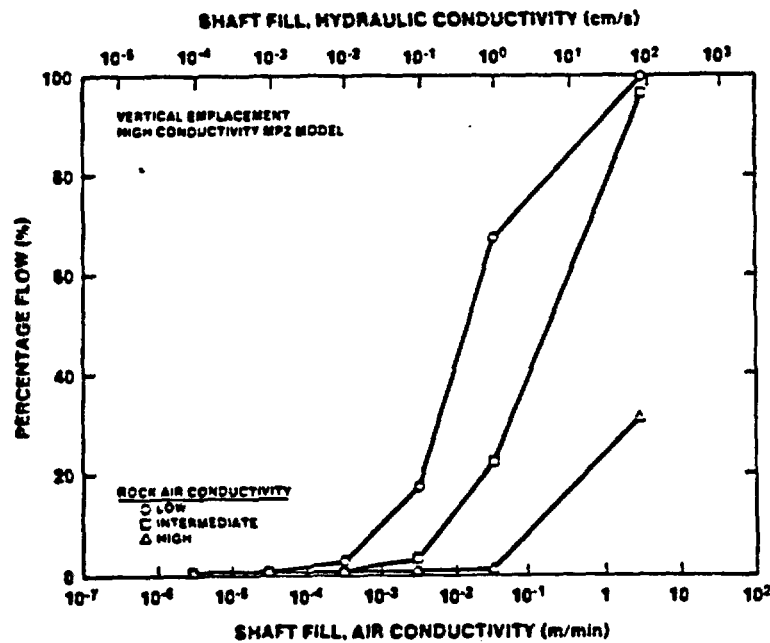


Figure 3-25. Air Flow Through ES-1 and ES-2 (Shaft Fill and MPZ Flow Included) as a Percentage of Flow Through Rock Over Repository (Vertical Emplacement and High Conductivity MPZ Model)

DRAFT

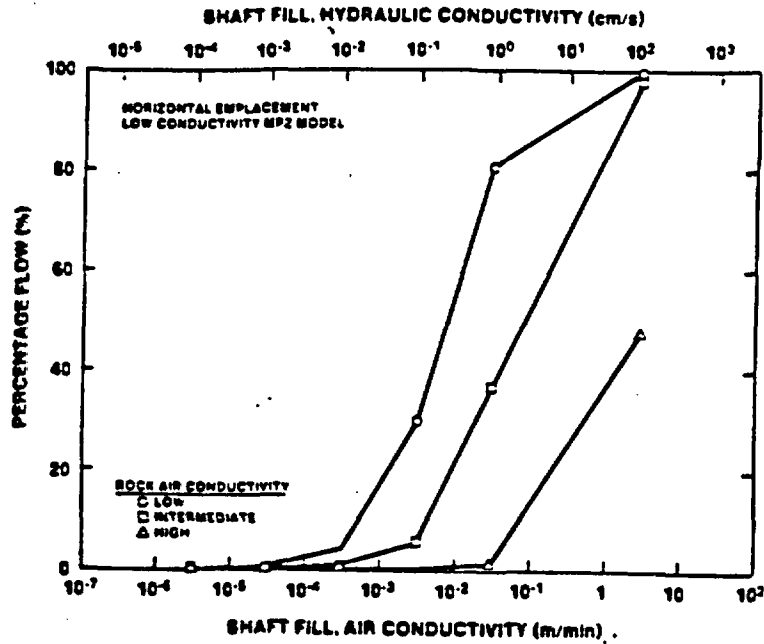


Figure 3-26. Air Flow Through ES-1 and ES-2 (Shaft Fill and MPZ Flow Included) as a Percentage of Flow Through the Rock Over Repository (Horizontal Emplacement and Low Conductivity MPZ Model)

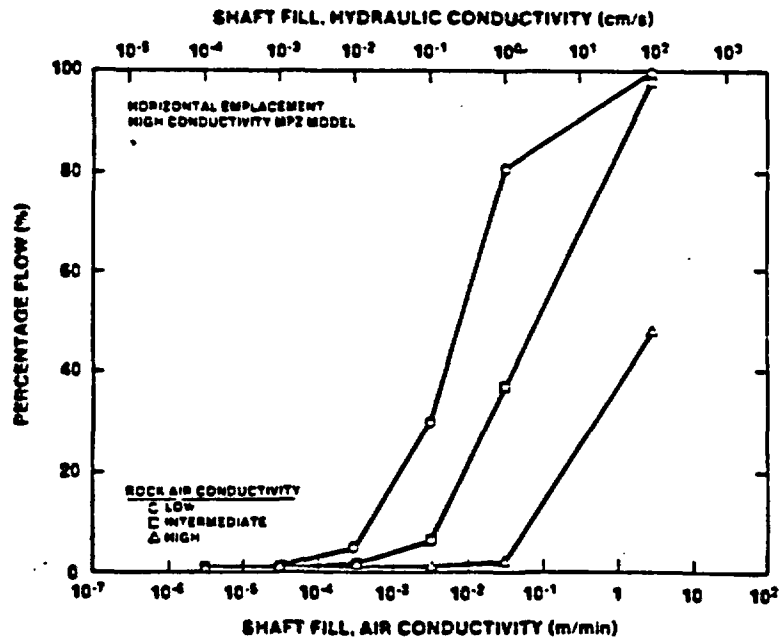


Figure 3-27. Air Flow Through ES-1 and ES-2 (Shaft Fill and MPZ Flow Included) as a Percentage of Flow Through the Rock Over Repository (Horizontal Emplacement and High Conductivity MPZ Model)

DRAFT

the assumption of the inlet shafts/ramps being at geothermal temperature is conservative for both emplacement modes.

The analysis indicates that the percentage of flow through ES-1 and ES-2 to total flow is also dependent on shaft fill, air conductivity. When the backfill conductivity is low, the percentage of flow through the shafts and ramps is also low, regardless of the existence of either a low or high conductivity MPZ. For example, for vertical emplacement, with a shaft fill having an air conductivity less than 3×10^{-4} m/min (equivalent to a hydraulic conductivity of 10^{-2} cm/s) the contribution of ES-1 and ES-2 shaft to total flow is less than 2.5 %. The percentage is somewhat higher for horizontal emplacement, and this attributable to a smaller roof area which tends to increase the percentage flow through ES-1 and ES-2. Nevertheless, for either emplacement mode the percentage is smaller than 2.5 % when the backfill air conductivity is less than 10^{-4} m/min.

3.3.5 Conclusions

From the preceding discussion, it is concluded that the exploratory shafts are not preferential pathways for gaseous radionuclide releases if the air conductivity of the shaft fill is less than about 10^{-4} m/min. When the air conductivity is greater than this value, the air flow through the shaft fill and MPZ is predominantly through the shaft fill. It is only when the conductivity of the shaft fill is low that flow through the MPZ is proportionally greater than flow through the backfill; however, the total air flow through the MPZ and the shaft backfill as compared to flow through the roof rock over the repository, is compared to flow through the roof rock over the repository, is extremely low. i.e., less than 2.5 %. Therefore, it can also be concluded that MPZ does not detrimentally influence the performance of the YMMGDS by enhancing the release of gaseous radionuclides. To reduce the potential for high convective air flows through the repository it is also prudent to fill the shafts and ramps with a material having a hydraulic conductivity of 10^{-2} cm/s.

DRAFT

3.4 Potential for Enhancing Radionuclide Release from Air Movement Due to Barometric Forces

This section evaluates the potential volumes of air displaced out of ES-1 or ES-2 due to barometric forces. These barometric forces are created by pressure differences that are induced by meteorological events occurring at the exploratory shaft locations. The purpose of the analyses in this section is to show what volume of air that is contained in the shaft and MPZ under unsaturated conditions can be displaced due to several meteorological events. If only a portion of the shaft and MPZ air volume is displaced when the pressure drop occurs at the surface, the surface air will be forced into the shaft and MPZ when the pressure reversal (pressure increase) occurs at the surface. As a result, contaminated air that reaches the shaft is not continuously displaced by barometric forces.

3.4.2 Model Description

Air pressure differences between the repository and the surface will cause air to move through shafts and ramps accessing the repository. Air movement may also be induced through the rock. The direction of air movement will be from areas of high pressure to those with low pressure. The magnitude of the flow rate will be proportional to the pressure difference, the air conductance, and the cross-sectional area through which air flows.

A one-dimensional, air flow model was developed to evaluate flow induced by barometric changes at the surface. Assumptions used in the development of the model include:

- o Darcy's law is valid for flow through the shafts and ramps; this assumption requires that air flow be laminar.
- o Atmospheric pressure follows a sinusoidal function. Individual pressure cycles occur within minutes to a year. The amplitude of the periodic functions are related to barometric pressure highs and lows found at Yucca Mountain for various events.

DRAFT

- o Air in the repository obeys the Ideal Gas law. For this analysis, the temperature of the repository is constant, while the mass of the air in the repository is allowed to change in response to barometric pressure variations.
- o Compressive storage of the air in the backfilled shafts and ramps and rock is negligible compared to the compressive storage of the repository.
- o The MPZ model is the same as that used in the previous analyses of convective flow.

This model is structured to describe porous media flow between the repository and the surface air in response to a sinusoidal variation in barometric pressure. The pressure within the repository will also vary sinusoidally as air leaves and subsequently reenters the repository by way of thirteen parallel pathways. In this model, these pathways are the backfills and modified permeability zones associated with all six shafts and ramps and the host rock mass itself.

3.4.2.1 Physical Model

For purposes of model development, the repository is conceived of as an enclosed volume with parallel conduits to the surface such as shown in Figure 3-28. Gas within the repository may enter or leave by ways of the parallel conduits and flow within each conduit is governed by Darcy's flow law. A pathway may consist of fill emplaced in a lined shaft or ramp, the surrounding modified permeability zone or the undisturbed rock. Because the fill and modified permeability zone associated with each shaft and ramp have different conductivities, flow areas, and lengths, they are treated as independent flow paths.

3.4.2.2 Mathematical Model and Assumptions

Flow through each conduit is described by Darcy's Law,

DRAFT

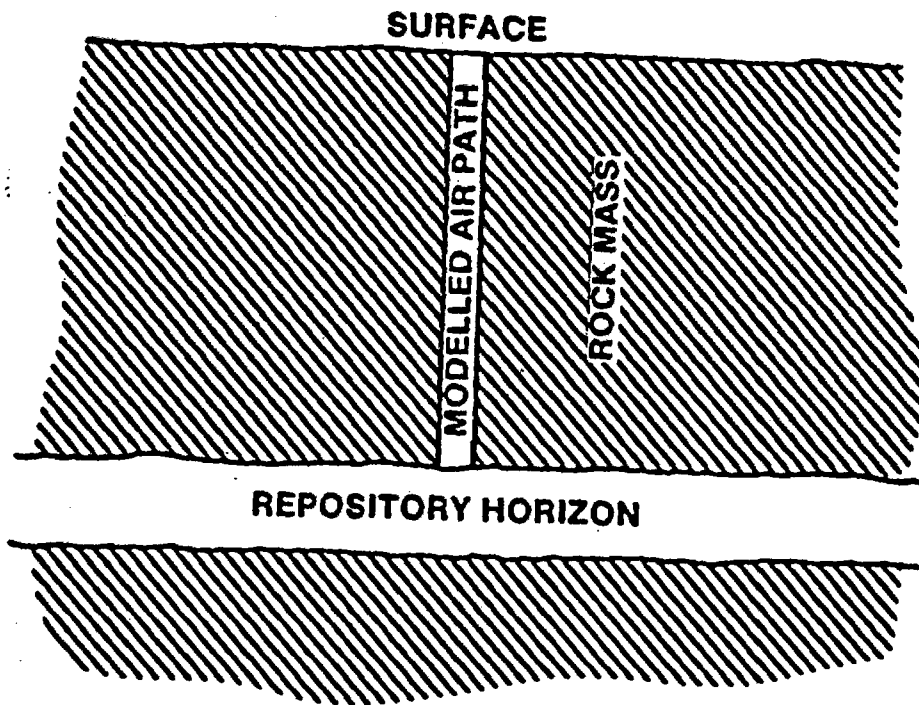


Figure 3-28. Schematic of Repository Use in Barometric Pressure Model

DRAFT

$$Q_i = \frac{K_i A_i}{L_i \rho g} (P_r - P_a) \quad (3-1)$$

where K_i - air conductivity of the i^{th} flow path,
 A_i - cross sectional area of i^{th} flow path,
 L_i - length of i^{th} flow path,
 ρ - average density of air within the permeable conduit,
 g - acceleration due to gravity,
 Q_i - volumetric flow rate (positive for flow out of repository),
 $P_a = P_a - \rho g Z_a$,
 $P_r = P_r - \rho g Z_r$,
 P_r - repository pressure variation,
 P_a - atmospheric pressure variation,
 Z_r - repository elevation above a reference datum, and
 Z_a - surface elevation above a reference datum

The use of P in Equation 3-1 inherently allows for variation in the static head due to repository and surface elevation differences. Hence, the difference $(P_r - P_a)$ is appropriate for all shafts and ramps.

The sum of the volumetric flow rates through all flow paths is also by a direct application of Darcy's Law:

$$Q = \sum_i \frac{K_i A_i}{L_i \rho g} (P_r - P_a) \quad (3-2)$$

This volumetric flow rate may then be expressed as a molar flow rate,

$$\frac{dn_r}{dt} = \frac{\rho Q}{M} \quad (3-3)$$

where M - the molecular weight of air,
 n_r - moles of air contained within the repository, and
 t - time.

The molar flow rate is also assumed to be related to the repository pressure through the ideal gas law so that

DRAFT

$$\frac{dn_r}{dt} = \frac{dp_r}{dt} \frac{V_r}{RT_r} \quad (3-4)$$

where V_r = repository volume,
 R = ideal gas constant, and
 T_r = repository temperature.

Noting that $\frac{n_r}{V_r} = \frac{\rho}{M}$ and combining Equations 3-2 through 3-4 yields an expression for the response of the repository pressure to atmospheric pressure variations.

$$\frac{dP_r}{dt} + c (P_r - P_a) = 0 \quad (3-5)$$

where

$$c = \frac{n_r RT_r}{\rho E V_r^2} \sum \frac{K_i A_i}{L_i} \quad (3-6)$$

The variation of atmospheric pressure with time is assumed to take the form of a sinusoid:

$$P_a = P_{a0} + m \sin \omega t \quad (3-7)$$

where P_{a0} = the average barometric pressure,
 m = amplitude, which is defined as $m = (P_H - P_L)/2$,
 ω = angular frequency = $2\pi/T$, and
 T = period.

The solution to this problem will be presented for various values of amplitude and frequency.

The significance of the constant c is that it is proportional to the ratio of the volumetric flow rate to the volume of the repository. It also influences the amplitude and phase relationships of the repository pressure under periodic conditions as described subsequently. The constant c is dependent on the air conductivity of all flow paths. The placement of

DRAFT

shaft fill under certain circumstances affects the pressure response of the underground repository.

The solution to Equations 3-5 and 3-7 is:

$$P_r = P_{ao} + \frac{m \sin(\omega t) - \frac{\omega m}{c} \cos(\omega t)}{1 + \frac{\omega^2}{c^2}} \quad (3-8)$$

The volumetric flow rate can be calculated by substituting the pressure relationships in Equations 3-7 and 3-8 into Darcy's Law (Equation 3-2).

$$Q = \sum \frac{K_i A_i}{\rho g L_i} \left[m \sin(\omega t) \left(\frac{c^2}{c^2 + \omega^2} - 1 \right) - \frac{c \omega m}{c^2 + \omega^2} \cos(\omega t) \right] \quad (3-9)$$

or expressed as a sinusoid with a lagging phase angle

$$Q = \sum \frac{K_i A_i}{\rho g L_i} \frac{m \omega}{\sqrt{c^2 + \omega^2}} \sin \left[\omega t - \pi + \sin^{-1} \left(\frac{c}{\sqrt{c^2 + \omega^2}} \right) \right] \quad (3-10)$$

Equation 3-10 may be integrated over half of any cycle to give the amount of air entering or leaving a shaft as a consequence of the assumed barometric pressure variation. Hence, the cyclic volume of displaced air, V , is given by

$$V = \sum \frac{2K_i A_i}{\rho g L_i} \frac{m}{\sqrt{c^2 + \omega^2}} \quad (3-11)$$

Further, the cyclic volume of displaced air may be computed for any flow path, i :

$$V_i = \frac{2K_i A_i}{\rho g L_i} \frac{m}{\sqrt{c^2 + \omega^2}} \quad (3-12)$$

DRAFT

3.4.3 Input to the Mathematical Model

The cyclic volumetric displacement relationship developed in the previous section suggests that the displaced volume is proportional to the

DRAFT

pressure amplitude and inversely proportional to the frequency of the weather event (proportional to the period). To cover a range of potential weather events, the following were considered:

- o A severe thunderstorm event with a time period of five days
- o A tornado event with a time period of one minute
- o A seasonal barometric pressure event with a time period of one year

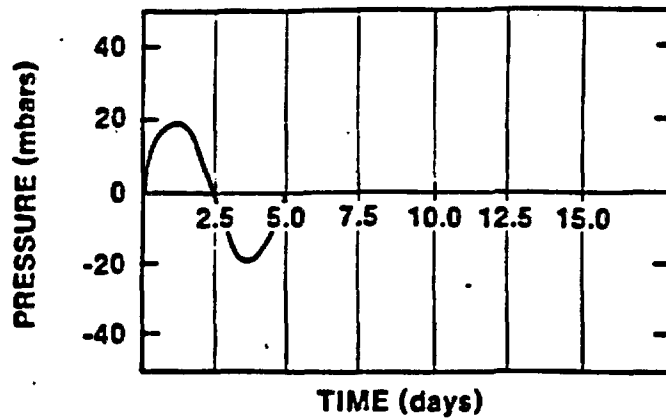
These events are indicated schematically in Figure 3-29 and include a low frequency/low amplitude seasonal event, an intermediate frequency/intermediate amplitude event and a high frequency/high amplitude tornado event.

The severe thunderstorm event represents a bounding event to typical atmospheric pressure fluctuations (movement of weather fronts) that might occur at Yucca Mountain. The average high and low pressures for the months January through December have been compiled by the U.S. DOE (1986, p. 3-48) and indicate that the pressure amplitude ranges from 8.6 mbars to 19.0 mbars (0.25 to 0.56 in. Hg). Various strip charts at Yucca Mountain have been reviewed and indicate that a typical period for thunderstorm events is approximately five days.

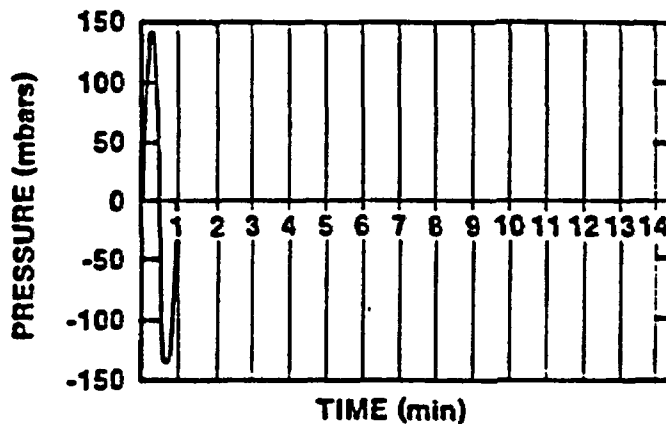
There are no published values for barometric pressure fluctuations for tornadoes which is due to pressure measurement difficulties during such events. An approximate value may be derived from the Bernoulli equation for conservation of energy for fluid flow and the equation of state for an adiabatic expansion of air. If it is assumed that the initial pressure is 850 mbars (25.1 in. Hg), and that the tornado event results in an air velocity of 200 mph (89.4 m/s), then the calculated drop in pressure is 132 mbars (3.9 in Hg). This calculated value may be compared to the difference between high and low pressure extremes recorded in the United States (Valley, 1986, p. 3-30). The high and low extremes are 1,063.3 and 954.8 mbars respectively with a difference of 108 mbars or an equivalent pressure amplitude of 54 mbars. It is further assumed that the tornado pressure event would hover over the exploratory shaft for approximately one minute (Church, 1987).

DRAFT

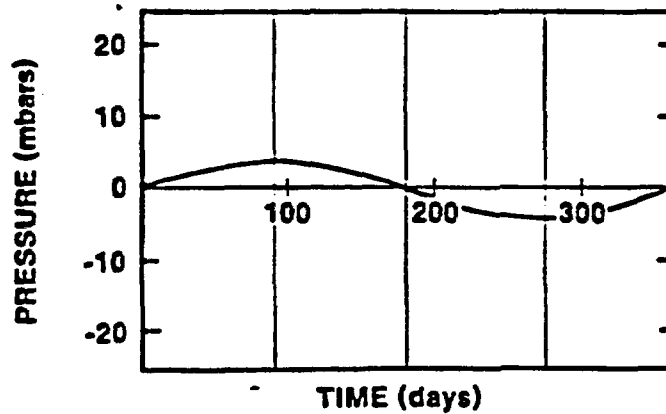
EVENT 1 - THUNDERSTORM



EVENT 2 - TORNADO



EVENT 3 - SEASONAL FLUCTUATION



DRAFT

Figure 3-29. Barometric Pressure Events

DRAFT

The seasonal fluctuation in barometric pressure is derived from differences between average pressures in January and June (U.S. DOE, 1986, p. 3-48). The calculated difference is 3.0 mbars (0.09 in. Hg).

Other parameters are required for conducting analysis, these include: 1) the air conductivities of the shaft fill, the surrounding MPZ, and the undisturbed rock; 2) the lengths and areas of the parallel flow paths; 3) the volume of the repository; and 4) the repository temperature.

In these analyses, the same range of shaft fill, air conductivities, the same combination of rock conductivities, and the same modified zone permeability zone models were used as the convective air flow analyses. The analyses were conducted for both vertical and horizontal emplacement options as in the convective air flow analysis. Tables 3-2 and 3-3 summarize cross-sectional areas and lengths for each of the flow paths.

The cross-sectional area of rock flow path was again taken to be equal to the combined roof area of all underground mains, submains and rooms (983,700 m² for vertical emplacement or 486,000 m² for horizontal emplacement). The area of modified permeability zones surrounding either shafts or ramps was taken as three times the excavated area. In addition, the temperature of the air underground was taken as 115°C for determining the mass of air in the repository.

3.4.4 Model Results

The results of the analysis are presented as a series of plots relating the ratio of total flow or displaced volume out of ES-1 to void volume in ES-1, and the surrounding MPZ versus backfill air conductivity. A series of six plots for vertical emplacement are presented in Figures 3-30 through 3-35 for the three pressure events and the two modified permeability zone models. The complementary set of six plots for horizontal emplacement are presented in Figures 3-36 through 3-41. Each plot presents three curves for the three cases of rock air conductivity presented previously.

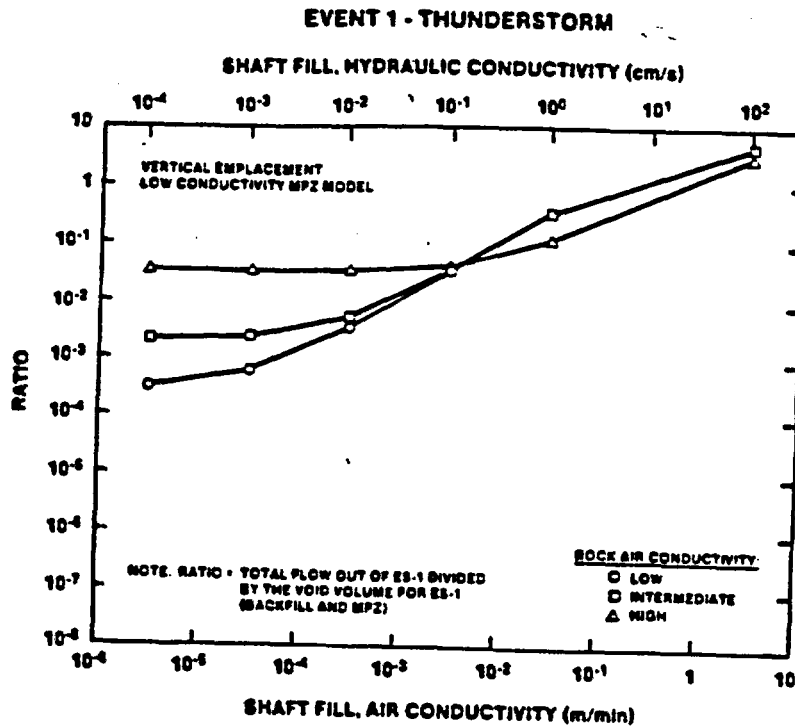
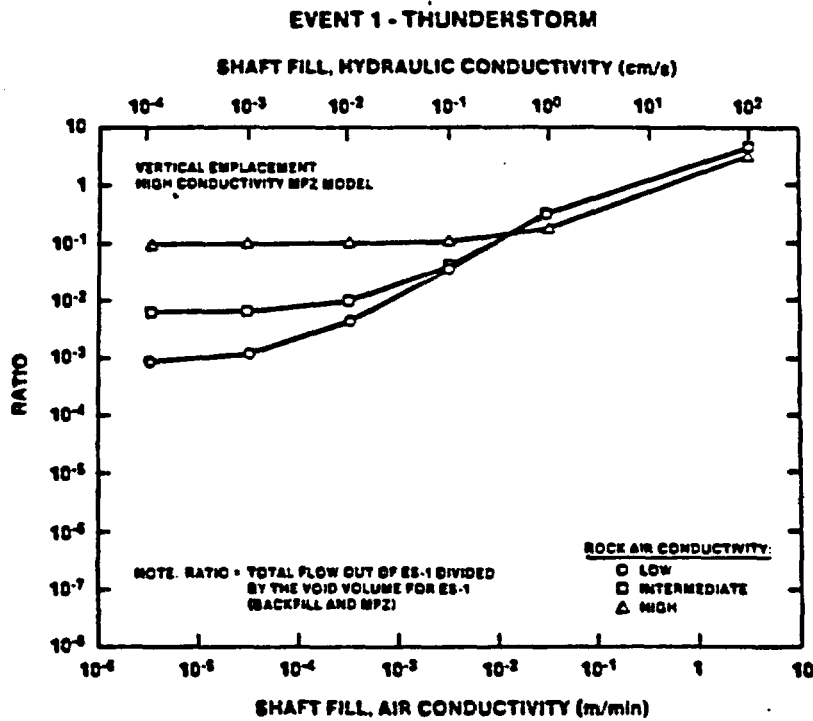


Figure 3-30. Ratio of Displaced Air Volume to Void Volume for ES-1 (Vertical Emplacement and Low Conductivity MPZ Model) for a Severe Thunderstorm Event



DRAFT

Figure 3-31. Ratio of Displaced Air Volume to Void Volume for ES-1 (Vertical Emplacement and High Conductivity MPZ Model) for a Severe Thunderstorm Event

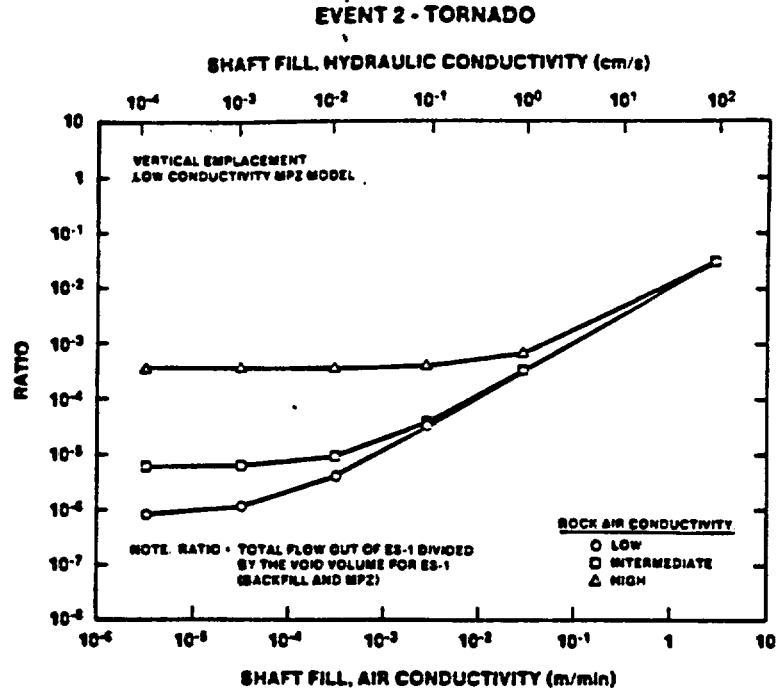


Figure 3-32. Ratio of Displaced Air Volume to Void Volume for ES-1 (Vertical Emplacement and Low Conductivity MPZ Model) for a Tornado Event

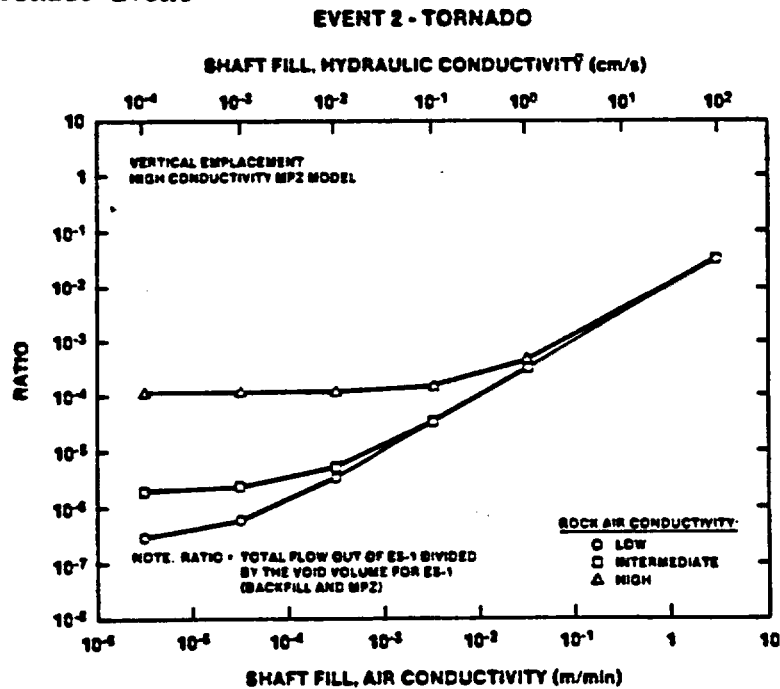


Figure 3-33. Ratio of Displaced Air Volume to Void Volume for ES-1 (Vertical Emplacement and High Conductivity MPZ Model) for a Tornado Event

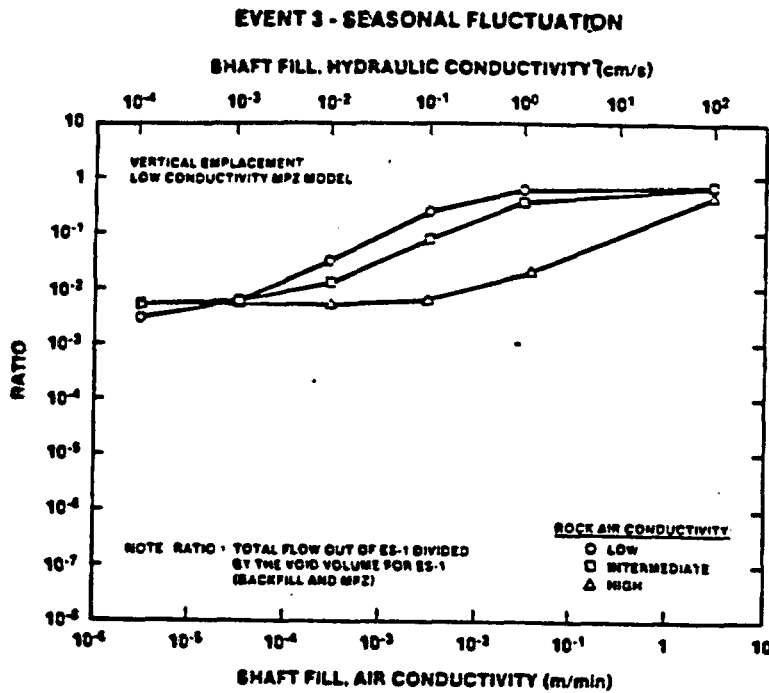


Figure 3-34. Ratio of Displaced Air Volume to Void Volume for ES-1 (Vertical Emplacement and Low Conductivity MPZ Model) for a Seasonal Event

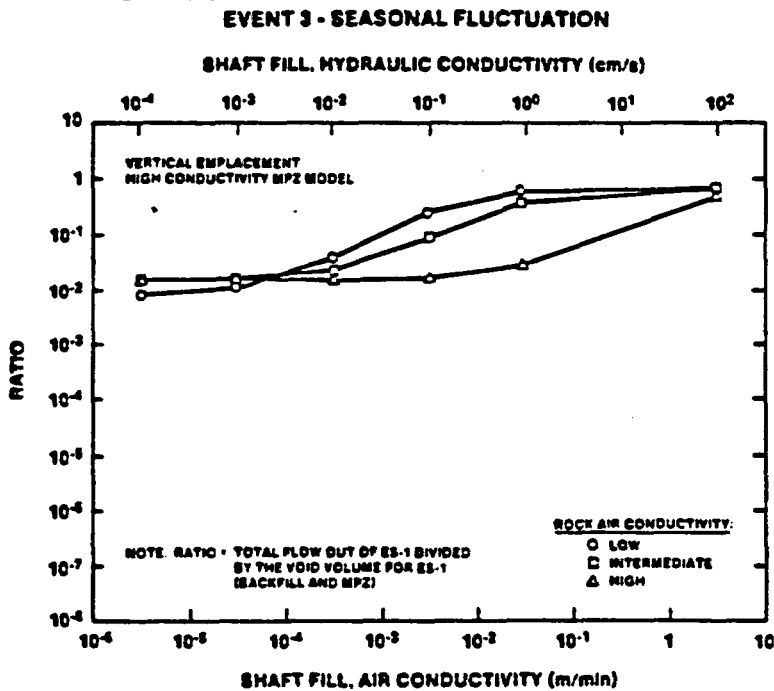


Figure 3-35. Ratio of Displaced Air Volume to Void Volume for ES-1 (Vertical Emplacement and High Conductivity MPZ Model) for a Seasonal Event

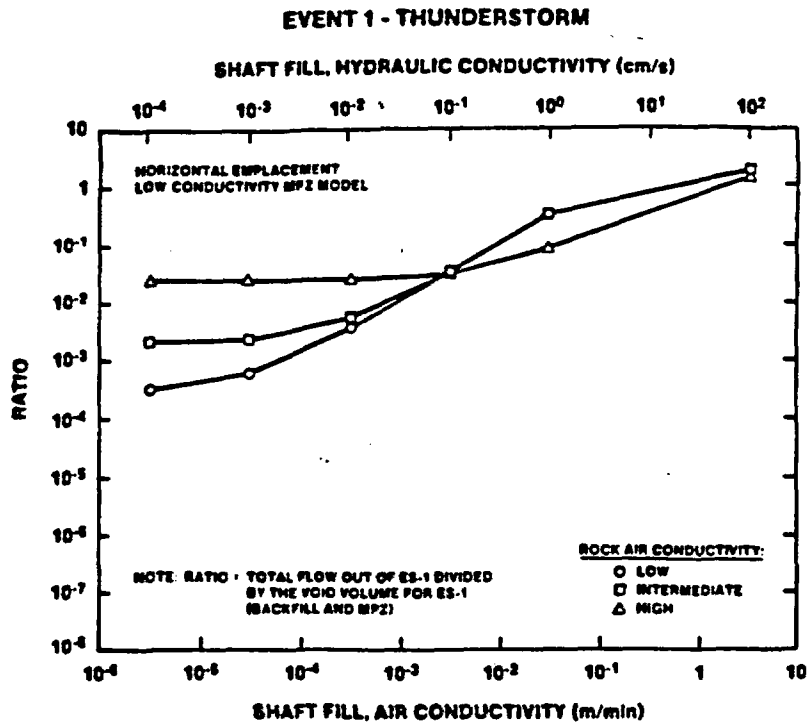


Figure 3-36. Ratio of Displaced Air Volume to Void Volume for ES-1 (Horizontal Emplacement and Low Conductivity MPZ Model) for a Severe Thunderstorm Event

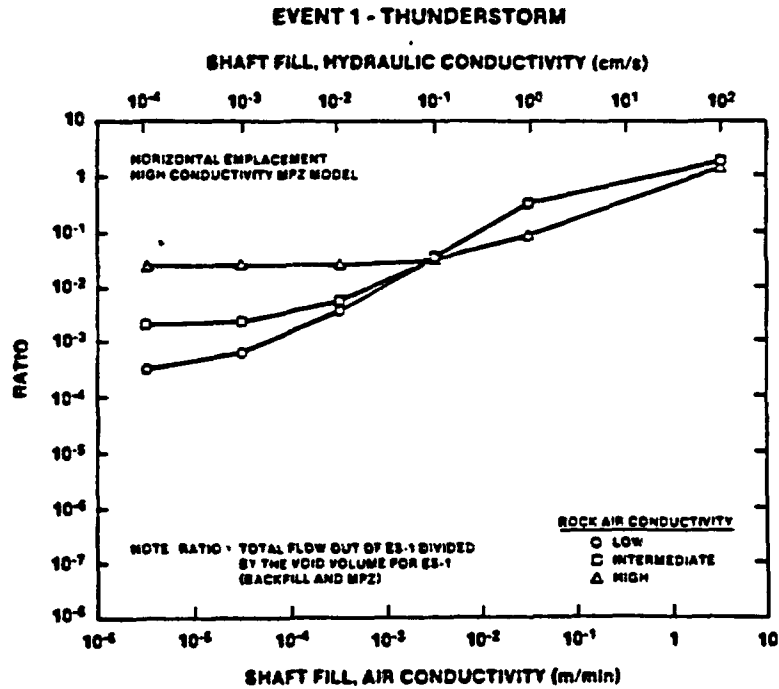


Figure 3-37. Ratio of Displaced Air Volume to Void Volume for ES-1 (Horizontal Emplacement and High Conductivity MPZ Model) for a Severe Thunderstorm Event

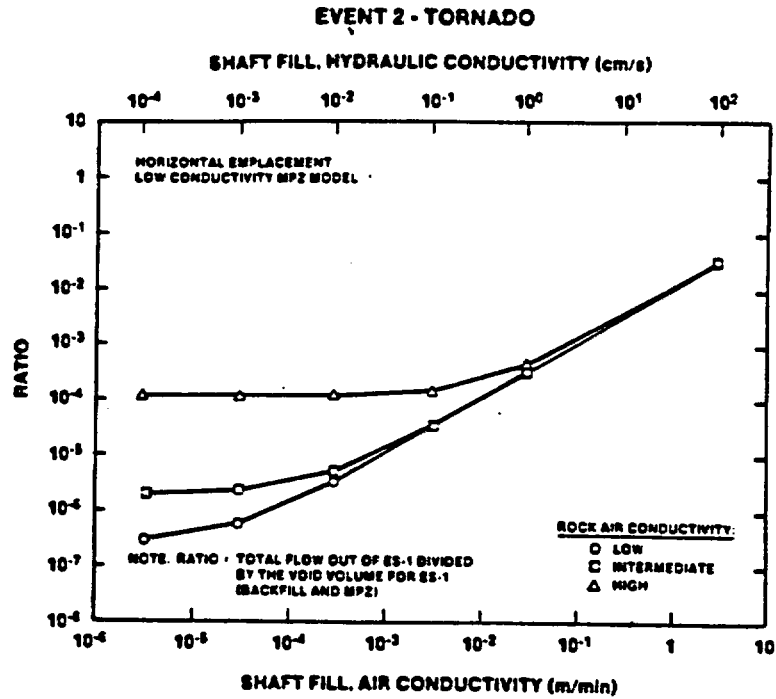


Figure 3-38. Ratio of Displaced Air Volume to Void Volume for ES-1 (Horizontal Emplacement and Low Conductivity MPZ Model) for a Tornado Event

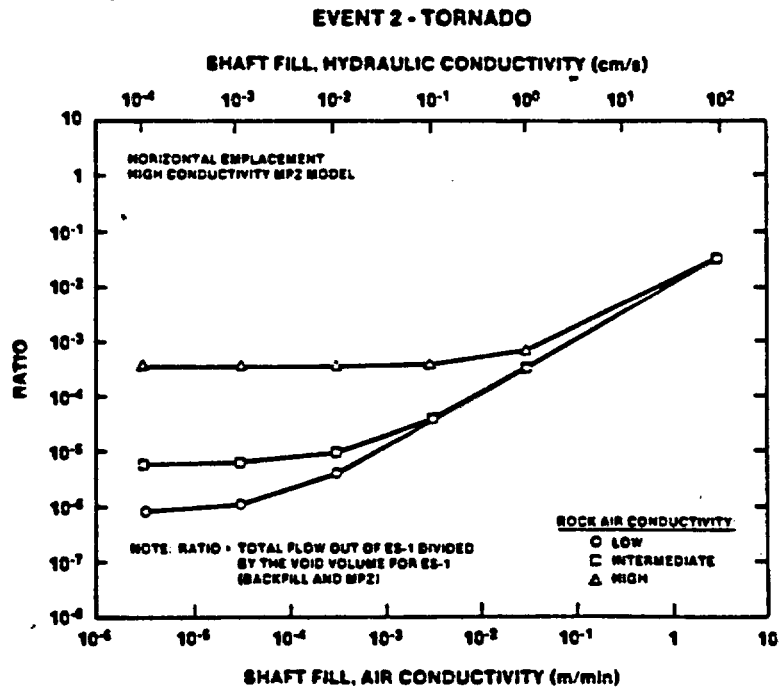


Figure 3-39. Ratio of Displaced Air Volume to Void Volume for ES-1 (Horizontal Emplacement and High Conductivity MPZ Model) for a Tornado Event

DRAFT

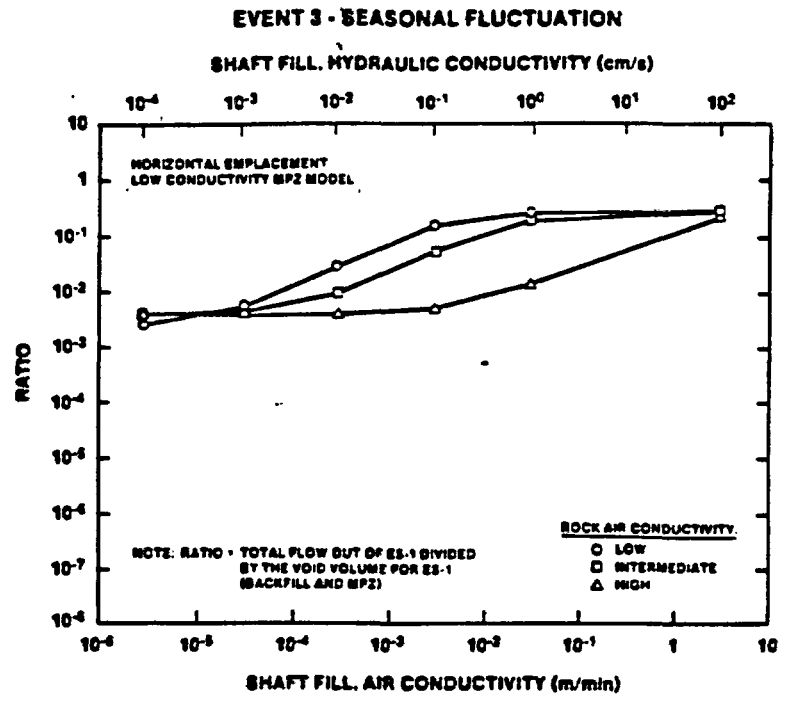


Figure 3-40. Ratio of Displaced Air Volume to Void Volume for ES-1 (Horizontal Emplacement and Low Conductivity MPZ Model) for a Seasonal Event

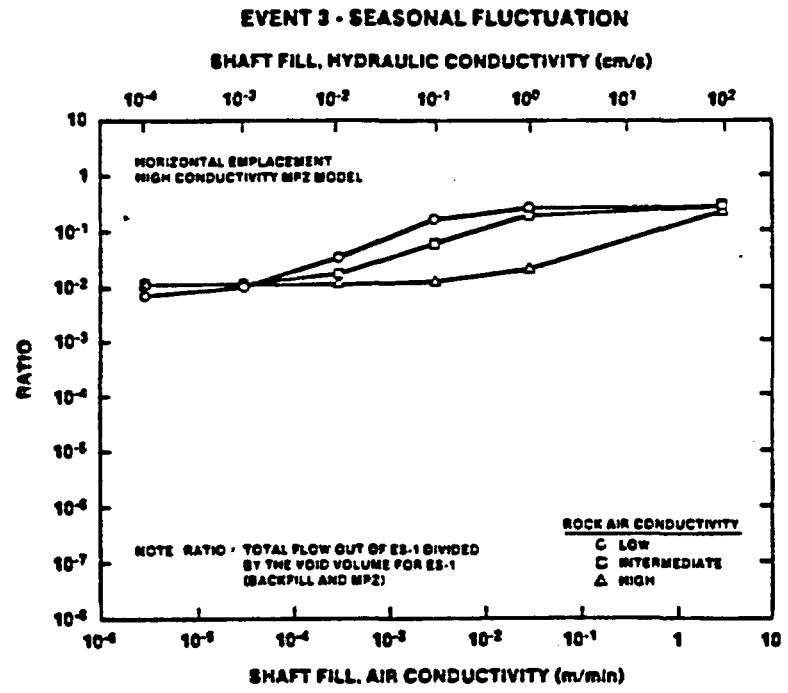


Figure 3-41. Ratio of Displaced Air Volume to Void Volume for ES-1 (Horizontal Emplacement and High Conductivity MPZ Model) for a Seasonal Event

The void volume in the shaft fill was calculated from the total volume of ES-1 within the lined shaft with a porosity of 30 % and the volume of the modified permeability zone, and an effective, unsaturated rock porosity of 4.2 %. The calculated volume of the exploratory shaft is 1,540 m³.

For vertical or horizontal emplacement, the results indicate that the displaced volume out of ES-1 is dominantly affected by flow through the shaft fill at high shaft fill, air conductivities and by flow through the modified permeability zone (MPZ zone conductivities is dependent on rock air conductivity) at low, shaft fill, air conductivities. For example, in Figure 3-30 for Event 1 and the low conductivity MPZ model, the analysis indicates that one to 10 times the void volume might be displaced if the shaft fill, air conductivity were greater than 1 m/min. The displaced volume is independent of both the MPZ and rock conductivity. For shaft fill, air conductivities less than 10⁻² m/min, the MPZ is more dominant, and the displaced air volume becomes independent of shaft fill, air conductivity for the high rock air conductivity combination. Similar trends are observed for the low and intermediate air conductivity combinations. The analysis indicates that 1/10,000 to 1/100 times the void volume would be displaced out of the shaft for frequently occurring weather events if a low conductivity backfill were emplaced in the shafts and ramps. The analyses indicate that placement of a low conductivity backfill will be very effective in reducing the flow volume if the surrounding MPZ has low conductivity.

It is interesting to note that a lower rock air conductivity results in the displacement of somewhat greater amounts of air at higher shaft fill, air conductivities. The "cross over" phenomenon is related to the pressure phase relationship that develops between the surface and the underground repository. As seen from Equation 3-8, if the characteristic constant c is large, then the atmospheric and repository pressures are in phase, and the differential pressure inducing the flow rate is smaller resulting in a smaller displaced volume (Equation 3-10).

DRAFT

In comparing displaced air volumes out of the exploratory shaft for various pressure events, it is apparent that the severe thunderstorm event is most significant, and the tornado event least significant. As seen from Equation 3-12, when the frequency of the event is high (equivalent to a small period), the displaced volume is inversely proportional to the frequency (proportional to the period), and the displaced volume is dominantly affected by the high frequency. The large pressure amplitude is of secondary importance for the tornado event. For the severe thunderstorm, the frequency is lower (by three orders of magnitude) and results in a higher displaced volume. The seasonal barometric pressure event is of intermediate significance. Because of the low frequency (equivalent to a large period) of this event, the ratio at large, shaft fill, air conductivities approaches a constant of 7/10 of the volume in the exploratory shaft. This may be seen from Equations 3-6 and 3-12 in which the frequency of the pressure event is much smaller than the c constant. The substitution of the relationship for the c constant (Equation 3-6) into the displaced volume relationship (Equation 3-12) results in the displaced air volume approaching a constant where the shaft fill, air conductivity is high, and flow is dominantly through the fill of shafts and ramps.*

The results of the analysis for the horizontal emplacement option are similar to the results for the vertical emplacement option at low backfill conductivities for the several events. This is because, at low, shaft fill, air conductivities, flow is dominantly through the modified permeability zone of the ES-1 which is identical for the two emplacement options. At high, shaft fill conductivities, the ratio of displaced air volume to void volume of the exploratory shaft is somewhat lower owing to the smaller mass of air in the underground repository for the horizontal emplacement option.

DRAFT

*The displaced air volume approaches an asymptote which is dependent on the initial air in the repository, the pressure amplitude, and the ratio of the conductance of the exploratory shaft (ES-1) flow path to the sum of the conductances of the other flow paths.

DRAFT

3.4.5 Conclusions

In previous convective air flow analyses, it was determined that a shaft fill, air conductivity of the order of 10^{-4} m/min (Fernandez et al., 1987) should be selected to restrict flow out of the shafts and ramps and surrounding modified permeability zones to a small percentage of air flow occurring through the surrounding rock. The present analyses of barometric pressure effects indicate that the selection of an air conductivity of 10^{-4} m/min fill would effectively isolate the repository air from barometric pressure fluctuations for a variety of events, and effectively restrict the displaced air volume out of the shafts and ramps to a small proportion of the shaft/ramp void volume.

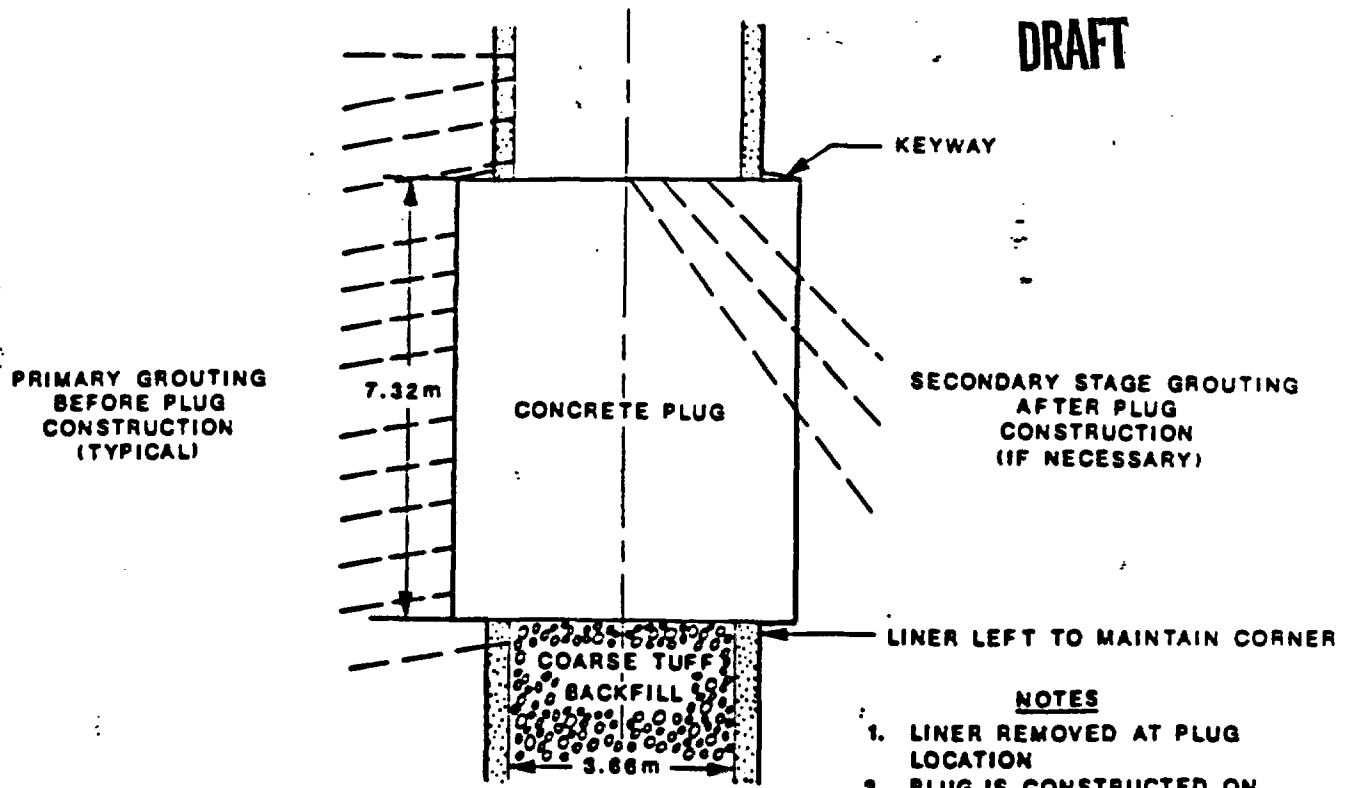
3.5 Remedial Measures to Restore the Modified Permeability Zone

When considering methods for the restoration of the MPZ, it is assumed that a plug would be constructed to reduce the flow of water down the shaft or the shaft/rock interface zone. It is further assumed that the plug would be keyed into the rock (Figure 3-42). This provides the most direct treatment or restoration of the MPZ, in that when a keyway is excavated, the more intensely fractured portion of the MPZ is removed. The structural performance of a plug keyed into the surrounding rock is also advantageous since overlying backfill loads would be transferred in bearing compression to the surrounding rock. A plug keyed into the rock should exhibit a higher rigidity when subjected to thermal or seismic loads than a simple plug.

DRAFT

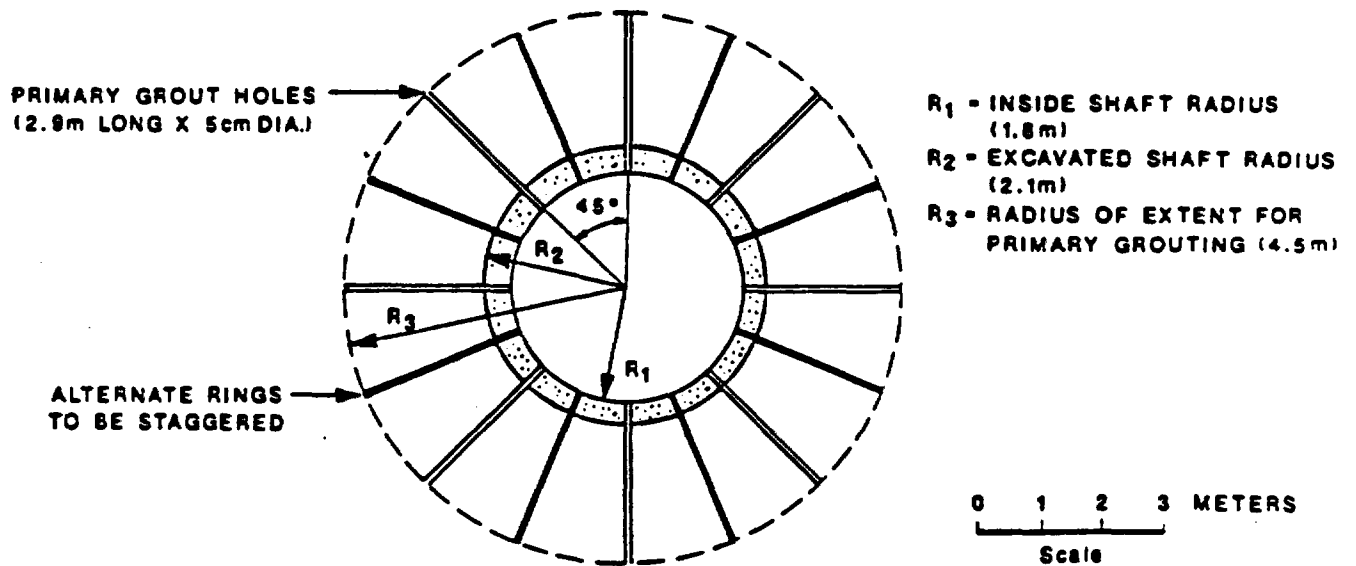
The construction sequence entails making saw cuts at the top and bottom of the plug, removing the liner, excavating the keyway, backfilling to the underside of the plug, placement of concrete, and contact grouting. Initial saw cuts ~23 cm deep around the top and bottom of the plug are made. A series of holes is drilled horizontally at the top of the seal to the full depth of the keyway and perhaps loaded with an expansive agent. Because of the high strength of welded tuff, mechanical excavation of a keyway may not be feasible, and other methods similar to those employed in

DRAFT



- NOTES**
1. LINER REMOVED AT PLUG LOCATION
 2. PLUG IS CONSTRUCTED ON COARSE TUFF BACKFILL

(a.) Plug Configuration



(b.) Primary Grout Pattern in Plan

Figure 3-42. Schematic of MPZ Restoration and Shaft Seal Emplacement

DRAFT

liner removal supplemented by hand methods could be used for rock excavation. The keyway is fragmented and excavated over a length of several meters to provide a larger working area. Excavation of the keyway then proceeds from the top to the bottom of the plug. To accomplish this excavation vertical holes on a precise pattern are drilled and loaded with an expansive agent from this working area to remove the rest of the keyway. The rock is removed to the surface. Fill is then emplaced to the base of the plug. The concrete is placed and allowed to mature for a period of time to achieve adequate strength and stiffness.

Methods for the treatment and restoration of the MPZ surrounding the keyway include:

- o The use of an expansive concrete and temperature control to develop interface stress and close fractures in the MPZ
- o Primary and secondary grouting of the MPZ.

DRAFT

3.5.1 Restoration of the MPZ Using Expansive Concrete

The use of an expansive concrete has been proposed elsewhere (Case et al., 1984). In this method, a concrete is selected that forms the expansive agent ettringite during cement hydration, resulting in volumetric expansion. The volumetric expansion in turn results in the development of interface stress, which will close fractures in the adjacent MPZ and thereby reduce the permeability in the MPZ. The degree to which volumetric expansion is effective depends on a number of factors: the temperature and moisture environment, evolution of the thermomechanical properties, and the degree of external restraint. Placement temperatures affect volumetric expansion of the concrete. A lower placement temperature results in elimination or reduction of the heating/cooling cycle and the development of higher interface stress. In using an expansive concrete, it is desirable to pour the plug (250 m³) in one operation to avoid potential leakage paths through construction joints. Auld (1983, pp. 209-211) describes methods of cooling aggregates and mixing water to eliminate undesirable thermal effects. An alternative is to provide pipes filled

DRAFT

with circulating water during cement hydration that are subsequently grouted.

The use of an expansive concrete to apply stress to the surrounding MPZ is most efficient where the stress-induced disturbance is caused by elastic deformation. If deformations are elastic, then the reapplication of stress would result in closure of open fractures. If deformations are inelastic, then stress reapplication might not result in the closure of fractures and restoration of permeability. The use of an expansive concrete would result in increased rigidity and increased confining stress in the plug and surrounding rock. The structural stability of the plug, when subjected to backfill, thermal, and seismic loads, would be enhanced. There would be less tendency for shear failure at the plug rock interface when the plug is subjected to combined loading.

The constructibility of the plug may be a key issue in the use of expansive concrete because use of an expansive concrete to restore an MPZ has not been demonstrated. As mentioned previously, the success of the method will be dependent on environmental control of moisture and temperature. Frequent sampling of concrete and monitoring of temperature would be required during construction. For these reasons use of an expansive concrete alone to restore the MPZ is not recommended.

3.5.2 Restoration of the MPZ by Grouting

DRAFT

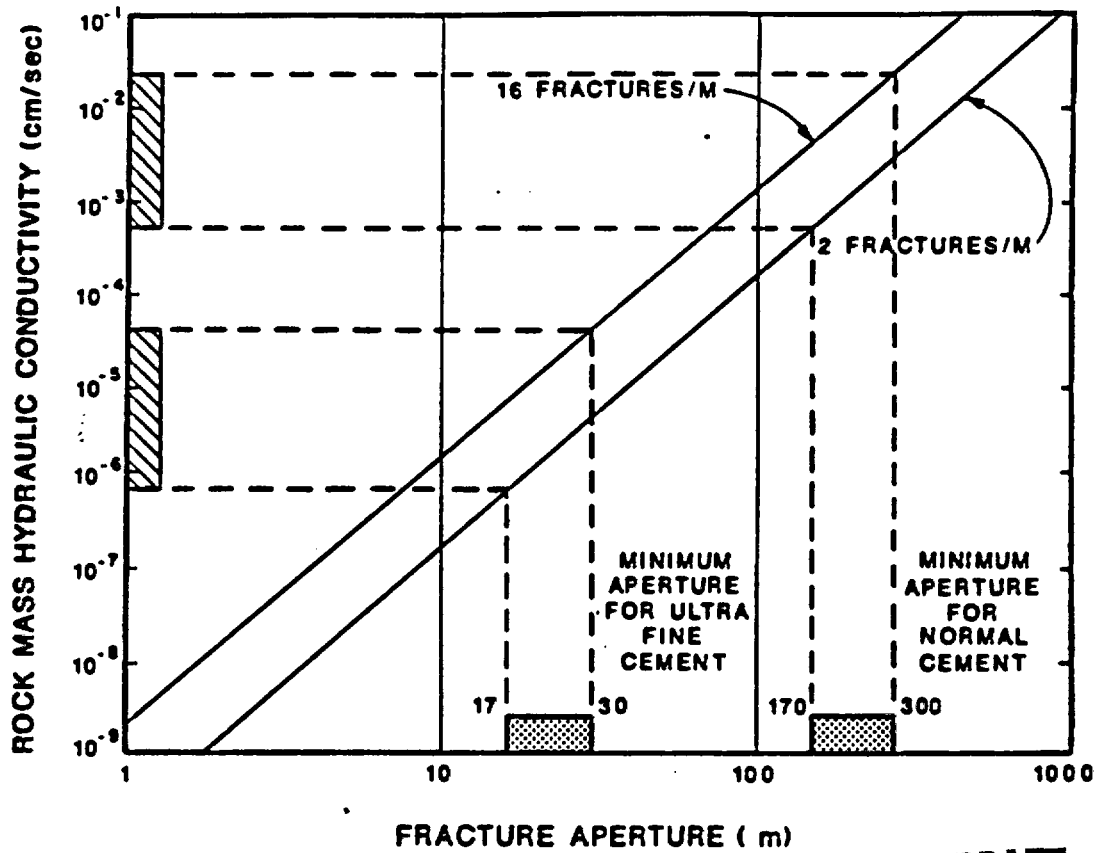
Emplacing grout in fracture is expected to reduce permeability in the MPZ. Grouting will reduce permeability in both the blast-induced and stress-induced fractures, irrespective of whether the rock deformed elastically or inelastically. However, grouting is not likely to increase rock mass strength significantly or increase structural stability. Grouting between the plug and the rock (contact grouting) may be required to provide a tight interface.

Grouting might be performed either before or after liner removal and plug emplacement (primary) or after liner removal and plug emplacement (secondary). There are advantages to pregrouting the plug location before

removal of the liner. After liner removal, there would be a gap of approximately 0.6 m or more between the work stage and the shaft walls. It is easier to locate grout pipes on the smooth surface of the concrete liner. The grouting pattern might consist of a series of eight holes with alternate rings staggered. This pattern would result in a hole spacing of approximately 1.5 m near the shaft and 3.5 m at a distance of 4.5 m from the shaft excavation. Note that the distance would depend on the size of the MPZ at the plug location. At the ends of the holes, only the open fracture zones would have continuity of grout between holes. By redrilling holes several times and grouting, an impermeable barrier would be formed by a "laced" grout structure similar to the pattern proposed by Kelsall et al. (1982, p. 122) for drilled cutoffs.

Primary and secondary grouting might be effective in reducing permeability of the MPZ. A series of holes is drilled to intercept conductive fractures either before (primary) or after (secondary) plug emplacement. The grout is selected to have a small particle size and high viscosity to penetrate under pressure into the thin fracture zones. Tests by Waterways Experiment Station, (Kelsall et al., 1982, p. 113) showed that the ratio of crack thickness to grout particle size should be at least 1.7 and preferably 3.0 or more for adequate penetration. For ordinary cements, the maximum particle size is about 100 μm , but this can be reduced to 10 μm using ultrafine cement. Therefore, the minimum size of aperture that could be grouted is 17 to 30 μm . The relationship of rock mass hydraulic conductivity to fracture aperture over a range of fracture spacing (Langkopf and Gnirk, 1986) is shown in Figure 3-43. Over the expected range of bulk rock, saturated hydraulic conductivities for welded tuff of 10^{-5} to 10^{-2} cm/s (Fernandez et al., 1987), grouting is feasible using either a normal cement for a welded tuff conductivity of from 10^{-3} to 10^{-2} cm/s or an ultrafine cement from 10^{-5} to 10^{-6} cm/s.

While there is precedence for pressure grouting of shafts and tunnels under a variety of conditions (Dietz, 1982, pp. 602-608), there are a number of operational factors to be considered in constructing a grout curtain. These include the distance and time for transporting the grout, the required injection pressure, frictional losses through pipes, and grout



DRAFT

LEGEND



MINIMUM CONDUCTIVITY THAT MAY BE GROUTED USING ULTRA FINE OR NORMAL CEMENT



MINIMUM APERTURE THAT MAY BE GROUTED USING ULTRA FINE OR NORMAL CEMENT

Figure 3-43. Minimum Conductivity for Grouting

DRAFT

setting time. At shallow depths, the use of packers may suffice to seal off sections of the injection hole; at greater depths, steel grout pipes may be required since greater injection pressures would be used to place grout in areas at greater distance from the shaft. Steel pipes enable grouting of fractures away from the shaft wall. These factors increase the complexity of the design prior to field operations and require sampling the grout for physical properties during grouting.

3.5.3 Conclusions

From the preceding discussion in this section and in Section 3.5.1, it is concluded that grouting in welded tuff is feasible and the preferred method for restoring the MPZ. This method is preferred because drilling grout holes allows a more direct examination of the modified permeability and provides a direct method for locating discrete fracture zones. Also, at present, it is not certain how large an interface stress can be developed through the use of only an expansive concrete or how effective such stress development would be in closing fractures.

Grouting the MPZ, however, does incur a greater cost. In Appendix D, the costs for liner removal in the vicinity of the plug and the construction of the plug are given. The estimated costs of primary and contact grouting add \$145,000 to the \$380,000 for plug construction. At this stage of the design process, these costs are intended to be used in a comparative way.

DRAFT

DRAFT

4.0 INFLUENCE OF THE SHAFT LINER ON THE PERFORMANCE OF THE YMMGDS

In this chapter, the influence of the shaft liner on the performance of the YMMGDS is evaluated. When a concrete liner is placed in the ESs, it will alter the ground-water chemistry and in turn be altered by the ground water. The expected changes are the result of leaching alkaline species from the cement. The concrete will become more permeable as minerals dissolve. Similarly, the ground water, coming in contact with the concrete liner, will become unstable when its pH is increased, and precipitates will form in the ground water. These precipitates will then lodge in pore spaces within the shaft fill and in the MPZ. The potential for changing the hydraulic conductivity of the liner is evaluated in Section 4.1 and the effect of precipitate formation is evaluated in Section 4.2.

4.1 Changes in the Hydraulic Conductivity of the Liner

It is anticipated that the concrete liner will be formed with conventional materials including aggregate, sand, and cement. For these formulations, the aggregate and sand portions of the concrete are essentially inert, and all chemical interactions occur during the cement phase. Also, the hydraulic conductivity of concrete is dependent almost completely on the hydraulic conductivity of the cement phase.

When ground water comes into contact with a cement, naturally occurring aqueous carbonate reacts with alkali and excess portlandite to modify the cement structure. Carbonate minerals are deposited within the pore structure of the cement, so that the natural tendency of the cement to shrink and crack will be partially offset by the deposition of new minerals.

DRAFT

In assessing how the hydraulic conductivity of the concrete liner may change due to chemical alterations, it is first important to know the initial hydraulic conductivity. The range of typical hydraulic conductivities for concrete is 10^{-8} to 10^{-6} cm/s, although hydraulic conductivities less than 10^{-10} cm/s are achievable (Mather, 1967). Values for saturated conductivities obtained through laboratory testing of a

grout, mortar, and a concrete, determined as part of the NNWSI Repository Sealing Program, varied from 1.6×10^{-10} to 9.5×10^{-10} cm/s (Fernandez et al., 1987, Appendix G).

DRAFT

Because the waste emplaced in the repository can elevate the rock temperature surrounding the waste disposal area, it is important to know how the elevated temperatures could affect sealing components. Hydrothermal experiments were performed at Pennsylvania State University (PSU) (Licastro et al., 1987) to determine the effect of temperature and moisture on selected seal materials. Two of the materials (grouts and mortars) had the same composition as the grout and mortar reported in Fernandez et al. (1987, Appendix G). The hydraulic conductivity of these materials was evaluated after the materials were exposed to water having a composition of J-13 water at 38°, 60°, and 90°C. Initial conductivities in all PSU cases ranged between 10^{-10} and 10^{-11} cm/s. These initial conductivities are at the low end of the conductivity spectrum for grouts. For all of the materials evaluated, no increase in hydraulic conductivity was observed at 38°C over a 1-year period. At 60°C, one cement sample showed a small increase in conductivity after 1 month, with no other changes noted after that. Finally, at 90°C, one sample showed a small increase in conductivity after 90 days.

DRAFT

Using the results of Blandford reported in Morales (1985), the temperature field at different portions of the liner can be approximated. We estimate that the top 80 m of the shaft will always be less than 38°C, the top 140 m always less than 60°C, and all but the 50 m above and below the repository horizon always less than 90°C. Because alteration of the shaft liner at 38°C and possibly 60°C will be limited, as indicated by the laboratory experiments cited above, surface-water infiltration through the shaft liner will be significantly impeded by the shaft liner.

4.1.1 Conclusions

From the discussion in the previous section, the potential for significant changes in the hydraulic conductivity of the concrete liner is low. Therefore, surface-water infiltration through the shaft liner will be impeded by the liner. Certainly, the assumption that the hydraulic

DRAFT

conductivity of the shaft liner is 10^{-2} cm/s* assumed in Chapter 3.0 is extremely conservative. This assumption implies that the hydraulic conductivity of the concrete liner would have to change from a range of 10^{-6} to 10^{-10} cm/s to 10^{-2} cm/s over the entire length of the shaft liner.

If the liner at the base of the shaft behaves in a similar way, water within the shaft fill would be impeded from draining into the surrounding rock. This discussion suggests that if restriction of surface-water flow is desired, leaving the concrete liner in place above the repository horizon, particularly in the upper portion of the shaft where the temperature field is lower, would be prudent. If water drainage from the base of the shaft is desired, removal of the liner below the repository horizon would probably be necessary.

4.2 Effect of Ground-Water Chemistry on the Hydraulic Conductivity of the Exploratory Shaft Fill and Modified Permeability Zone

In addition to modification in the hydraulic conductivity of the shaft liner, the liner itself will cause minor modifications to the ground water. These water chemistry changes may cause the ground water to become supersaturated with some minerals, and precipitation could then occur. The amount of these precipitates as well as their eventual destinations is projected in Section 4.2.3.

DRAFT

Water entering the ES could have a range of possible concentrations depending upon the source of the water. The primary source of water could have a variety of compositions. It could be rainwater, water equilibrated with alluvium, water equilibrated with tuff, or any of a variety of ground waters. In this paper, we have assumed that the starting water composition is that of J-13 water (Ogard and Kerrisk, 1984, pp. 9-12). In future work, we will consider the other possible choices through the use of the computer code EQ 3/6 (Wolery, 1979).

*This value is representative of a silty sand.

DRAFT

Further, we have assumed that local equilibrium will apply throughout the ES. In actuality, there are several rate phenomena that are operative. The leaching of minerals from the cement is governed by the diffusion of ionic species in the pore spaces of the cement and by the diffusion and dispersion of those same chemical species in the rock backfill and MPZ. Lastly, there are chemical kinetic rate processes to be considered. The above-mentioned rate processes will tend to limit pH increase of the ground water and the amount of precipitate released. Hence, the assumption of local equilibrium is a conservative one that leads to the maximum calculable change in the ground-water chemistry. The assumption of local equilibrium will be very closely approached in practice because of the extremely low fluid velocities the great majority of the time.

4.2.1 Leaching of Alkaline Species From the Concrete Liner

DRAFT

A typical Portland cement is composed of three major hydrated phases: calcium silicate hydrate, tricalcium aluminate hydrate, and tetracalcium aluminoferrite hydrate. In the presence of sulphate, we also have an ettringite phase. In addition to these major phases, minor amounts of unreacted portlandite, $\text{Ca}(\text{OH})_2$, and sodium and potassium alkalis are present. A typical portland cement will contain between 0.05 % and 0.15 % of dissolvable alkali (Glasser et al., 1984). It is these alkalis that are primarily responsible for increasing the pH of any water that contacts cement. Moreover, the cement pore fluid will contain increased concentrations of H_4SiO_4 , Na^+ , K^+ , OH^- , and perhaps SO_4^- . The actual concentration of these species in the ground water contacting cement will depend on the water flow rate, whereas higher concentrations are expected at lower flow rates. Barnes (1983, p. 298) gives the pore fluid concentration of alkali after 7 days of hydration as 0.75 M. This corresponds to a pH of 13.88 for the pore fluid. After this initial small percentage of alkali has been leached from the cement, the pH of the pore fluid is dominated by the $\text{Ca}(\text{OH})_2$ equilibrium (Glasser et al., 1984), and the pH of the pore fluid is expected to drop to 12.5 (Lea, 1971, p. 185).

DRAFT

Leaching of cement is represented by the diffusion of Na^+ , K^+ , OH^- , and possibly SO_4^- through the pore spaces of the cement. All other ionic species are not expected to be present in significantly increased concentrations. In related experimentation at PSU, B. E. Sheetz and D. M. Roy (1987) have considered the leaching of a particular ettringite bearing cement, formulation 82-022, by J-13 ground water, where the water-to-cement mass ratio was 10:1 and the test was conducted at 90°C for 3 months. Results of this experimentation are shown in Table 4-1.

DRAFT

As may be seen in the table, only ions Na^+ , K^+ , SO_4^- , and OH^- are significantly greater than the J-13 composition. All other species, are no more than 1 mg/l greater than their starting composition. Of these species, OH^- is the most important in affecting the performance of the ES, as will be discussed in 4.2.2.

A diffusion model of the cement liner is postulated to estimate the concentration of ions that reach the ground water. The cement liner is considered to be a slab 30.5 cm thick, where the cement pore fluid assumes an equilibrium value and the surface of the liner has a concentration assumed to be zero. Under this assumption the maximum flux of any ionic species is given by (cf. Bird, Stewart, and Lightfoot, 1960, p. 355).

$$\text{Flux} = \frac{2D_e (C_o - C_{\text{initial}})}{L} \quad (4-1)$$

where $C_o - C_{\text{initial}}$ is the concentration in excess of the ground-water concentration of any ionic specie within the cement pore fluid, L is the half thickness of the cement slab, and D_e is related to (Smith, 1970, p. 416) the cement void fraction, ϵ , and the molecular diffusivity D_{AB} by

$$D_e = D_{AB}\epsilon^2 \quad (4-2)$$

The concentration of species in the ground water passing below the shaft liner is then estimated by

DRAFT

DRAFT

TABLE 4-1

CHEMICAL ANALYSIS OF WATER BEFORE AND AFTER CONTACT WITH PSU 82-022 CEMENT

Species	J-13 Concentration		Concentration After 3 mo. With PSU82-022 Cement	
	(mM)	(mg/l)	(mM)	(mg/l)
Al	9.27×10^{-4}	.025	.008	.216
Ca	.287	11.5	.181	7.25
Fe	1.97×10^{-4}	.011	.006	.34
K	.135	5.28	1.48	57.9
Mg	7.24×10^{-2}	1.76	.013	.316
Na	1.96	95.1	5.70	131
Si	1.13	31.7	2.14	60.1
NO ₃	.163	10.1	.150	9.3
SO ₄	.188	18.0	.542	52.0
HCO ₃	2.33	142	1.85	113

pH	6.9		9.9	

$$C = C_{\text{initial}} + \frac{(C_o - C_{\text{initial}}) 2D_e A_{\text{shaft}}}{L Q} \quad (4-3)$$

where A_{shaft} is the shaft liner surface area and Q is the volumetric flow rate through the shaft and the MPZ. In Equation 4-3, the following values are used to determine the concentration:

$$\begin{aligned} A_{\text{shaft}} &= 4.17 \times 10^7 \text{ cm}^2 \\ \epsilon &= 0.28 \\ D_e &= 10^{-5} \text{ cm}^2/\text{s} (0.28)^2 = 7.84 \times 10^{-7} \text{ cm}^2/\text{s}. \\ L &= 15.24 \text{ cm} \end{aligned}$$

Focusing our attention on the concentration of hydroxide, for an initial pH of 6.9, the initial molar concentration is 7.94×10^{-8} M. The concentration of hydroxide in the cement pores, C_o , is 0.75 M. To

DRAFT

DRAFT

evaluate the concentration of hydroxide in the ground water after contact with cement, the flow rate through both the shaft and the MPZ must be estimated. Flow in the shaft fill and the MPZ will be unsaturated most if not all of the time. We have, however, allowed for the possibility of saturated flow in these zones; and during saturated flow periods, the flow rate is governed by the hydraulic conductivity of the shaft fill and of the MPZ. The concentration of hydroxide, expressed as pH, as a function of flow rate is shown in Figure 4-1. The concentration of other ionic species will follow the pH curve shown in Figure 4-1.

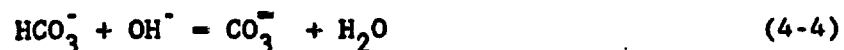
4.2.2 Chemical Equilibrium Model of Ground-Water Reactions

When ionic species are leached from the cement, these ions will interact with ground water. As a consequence, some precipitation is expected. These precipitates may then lodge in existing pores to reduce the hydraulic conductivity of both the MPZ and the shaft fill.

For the present analysis, we only estimate the nature and quantity of the precipitates formed from the interaction of ground water with a concrete liner. We leave, as a necessary adjunct to the present work, a detailed analysis of the interaction between ground water, tuff, and cement as a function of temperature. The estimates provided here, however, do provide an indication of the likely consequences of having a cement liner contact ground water.

DRAFT

A consideration of a single equilibrium, that of CaCO_3 , will show that at least one species is likely to precipitate as the pH of the ground water is increased. In Table 5-1, the concentration of Ca^{++} in solution is reduced after coming into contact with cement. This reduction in Ca^{++} concentration is verified by calculations of chemical equilibrium when the pH of the water is increased. The chemical equilibrium between HCO_3^- , CO_3^{--} , and Ca^{++} is expressed in the following equations:



DRAFT

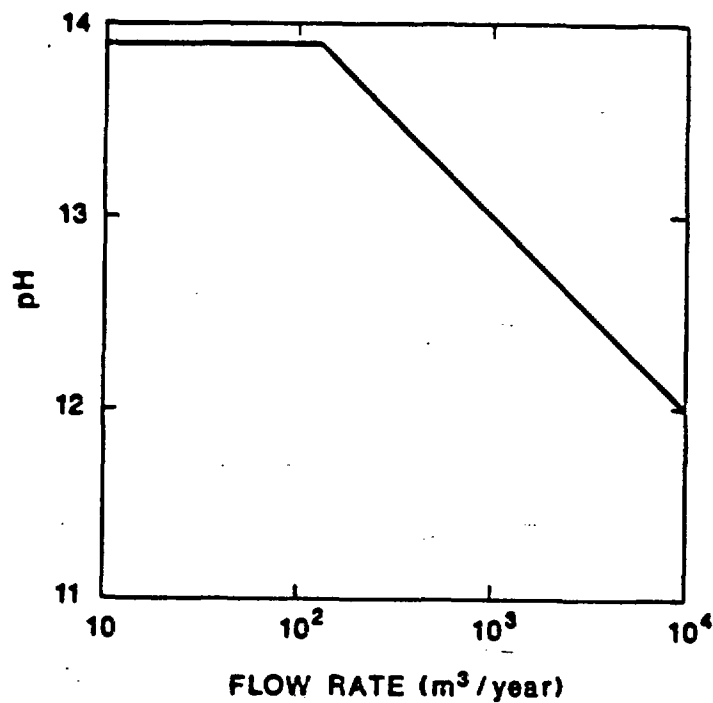
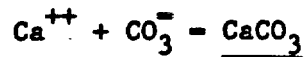


Figure 4-1. Plot of pH of Water from Below the Shaft Liner as a Function of the Volumetric Flow Rate of Water Through the Shaft or MPZ.

DRAFT



(4-5)

When OH^- is added to ground water according to Equation 4-4, more CO_3^- is formed. This CO_3^- may then react with Ca^{++} according to Equation 4-5; and if the solubility product of CaCO_3 is exceeded, then CaCO_3 will form to reduce the solution concentration of Ca^{++} . Using the equilibrium constants at 25°C for Equations 4-4 and 4-5, precipitation first occurs when a pH of 9 is reached.

A consideration of a single equilibrium, such as that illustrated in Equations 4-4 and 4-5, however, dramatically oversimplifies the interactions that occur when a cement liner is allowed to contact ground water. In actuality there are hundreds of these equilibria that must be considered simultaneously. Also, the effects of interaction with tuff, cement, and ground water, are dependent upon the order of contact as well as the temperature of the environment. While we do plan a more detailed study of this problem, we have examined the equilibrium of J-13 water after several changes have been superimposed on the water chemistry. The base case was J-13 water using the water analysis presented in Ogard and Kerrisk (1984). Variations on this base case are increasing the pH to 9.5, increasing the temperature to 100°C, and increasing the Na^+ , K^+ , SO_4^- , and SiO_2 concentrations, each by an order of magnitude. These studies were performed using a water chemistry equilibrium code, WATEQ, developed by Truesdale and Jones (1974).

For the base case, the J-13 water pH was taken to be 6.9, the water temperature 25°C, and the Eh -0.256 volts. WATEQ examined more than 100 equilibria and reported both ion activity products and equilibrium constants. When the ion activity product was greater than the equilibrium constant, a mineral would have a tendency to precipitate. In the base case 22 minerals had already exceeded their equilibrium solubility products. In every case, however, these minerals were aluminum bearing, with the least soluble of these being clay minerals. Further, the concentration of Al in J-13 water was reported to be 0.03 mg/l. By varying the aluminum concentration in J-13 water, it was determined that the maximum concentration of soluble aluminum was 1 % of 0.03 mg/l; or by implication,

DRAFT

practically all of the aluminum in J-13 water is present in microscopic clay particles carried along with the water. It is assumed that these clay particles are so small that they would have no tendency to clog pores within the MPZ or the shaft fill.

Next we consider the effects of increasing the pH of the water to 9.5. In this case, 12 new minerals exceeded their solubility products. These minerals were aragonite (CaCO_3), calcite (CaCO_3), diopside ($\text{CaMgSi}_2\text{O}_6$), hematite (Fe_2O_3), maghenite (Fe_2O_3), magnetite (Fe_3O_4), goethite ($\text{FeO}(\text{OH})$), siderite (FeCO_3), clinoenstatite (MgSiO_3), talc ($\text{Mg}_3\text{Si}_4\text{O}_{10}(\text{OH})_2$), sepiolite ($\text{Mg}_2\text{Si}_3\text{O}_7 \cdot 0.5\text{OH} \cdot 3\text{H}_2\text{O}$) and chrysotile ($\text{Mg}_3\text{Si}_2\text{O}_5(\text{OH})_4$). The least soluble of these minerals, as determined by increasing the pH in small steps, is the iron mineral hematite, followed by the magnesium and calcium minerals, talc and calcite. If we assume that the iron, magnesium, and calcium are all deposited as their least soluble mineral, then 37.9 mg/l of precipitate will form as a consequence of raising the pH of the J-13 ground water. Equivalently, the total volume of this precipitate formed per volume of solution is 1.394×10^{-5} , to be referred to as ν in the following text.

Other possible changes to the ground water were also considered in addition to raising the pH. We raised the temperature to 100°C , and increased the concentration of Na^+ , K^+ , SO_4^- , and SiO_2 by one order of magnitude in each case. These additional changes cause some variation in the solubilities of the various minerals, but are considered to be small. For example, when the temperature is increased, calcite is actually less soluble than at lower temperature. Thus, the mineral that accounts for the most precipitate will tend not to redissolve as the temperature is raised. Increasing the concentrations of Na^+ , K^+ , SO_4^- , and SiO_2 similarly appear to have small additional effects, and detailed analysis of their effects is postponed until a later date.

4.2.2.1 Migration of Precipitates

DRAFT

The precipitation of minerals from a supersaturated solution is a rate-controlled process. When considering the formation of calcite, solid

DRAFT

calcite is found to precipitate at nucleation sites on existent solid surfaces rather than homogeneously (Berner, 1980). The rate at which further precipitate forms on existing nucleation sites is governed by diffusional rate processes. In a quiescent fluid where the bulk of the fluid is supersaturated, excess ions will migrate to the solid surfaces and then precipitate to cause the concretion to grow. When fluid is moving through pores or fractures, the process of solid deposition is controlled by the diffusion of ions from the bulk of the fluid to the pore or fracture wall. Where pores or fractures are narrowed by ongoing precipitation, further precipitation is favored because of the reduced diffusional path length (Figure 4-2).

This local restriction in the fluid pathway will result in spreading the precipitate out over a thin shell to reduce fluid motion and hydraulic conductivity. Moreover, the precipitate will tend to seal off the MPZ and the shaft fill so that high conductivities will be locally reduced.

To estimate how rapidly this shell will form, consider the time required for ions in the center of a pore to migrate to a pore wall. If we make use of the conservative Einstein relationship to describe diffusion, then

$$t = \frac{x^2}{D}$$

DRAFT

(4-6)

where t is the time for a molecule to migrate in a random way through a distance, x , in a fluid with a diffusion coefficient, D . The aperture assumed is $50 \mu\text{m}$. Therefore, the value of x used in Equation 4-6 is $25 \mu\text{m}$. Using a representative liquid diffusivity of $10^{-5} \text{ cm}^2/\text{s}$, the time for ions to migrate from the stream centerline to the wall is given by Equation 4-6 to be 0.6 s . In the more likely case, where flow occurs primarily within the matrix, the pore diameters are inferred from matrix hydraulic conductivities to be $0.05 \mu\text{m}$. In this instance, the migration time is $0.5 \mu \text{ s}$. Hence, we conclude that supersaturated solutions will not persist and precipitate deposition will be almost instantaneous.

DRAFT

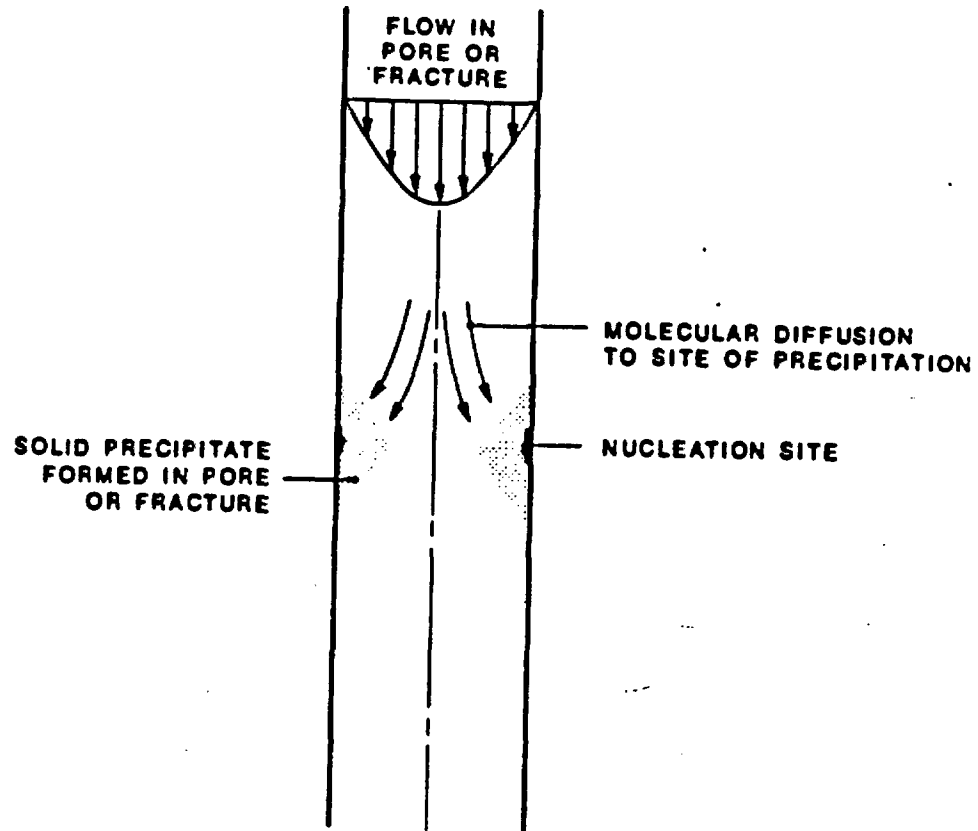


Figure 4-2. Schematic of Deposition of Precipitate

4.2.2.2 Model for Precipitate Deposition

A model describing the rate of buildup of solid precipitate in porous media flow has been proposed by Berner (1980). In this model, a front of solid precipitate progresses through the porous media, where the void spaces behind the front are assumed to be completely filled. A small residual permeability is allowed so that the deposition process may continue. Beyond the front, the water is saturated so that no further deposition is assumed. Berner describes the frontal velocity, U_F , as

$$U_F = \frac{\nu Q}{A(\Phi_U - \Phi_d)} \quad \text{DRAFT} \quad (4-7)$$

where ν is the volume of precipitate per unit volume of water, Q is the volumetric water flow rate, A is the cross-sectional area for flow, Φ_U is the undisturbed porosity, and Φ_d is the porosity behind the deposition front. After Berner we assume that Φ_d is zero. Equation 4-7 may be applied to two regions: the shaft fill and the MPZ. Equation 4-7 is also applied for the normal flow rate of $44.2 \text{ m}^3/\text{year}$ and for flooding events where the fractures are saturated. This latter type of flow will be very transient in nature (flow for less than 1/2 year per event) and is expected to occur only infrequently over the lifetime of the repository.

4.2.3 Results and Conclusions

For normal annual water passage through the MPZ and the shaft fill, flow will occur in an unsaturated manner. Within the MPZ unsaturated flow will occur within the matrix where the undisturbed porosity (taken from the Reference Information Base, Zeuch and Eatough, 1986) is 0.1062. Within the shaft fill the porosity is assumed to be 0.3. The total flow of $44.2 \text{ m}^3/\text{year}$ is partitioned between the MPZ and shaft fill in proportion to the relative conductivities and areas. The frontal velocities in each case are then calculated from Equation 4-7 to be

$$U_F \text{ MPZ} = 0.1 \text{ mm/1000 yr}$$

$$U_F \text{ shaft fill} = 0.2 \text{ m/1000 yr}$$

DRAFT

In the anticipated water passage case, we conclude that no significant migration of precipitate occurs.

At the other extreme of the water flow spectrum is the PMF scenario. In this case, we assume that water flow fills the fracture and saturated flow results. Up to 20,000 m³ may enter the shaft in a single event. The hydraulic conductivity of the backfill is assumed to be 10⁻² cm/s, while that of the MPZ may vary between 60 x 10⁻² and 20 x 10⁻⁵ cm/s. The porosity of the MPZ for flow in fractures is assumed to vary between 0.001 and 0.0001. The frontal advance in the MPZ behind the shaft liner is shown in Figure 4-3, estimates for natural fractures (Erickson and Waddell, 1985, p. 1). Within the shaft fill, the frontal advance is never greater than 0.08 m for any of the above cases.

While the advance of the precipitation front (Figure 4-3) may become as large as 60 m for a maximum flooding event, this advance rate is appropriate only for flow behind the shaft liner. Once the flow advances beyond the base of the liner the appropriate porosity is no longer the very small value assigned for fracture flow in the MPZ. Here, because of the intimate communication between the shaft fill and the MPZ, the porosity of the backfill allows the interstitial flow rate to decrease. As a result, the maximum frontal advance below the shaft liner will be 0.016 m/event. Hence, the deposition of solids from the interaction of the shaft liner with ground water will be a localized phenomenon.

DRAFT

4.3 Remedial Measures to Remove the Liners From the Exploratory Shafts

The removal of the shaft liner will require breaking the concrete over some portion of the shaft, removal of the chunks of concrete to the surface, and backfilling. The breakage methods are described first, followed by the mucking and backfilling operations. In the initial

DRAFT

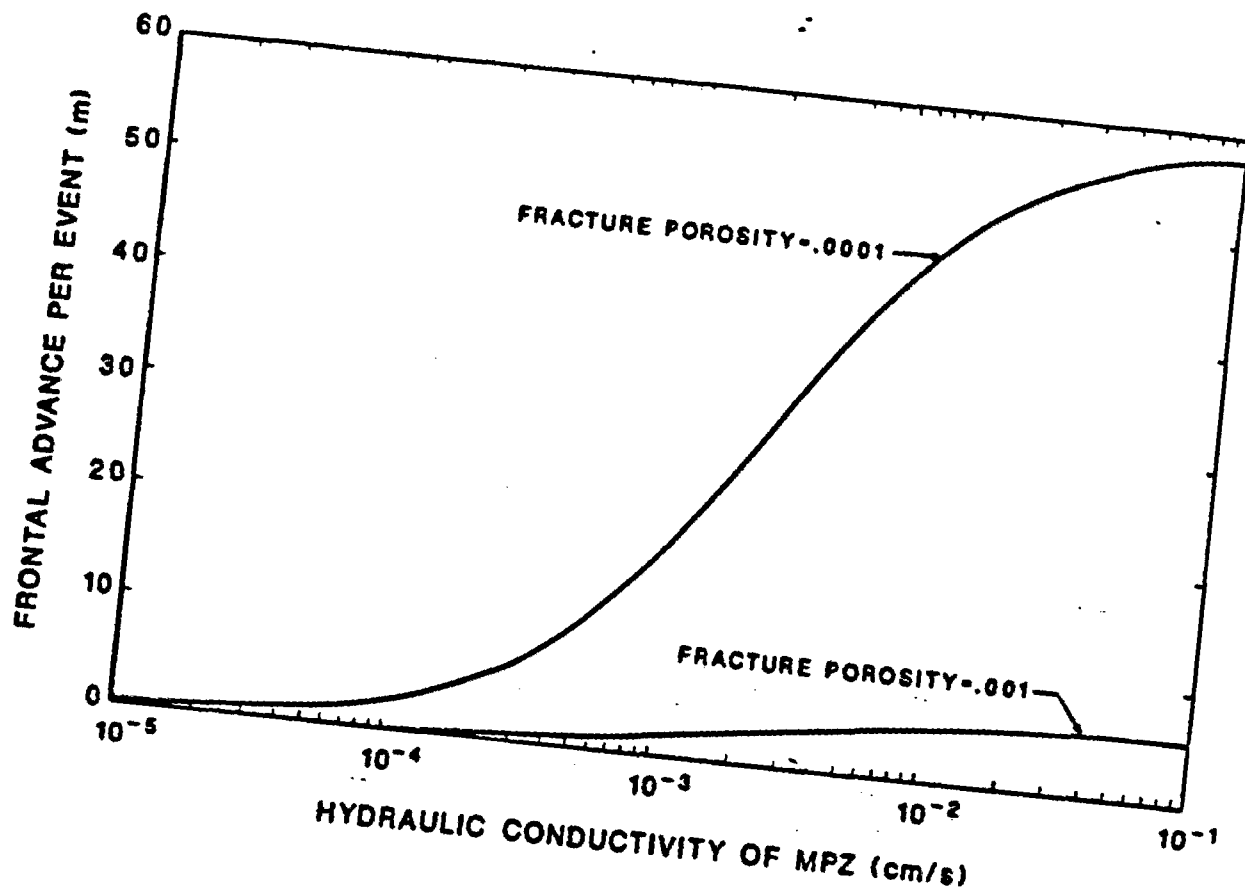


Figure 4-3. Frontal Advance of the Precipitation Front in the MPZ

screening, six methods were identified for concrete breakage:

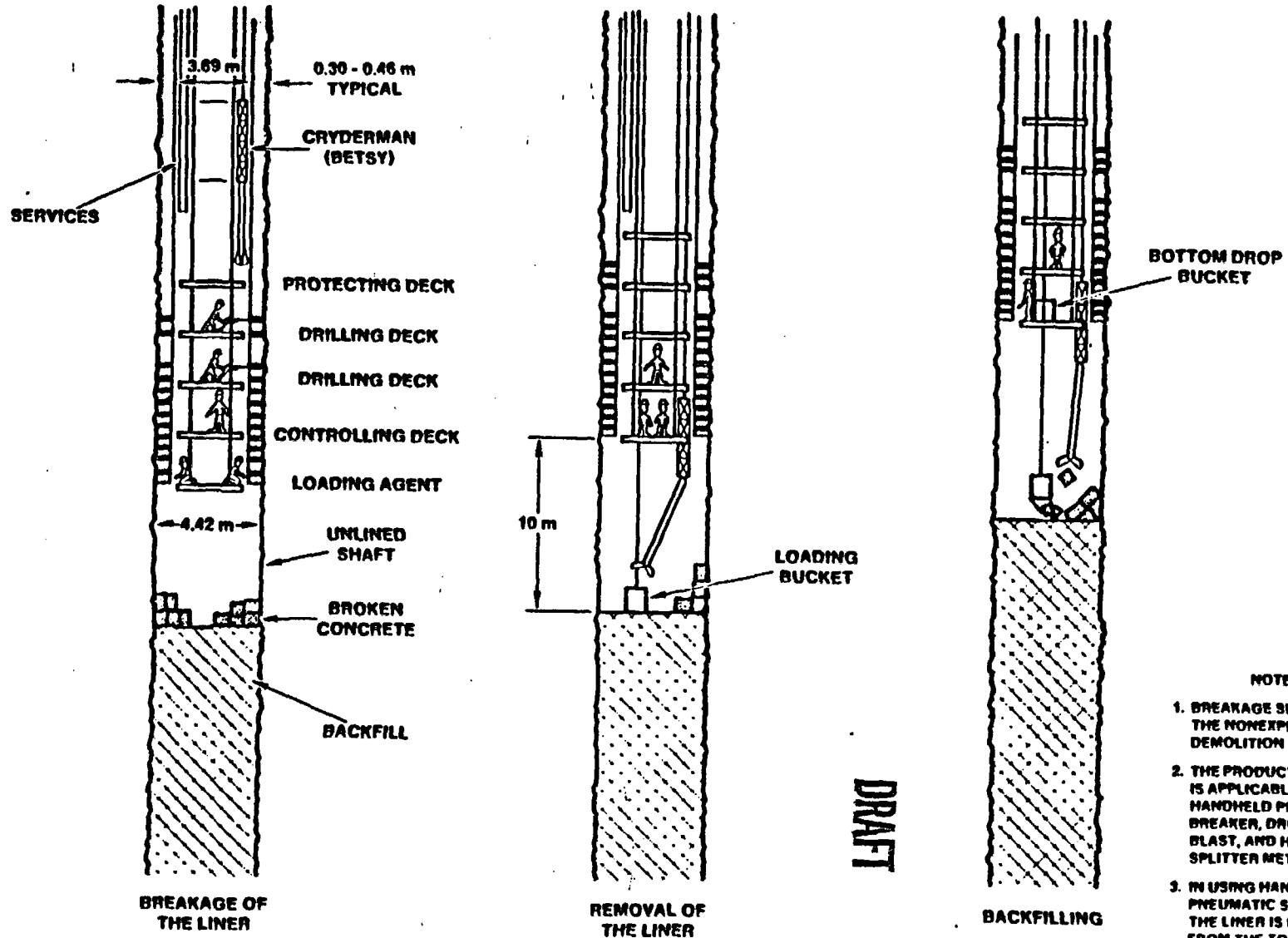
- o Hand-held pneumatic breakers
- o Drill and blast
- o Drill and the use of a hydraulic splitter
- o Drill and the use of a nonexplosive demolition agent
- o Impact breaker
- o Roadheader boom

DRAFT

In the first four methods it is assumed that several operations (drilling and breakage, liner removal, and backfilling) would be performed from a single stage retreated out of the repository (Figure 4-4). In the production cycle, the concrete lining is removed upward, and the backfill is placed below the working stage (the length of unsupported rock sides would be approximately 10 m). It may be necessary to install occasional temporary support to facilitate muck removal and reduce the unsupported length in weaker zones. In the last two methods, the impact breaker or the roadheader boom (Figure 4-5) would be mounted on the base of one stage with mucking and backfilling occurring from a second stage.

Hand-held pneumatic breakers have been used to break high-strength concrete. In one unpublished experience, they were used to remove an 0.5-m, tunnel, spillway lining of concrete with unconfined compressive strength ranging from 28 to 55 MPa. In this method, it is essential to maintain support for the breaker point; otherwise, when the liner fractures, the support is lost, and the breaker drops suddenly. To avoid this problem, the liner would be removed over 10 m in a downward direction. In this method, it is estimated that horizontal drill holes spaced approximately on 0.3-m centers would be required to break out the concrete.

The drill and blast method would require that horizontal drill holes with a horizontal spacing of 0.5 m, and vertical spacing of 0.3 m be loaded with approximately 0.23 kg of plastic explosive and detonated. Drilling and loading operations are performed in series. During blasting, the stage would be raised and personnel would be kept clear for 30 min



- NOTES**
1. BREAKAGE SHOWN IS BY THE NONEXPLOSIVE DEMOLITION AGENT
 2. THE PRODUCTION CYCLE IS APPLICABLE TO THE HANDHELD PNEUMATIC BREAKER, DRILL AND BLAST, AND HYDRAULIC SPLITTER METHODS
 3. IN USING HANDHELD PNEUMATIC SPLITTERS, THE LINER IS BROKEN FROM THE TOP DOWN OVER 10 m.

Figure 4-4. Production Cycle for Breaking and Removing the Liner and Placement of Backfill

DRAFT

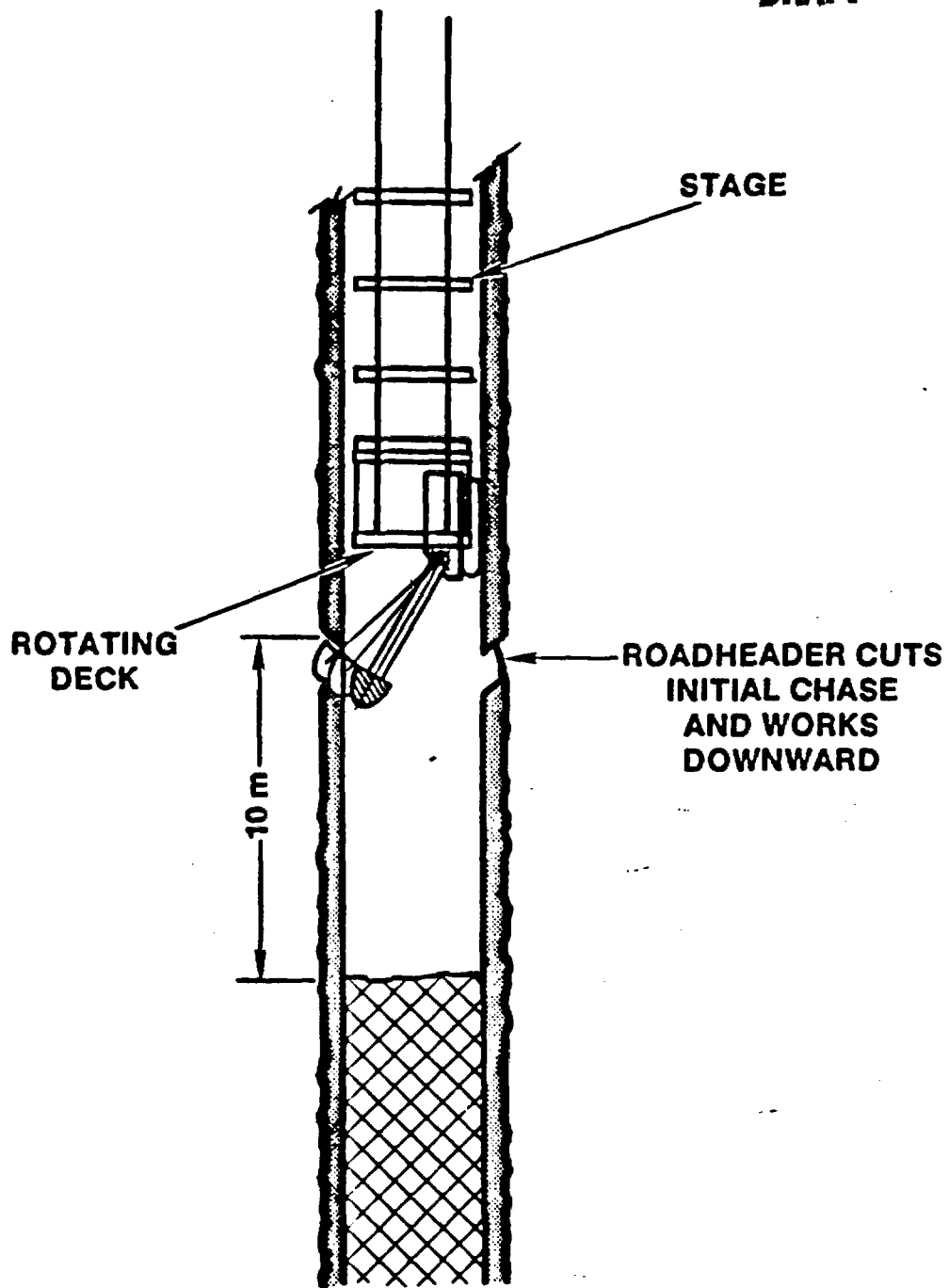


Figure 4-5. Liner Breakage by the Roadheader Method

following each blast. Hole lengths would penetrate the surrounding rock. The method would be suitable where removal of the liner is performed to enhance drainage as discussed previously.

DRAFT

The drill and hydraulic splitter operate on the plug-and-feather principle. In a series of holes penetrating the liner, wedge pairs inserted into the drillhole series are forced apart, resulting in tension and splitting. It is estimated that twice as many holes would be required as in the drill-and-blast method. To retrieve the splitters from the broken concrete, it is necessary to suspend them on chains. Hydraulic splitting is accomplished at the lower platform of the stage with drilling operations performed on the higher platforms.

The drill and nonexplosive demolition agent method consists of drilling holes and loading them with an expansive agent. The technique has been described by Dowding and Labuz (1982, pp. 1289-1299), who describe a series of tests to fracture rock and concrete in a series of case histories that include fracturing of plain concrete. These authors, and subsequent investigators (Ingraffea and Beech, pp. 1205-1208), have interpreted tests on the basis of linear elastic fracture mechanics. It is estimated that a similar number of holes would be required as with the hydraulic splitter method. The fracturing of the liner would take place 24 to 48 hours after placement of the agent.

The impact breaker is mounted on a hydraulically operated boom below the stage and is suspended on ropes. Impact breakers mounted on rubber-tired base units have been successful in breaking concrete in surface operations. The unit breaks at a high rate and would have to be supported in a similar fashion to the hand-held breaker. Using this method, it would be necessary to break out a chase every 10 m to allow breaking out the liner in the downward direction. Because of space restrictions, it would not be possible to muck out the broken liner and backfill unless the stage was removed after every 10-m lift.

Roadheader booms are used extensively in underground mining operations. The single head or two cutting heads are capable of excavating medium-hard rock (D'Appolonia, 1976, pp. 2-62 through 2-66) and would be suitable for concrete liner removal. In this method, the roadheader boom is mounted below the base platform of the stage and would be capable of reaching the liner from a single support point. It is best suited for cutting downward. It has the advantage over the impact breaker that it can cut as it is being swung into the concrete lining so that it can readily cut the starting chase to allow downward excavation.

Two methods are identified for muck removal and backfilling operations since there are space restrictions in the small-diameter exploratory shaft; these include the following:

- o Cryderman mucker (The Betsy)
- o Remote controlled, orange-peel-type grab.

The smallest size Cryderman mucker would suit the small, 3.66-m, finished diameter of the exploratory shafts. This unit is normally suspended on a winch from the surface and held against the side of the shaft excavation or concrete lining by a frame-and-bolt arrangement. The unit is pneumatically operated and may be hoisted out of the shaft stage area while drilling and breakage operations are in progress. During mucking operations, the unit would remove broken concrete and place it in a conventional bucket hoisted through a trap door to the surface. During backfilling operations, the conventional bucket is replaced by a bottom drop bucket.

The other mucking method is the orange peel type grab unit that operates below the stage (Figure 4-6). This unit is raised and lowered by a hoisting winch that operates from the bottom of the shaft stage. The broken concrete liner is loaded into a bucket that may be hoisted to the surface.

DRAFT

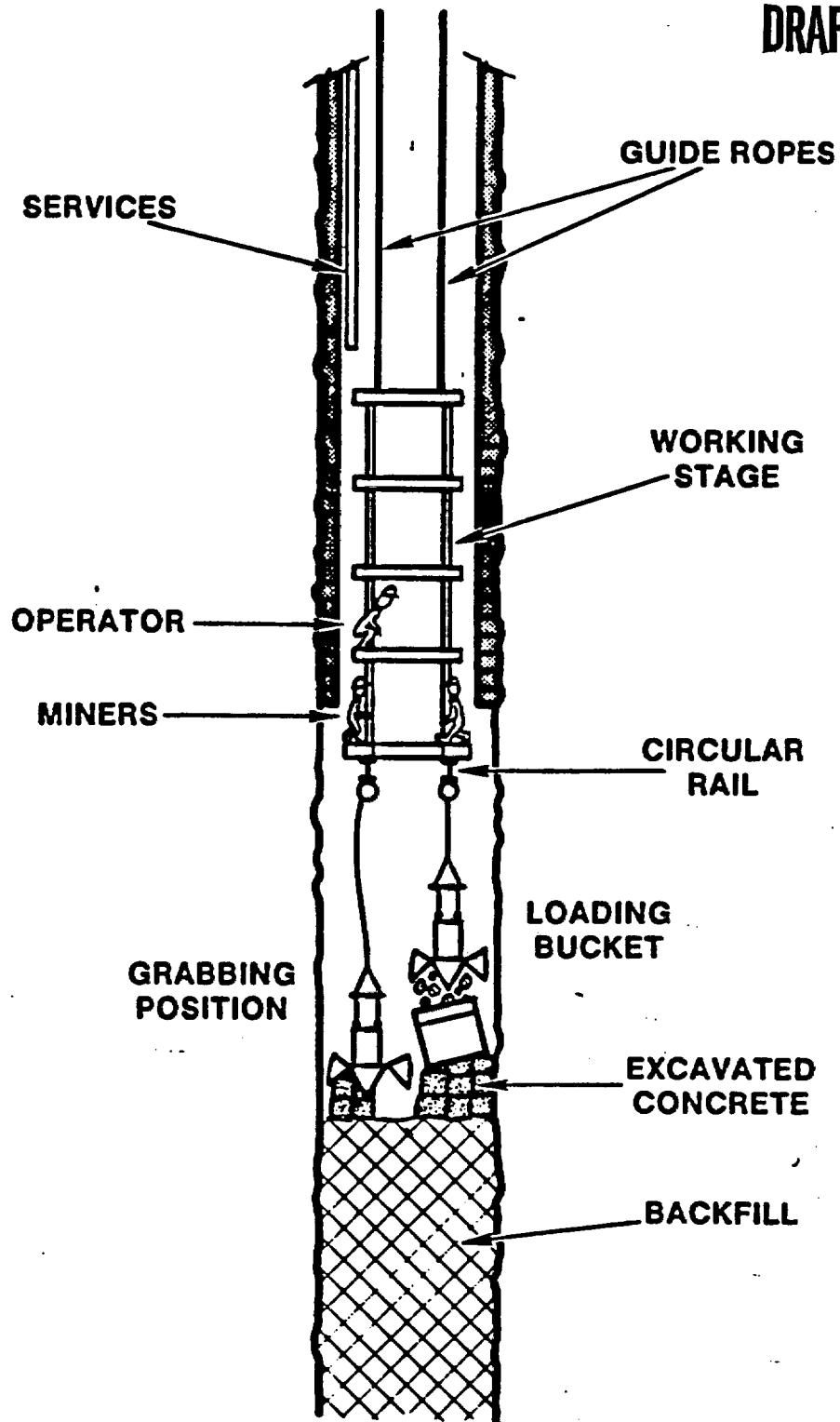


Figure 4-6. Removal of Concrete Using the Orange Peel Grab

DRAFT

The advantages, disadvantages, and equipment/material costs for the several methods for liner removal are summarized in Table 4-2. This study places emphasis on conventional methods and gives preference to the use of "off-the-shelf" equipment. The impact breaker and roadheader methods are not as practical for removing concrete from the muck pile; either the impact breaker or the roadheader boom would have to be retreated from the shaft for removal of concrete and placement of backfill. It is noted that if the entire liner were to be removed, the initial fixed costs for stage modifications might be offset by the higher production rates of these two methods.

Further comparisons of production cycle times and costs for the remaining four methods are presented in Tables 4-3 and 4-4, respectively. These costs apply to complete removal of the liner from the base of the shaft to near the repository horizon. This cost comparison would suggest that the drill and hydraulic splitter method is the most economical, although when off-site preparation, on-site preparation, and other costs are factored in (Appendix D), the differences in adopting any single method are not significant.

4.3.1 Conclusions

DRAFT

Evaluation of the advantages and disadvantages suggests that the hydraulic splitter method is the favored approach for liner removal. Conventional equipment with the slight modification of suspending the splitters from chains may be used. The costs are somewhat more favorable. It is possible that drilling and splitting patterns could be optimized through analysis of superpositions effects from an array of splitters. The method does not leave any undesirable chemical residue. While supplemental hand methods may be required, this is not considered a significant disadvantage.

Table 4-2

Summary of Advantages, Disadvantages, and Cost of Liner Removal Methods

Removal Method	Advantages	Disadvantages	Equipment and Material Costs ^(a)
1. Hand-held pneumatic breakers	There is experience in removing concrete liners.	<p>The method is labor intensive and requires more production time.</p> <p>The method poses a potential safety problem if the breaker dropped suddenly.</p>	The cost of 8 breakers and 4 drills is approximately \$15,000. Drilling equipment spares cost \$120,000.
2. Drill and blast	The method is well known,	An overbreak zone may form. Drilling and loading operations cannot be performed simultaneously. Blasting would require raising the stage and clearing the area after each detonation.	The cost of 6 drills and 4 breakers is \$15,000; the cost of drilling equipment spares is \$57,000. The cost of explosives and caps is \$51,000.
3. Drill and hydraulically split	<p>Drilling and splitting may occur simultaneously.</p> <p>The method is clean and does not leave chemical residue.</p>	<p>It is not as efficient as drilling and blasting. The method may need to be supplemented with hand methods such as the hand-held pneumatic breakers.</p> <p>The splitters must be suspended to avoid being dropped into broken concrete.</p>	The cost of 6 drills and 4 breakers is \$15,000. Drilling equipment spares cost \$102,000. Rental costs for the splitters are estimated at \$54,000.

4-23

DRAFT

^(a)Note that the costs apply to complete removal of the liner.

Table 4-2 (Continued)

Summary of Advantages, Disadvantages, and Cost of Liner Removal Methods

Removal Method	Advantages	Disadvantages	Equipment and Material Costs ^(a)
4. Drill and use a nonexplosive demolition agent	<p>Drilling and splitting may occur simultaneously.</p> <p>Experience in fracturing plain concrete (Dowding and Labuz, 1982, p. 1297)</p>	<p>Operations must be carefully planned since a period of 24 to 48 hours is required for liner fracturing.</p> <p>The chemical agent could not be recovered from the muck pile.</p>	<p>The cost for 6 drills and 4 breakers is \$15,000. Drilling equipment spares cost \$102,000. The cost of the expansive agent is \$306,000.</p>
4-24 5. Impact breaker		<p>Mucking and backfilling operations must be performed from a second stage.</p> <p>The breaker point must be supported.</p>	<p>The initial costs of power and stage modifications are \$16,000 and \$8,000, respectively. A suitable unit with equipment spares may be rented at a rate of \$100.00/hour, or an estimated cost of \$300,000.</p>
6. Roadheader boom	<p>No drilling is necessary and the production rate is high.</p> <p>It can cut as it is being swung into the concrete lining so that it can readily cut the starting chase to allow downward excavation.</p>	<p>Mucking and backfilling operations must be performed from a second stage.</p> <p>Little experience in shaft operations.</p>	<p>The initial costs of power and stage modifications are \$18,000 and \$8,000, respectively. A suitable unit with equipment spares may be purchased for \$125,000.</p>

DRAFT

TABLE 4-3

COMPARISON OF PRODUCTION CYCLE TIMES FOR VARIOUS METHODS
USED TO REMOVE CONCRETE LINERS^(a)

<u>Activity</u>	<u>No. of Shifts</u>
<u>Drill and Blast</u>	
Drill approximately 800 holes 0.6 m deep	2.0
Load 60 % of the holes and blast	3.0
Muck out broken liner	1.5
Backfill 160 m ³	1.5
Remove 9 m of service lines	0.5
Allow for other hoist runs, movement of stage	<u>0.5</u>
Total	9.0
<u>Drill and Hydraulic Splitter</u>	
Drill 1,700 holes 0.6 m deep	4.0
Simultaneously use splitter in 25 % of the holes	1.5
Muck 62 m ³	1.5
Backfill 160 m ³	0.5
Remove 9 m of service lines	0.5
Allow for other hoist runs, movement of stage	<u>0.5</u>
Total	8.0
<u>Drill and Nonexplosive Expansive Demolition Agent (NEDA)</u>	
Drill 1,700 holes 0.6 m deep	4.0
Simultaneously load 25 % of the holes with NEDA	1.5
Muck 62 m ³	1.5
Backfill 160 m ³ (loose)	0.5
Remove 9 m of service lines	0.5
Allow for other runs, movement of stage	<u>0.5</u>
Total	8.0

(a) Cycle times are calculated for a 9-m length.

Note: For the hand-held pneumatic breaker method, the estimated production cycle time is 15 shifts for breaking out the liner. The total production cycle time is estimated at 19 shifts.

DRAFT

TABLE 4-4

COMPARISON OF COSTS FOR BREAKING OUT THE CONCRETE LINING AND ROCK^(a)
(\$ THOUSANDS)

Cost Item	Hand-Held Pneumatic Breakers	Drill & Blast	Drill & Hydraulic Splitter	Drill & NEDA
1) Time-related	3,447	1,149	912	912
2) Equipment-related				
Drilling	15	15	15	15
Blasting Winch Rental		2		
Blasting Cable		17		
Firing Switch, etc.		2		
3) Consumables-related				
Drilling	120	57	102	102
Explosives & Caps		51		
Rental of Splitters		6	54	
Bristar				306
Total	3,582	1,299	1,083	1,335
Weeks	42.6	14.2	11.2	11.3

^(a) Includes only costs directly related to breaking out the concrete liner from the shaft.

DRAFT

5.0 INFLUENCE OF THE ES PENETRATION INTO THE CALICO HILLS UNIT

5.1 Changes in the Sorptivity of the Calico Hills Unit Due to Elevated Ground-Water Temperature

5.1.1 Temperature Elevation of Water Entering The Shaft

The temperature of the ground water within the Calico Hills unit will be increased globally by the presence of the repository. Calculations by M. L. Blandford (Morales, 1985, pp. 36-39), carried out assuming a thermal load by the repository of 57 kW/acre indicate that the temperature expected at the top of the Calico Hills unit at 500 years after emplacement will be 63°C and that the maximum temperature will be 76°C. These temperatures are calculated assuming that conduction of heat is the primary heat transfer mechanism. These calculations indicate that the temperatures are relatively constant within the repository perimeter and fall off rapidly as one moves away from the repository. Further, these calculations do not consider the effect of the barrier pillar around the shafts. Such a non-waste emplacement area will tend to lower the temperature of the rock mass around the shaft.

To address the thermal impact of the exploratory shaft on water that might enter the Calico Hills, a separate analysis (see Appendix E) was conducted assuming various water flow rates downward through the shaft fill and the MPZ around the ES. These calculations were directed at determining the maximum water temperature at the base of the ES, entering the Calico Hills unit. Conservative assumptions were involved in all cases to reveal that the fluid temperature never deviated greatly from the formation temperature. Under normal expected water flow conditions where the temperature at the top of the Calico Hills unit was 76°C, the water temperature was 76.03°C. Increasing the water flow rate to its maximum permissible value, i.e., the maximum hydraulic conductivity of the modified permeability zone, increased the water temperature to 77.6°C. Hence, the formation temperature computed assuming conduction alone completely dominates the influence of the ES, and the ES has little additional impact on the ground-water temperature.

DRAFT

5.1.2. Impact of Increased Ground-Water Temperature on the Sorptivity of the Calico Hills Unit

Within the Calico Hills unit, the principal zeolite phases are clinoptilolite, mordenite, and analcime. Of these, clinoptilolite is the most important sorptive phase. Moreover, the sorptivity of the Calico Hills at elevated temperature depends on two factors: the dependence of the distribution coefficient, (e.g., K_d^*), temperature, and the hydrothermal stability of the mineral phase, clinoptilolite. Also, as has been shown above, the upper limit of temperature considered in this discussion is approximately 80°C. The concern at the upper margin of the Calico Hills does not involve extreme temperatures but rather represents the impact of more moderate temperatures on the sorptivity.

The dependence of the distribution coefficient, e.g., K_d , on temperature has been addressed in several studies (Wolfsberg et al., 1979; Daniels et al., 1982). In these studies, increases in K_d with temperature are reported in every case for temperature increases of up to 100°C. Hence, it may be stated that the distribution coefficients of the Calico Hills minerals improve as temperature increases.

The second phenomenon to be addressed is the hydrothermal stability of the zeolite phases within the Calico Hills unit. Smyth (1981 and 1982) reports on two types of stability. These are dehydration stability and mineralogical stability. Dehydration reactions occurring up to 200°C are found to be reversible and will not be considered further. However, irreversible, deleterious, mineralogical reaction is also observed. Clinoptilolite is a thermally sensitive mineral and undergoes transformations to mordenite and analcime. While the consequence of these

*The distribution coefficient is a parameter commonly used to describe the sorption behavior of radionuclides in geologic systems. K_d is defined as "the concentration per gram of a species on a solid phase divided by its concentration per milliliter in the liquid phase at equilibrium" (Wolfsberg et al., 1979, p. 4). The higher the K_d value, the higher the sorption potential of the material being evaluated.

DRAFT

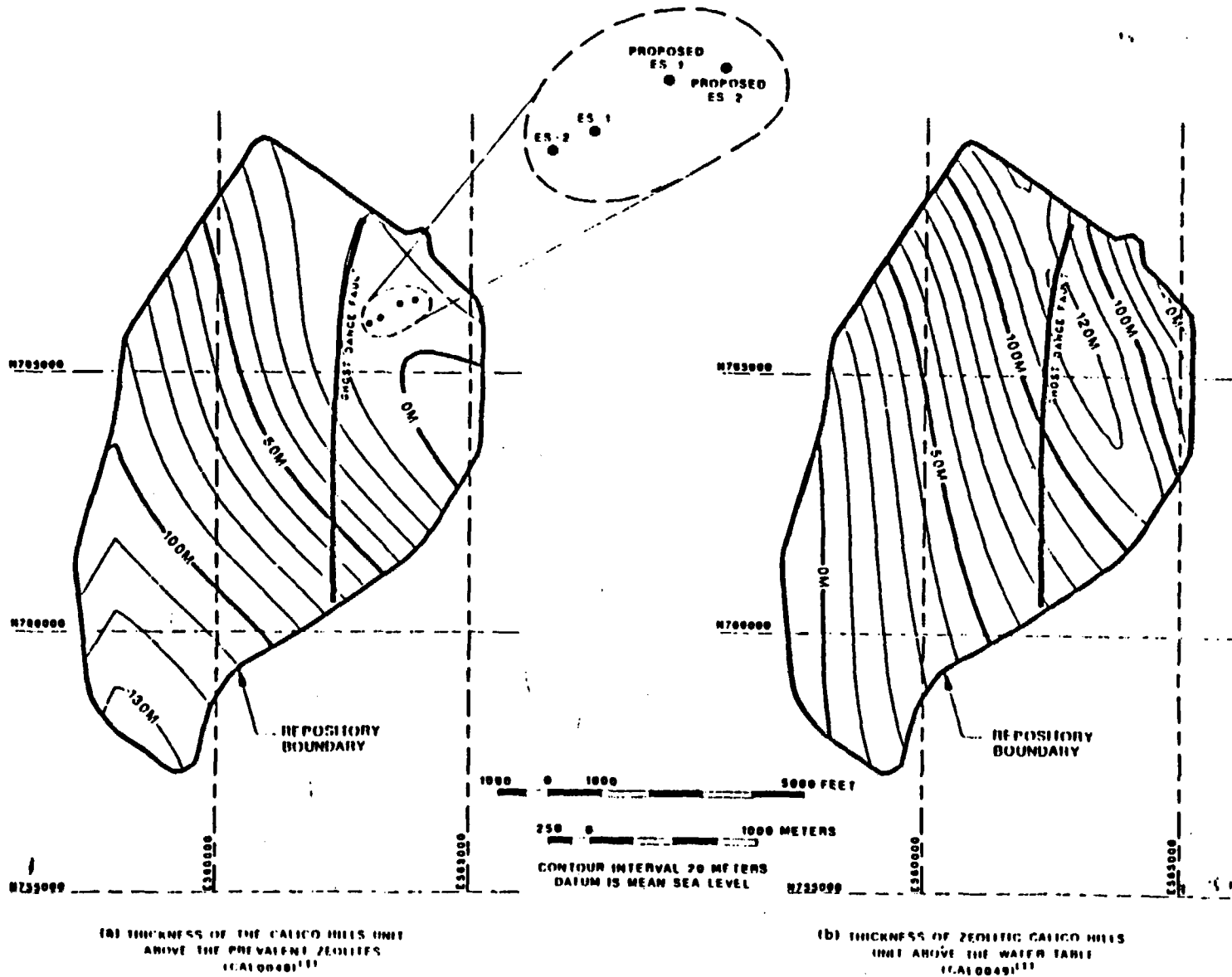
transformations has not been investigated, it is assumed that the sorptivity will decrease. The exact transition temperature being dependent on sodium concentration and pH. For conditions found at Yucca Mountain, Smyth predicts a transition temperature of 105°C; at extreme sodium concentration levels, this transition temperature may drop to 95°C. Other investigators* at Los Alamos National Laboratory feel that cristobalite may also influence the stability of clinoptilolite and that the irreversible mineralogical transition temperatures of Smyth may be inappropriate and will probably be higher. In any case, all data gathered to date indicate that the actual temperature of any part of the Calico Hills unit will be less than that required to cause any reaction of clinoptilolite.

5.2 Changes in the Thickness of the Tuffaceous Beds of Calico Hills Above the Ground-Water Table

An additional consideration associated with the ES-1 is its penetration into the zeolitic Calico Hills unit. Such a penetration can reduce the effective thickness of the Calico unit used in performance assessment calculations. The current NNWSI Project position is that any penetration associated with the ESF including the ES-1 should not reduce the effective thickness of the zeolitic portion of the Calico Hills to a thickness less than its minimum thickness occurring anywhere within the repository boundary. Figures 5-1a and 5-1b illustrate this point.

The Calico Hills unit can be divided into a nonzeolitic portion and a zeolitic portion. In the ES-1 location, the Calico Hills unit above the prevalent zeolites is zero. The thickness of the zeolitic portion of the Calico Hills unit (Figure 5-1b) is approximately 100 m. Because the proposed penetration into the zeolitic portion of the Calico Hills unit is 15 m, the thickness of the Calico Hills unit will be about 85 m. This thickness is above the minimum thickness of 70 m illustrated on Figure 5-1b. The total thickness of the Calico Hills Unit at the exploratory shaft locations can be obtained by adding the thicknesses of the vitric and zeolitic portions of the Calico Hills as shown by both Figures 5-1a and 5-1b.

*C. J. Duffy, 1987, personal communication.



DRAFT

Figure 5-1. Contours of the Thickness of the Unsaturated Portion of the Calico Hills Unit Beneath the Repository

DRAFT

5.3 Conclusions

The impact of the ES on the sorptivity of the Calico Hills unit has been found to be negligible. First, water passing through the ES will be completely separated from waste stored in the repository and will not constitute a preferred pathway. Second, the minimum thickness of the Calico Hills unit will be preserved, while allowing much valuable information to be gained by sinking the ES into the upper margin of the Calico Hills. Third, the variation in the global temperature field of the repository caused by the ES is negligible. Last, the elevation of the temperature of the ground water percolating through the shaft fill is computed to be a maximum of 77.6 C at the top of the Calico Hills unit. This value is less than the minimum value of 95 C (Smyth, 1982, p.195) observed to cause mineralogical transition of zeolites. Therefore, there is no impact of water percolating through the shaft fill on the zeolites in the Calico Hills unit.

ROUGH DRAFT

DRAFT

6.0 CONCLUSIONS AND RECOMMENDATIONS

The analyses in the report support the tentative conclusion that the design and construction of the ESs, as currently planned, do not negatively influence the performance of the potential nuclear waste repository at Yucca Mountain. Specific design and construction actions of concern include: (1) construction of a concrete liner and leaving the majority of the concrete liner, as constructed during the preclosure period, in place during the postclosure period, and (2) controlling blasting to enhance the vertical advance, limit damage in the rock surrounding the shaft, and produce acceptable-sized rock fragments. Nevertheless, there are some actions that can be taken in constructing the ESs to enhance the performance of the repository. These recommended actions are stated below.

- o The proposed construction method should not preclude nor unnecessarily complicate the removal of the concrete liner associated with the exploratory shafts. This is particularly true for that portion of the liner below the repository station.
- o The paste portion of the concrete liner placed in the lower portion of the shaft, i.e., the sump, should not infiltrate the fractures of the rock mass to the point where it could not be removed.
- o Overbreak that occurs while excavating the ESs should be recorded.
- o The current performance analyses assume that the MPZ is not greater than 20 to 60 times the undisturbed rock mass hydraulic conductivity one radius from the edge of the liner. We believe that this model is very conservative, and excavation of the shaft liner should not create a condition more severe than that estimated by the MPZ model. However, it is prudent to exercise as much control as possible and practical while excavating the ESs, so that blasting damage is reduced.
- o Although a special mixture of concrete is not necessary, increasing the silica content of the concrete could provide greater stability

ROUGH DRAFT

ROUGH DRAFT

of the liner. The addition of excess, reactive silica consumes calcium hydroxide and creates a more stable calcium silicate hydrate. Based on preliminary, laboratory testing, it is desirable if the concrete mixture contains excess silica such that the molar ratio of CaO to SiO₂ is approximately 1. Reactive silica can take the form of silica flour, silica fume, or fly ash.

- o It is preferred that no grouting occur behind the shaft liner. If future analyses indicate that grouting is necessary or desirable to achieve enhanced repository performance, it is possible that a previously grouted zone could not meet newly established, long-term performance objectives. Not grouting in water-producing fracture zones would simplify any grouting action that might be required for long-term performance.

Perspective into Radionuclide Transport

The purpose of this appendix is to provide a perspective into the potential for radionuclide transport due to the presence of the ESs. To achieve this perspective descriptions of several mechanisms that can potentially enhance radionuclide releases from the underground facility are given. These descriptions are supplemented by simple calculations that compute the travel distance and/or travel time of the transporting medium. The authors recognize that these mechanisms do not represent a comprehensive evaluation of all conceivable mechanisms. However, these mechanisms do represent some of the more commonly thought of mechanisms that could affect radionuclide transport due to the presence of shafts. The mechanisms considered include:

- o downward water movement through the shafts,
- o upward movement of water in the sumps of shafts,
- o transport of radioactive solids through shafts,
- o gaseous transport through drifts and shafts due to gaseous diffusion,
- o gaseous transport through drifts and shafts due to convective forces, and
- o gaseous transport through shafts due to barometric forces.

DRAFT

A.1 Downward Water Movement Through Shafts

Shafts are pathways to the underground facility that could potentially increase the amount of water that could enter into the waste disposal areas. The analyses presented below illustrate the time required to saturate shaft fill to a 300 m depth assuming a constant supply of water at

DRAFT

the upper portion of the shaft. It is presumed in the analysis that if water does not reach the repository horizon over a substantial period of time, there is no potential for water to reach the waste disposal areas and this mechanism should not be considered further.

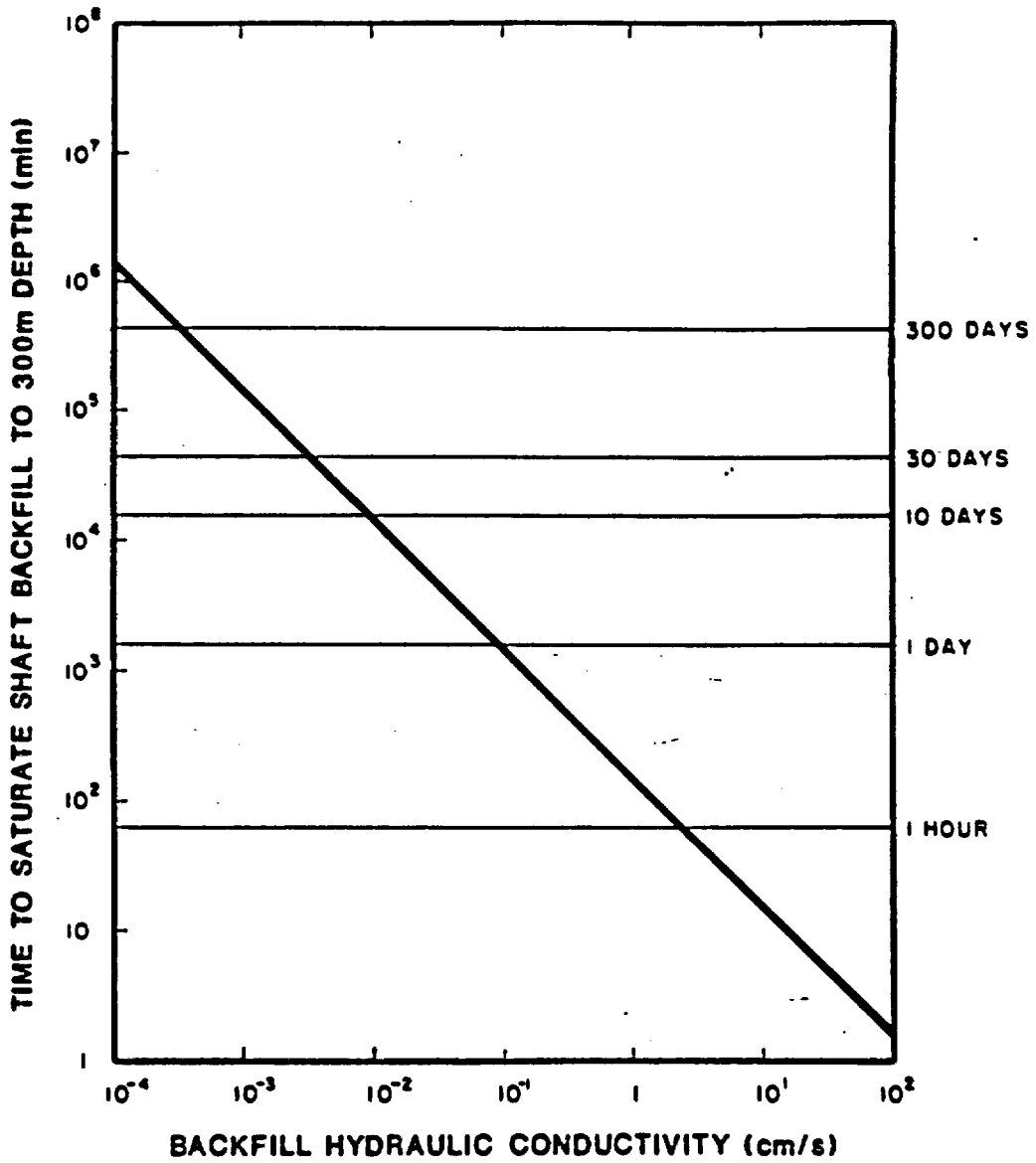
The approach used was to compute the downward infiltration of water through the shaft fill which is assumed to be initially dry. The Green and Ampt solution (Hillel, 1971, pp. 140-143) was used to calculate the saturated vertical infiltration into the initially dry shaft fill. The discussion of how the Green and Ampt solution is applied is provided in Fernandez et al. (1987). The results illustrating the time to saturate 300 m of backfill is given in Figure A-1. This figure suggests there is a time delay for a fully saturated front to reach the repository horizon. Depending on the hydraulic conductivity of the shaft fill, this time delay can vary over many orders of magnitude. Figure A-1 also illustrates that if a coarse material is placed in the shaft, water from the surface is transmitted to the repository level over a short time. Because there is some potential for water to be transmitted down to the repository horizon (depending on the condition encountered at the surface), this mechanism is considered further in Chapter 3 of this report.

A.2 Upward Movement of Water in the Sumps of Shafts

The mechanism discussed in this section involves the transport of standing water at the base of a shaft upward due to fracture and matrix capillary forces. This mechanism assumes that standing water occurs and radionuclides are in solution at the base of the shaft implying transport of contaminated water to the shaft. This assumption of transport of contaminated water to the shaft, in itself, may totally negate the feasibility of this mechanism to occur because one constraint placed on the drift grades in the underground facility is to establish a drainage pattern for the access and emplacement drifts so that no drainage occurs from these drifts into ES-1. This constraint, therefore, significantly reduces the possibility of radionuclides to reach ES-1. The following discussion nevertheless, presents discussions and calculations evaluating the effect of this mechanism.

DRAFT

DRAFT



DRAFT

Figure A-1. Results from Green and Ampt Solution for Transient Flow Through Shaft Backfill

Because the sump at the base of ES-1 is located predominantly in welded tuff which is highly fractured, the capillary forces in the modified permeability zone is controlled by the fractures. Therefore, upward transport of water in fractures due to capillarity was computed using the formula

$$h = 2\sigma \cos \theta / \rho g b$$

(Lohman, 1972, p. 2)

where h = height of water in a fracture, m
 σ = surface tension of water against air, newton/m
 θ = contact angle between the water in the fracture and the tuff (assumed to be zero degrees),
 ρ = density of water, kg/m³
 b = fracture aperture, m, and
 g = acceleration due to gravity, m/s².

This situation could be applied to fractures penetrating saturated zones such as the water table or a shaft containing water at the base. For fractures having aperture widths of 71 μm (Sinnock et al., 1984, p. 12) and 25 μm , the rise of water in the fracture was computed to be approximately 0.21 and 0.58 m, respectively. The temperature of the water was assumed to be 30°C. At 100°C, the rise of water in fractures having apertures of 71 and 25 μm would be 0.18 and 0.50 m respectively. Because of the limited extent to which capillary forces within a fracture can transport water upward, radionuclide transport upward in a fracture is considered insignificant.

If standing water occurs within the shaft fill portion of the shaft sump, movement of water upward in the shaft fill by capillary forces is possible. The rise of water above the fully saturated level or the phreatic surface is termed the capillary rise. The extent of capillary rise depends on the pore sizes of the shaft fill. For example, capillary rise in a material that has larger pore sizes, such as a coarse sand, would be low (2-5 cm). For a shaft fill having small pore sizes such as a clay, the capillary rise could range from 200 to 400 cm (Bear, 1976 p. 481). Under either case, i.e., a shaft fill that is representative of a coarse

DRAFT

sand or clay, the capillary rise would be a function of the total length of the shaft. Therefore, because (1) capillary forces within the shaft fill can transport water over a limited extent, (2) transport of radionuclides to the shaft sump is unlikely, and (3) duration of ponding of water, if it occurs at all, is anticipated to be short because it is postulated that water can be effectively drained through the base of the shaft, radionuclide transport upward due to capillary forces in the shaft fill is considered insignificant.

A.3 Transport Due to Solid-Solid Diffusion

Using a one-dimensional solution to Fick's second law, the time for solid diffusion of radionuclides can be computed. The formula used to compute the time for radionuclide migration, for the specified conditions, is

$$\frac{C_A}{C_{A_0}} = \operatorname{erfc} \frac{X}{\sqrt{4\phi_{AB} t}} \quad (\text{A-1})$$

(Freeze and Cherry, 1979, p. 393)

where

- C_A - concentration of A at point X, moles/l
- C_{A_0} - concentration of A at point of origin, moles/l
- X - distance from original point of diffusion, m
- ϕ_{AB} - binary diffusivity for system A-B, m^2/s
- t - time over which diffusion occurs

The most significant unknown in this formula is the diffusion coefficient for uranium through welded tuff. The diffusion coefficient used below is $10^{-15} \text{ cm}^2/\text{s}$, which is believed to be extremely conservative because it is at the higher end of the diffusion coefficients of some solid-solid diffusion coefficients given in Bird, Stewart, and Lightfoot (1960, p. 505). Using this diffusion coefficient and evaluating the condition where the solid portion of the radioactive waste migrates 0.1 m and its concentration is 99 % of its original concentration, a transport time of about 10^{13} years.

DRAFT

is computed. However, the diffusion coefficient of uranium or uranium oxide because of its molecular size would probably be less than the value of 10^{-15} cm²/s used above. A diffusion coefficient of 10^{-30} cm²/s yields a transport time of 10^{28} years. Because of these long transport times, radionuclide release by solid-solid diffusion is considered to be insignificant.

A.4 Gaseous Transport Due to Diffusion

Some radionuclides can be released in a gaseous form and therefore the significance of binary-gaseous diffusion is considered here. Some potential gaseous species (Xe isotopes, Rn, Kr-85, and H-3) can be eliminated from concern because of their short half-lives, assuming the containment period to be 300 to 1000 years. The radionuclides that could potentially enter the repository in a gaseous state are C-14 and I-129 (Van Koynenburg et al., 1984, p. 1). Equation A-1 is used to compute the relative concentration-versus-time curves for I-129 and C-14. However, in order to apply Equation A-1, the diffusivity values for the gaseous forms of I-129 and C-14 are needed. It is assumed that I-129 occurs as I₂ and C-14 occurs as CO₂. Using an approach described in Reid et al., (1977, pp. 548-550) for binary-gas diffusion coefficients and in Smith (1970, p. 406) for Knudsen diffusion coefficients, diffusivities are computed for air-iodine and air-carbon dioxide systems. The computed binary diffusion coefficients for these two systems are 0.081 cm²/s for the air-iodine system and 0.156 cm²/s for the air-carbon dioxide system. The computed Knudsen diffusion coefficients are 10.6 cm²/s for iodine and 25.3 cm²/s for carbon dioxide. These diffusivities are combined by the method described in Mason and Evans (1962, p. 362) to give overall gaseous diffusion coefficients of 0.080 cm²/s for the air-iodine system and 0.155 cm²/s for the air-carbon dioxide system. These diffusivity values assume open drifts and shafts. If backfilling is emplaced, a partial restriction of the migration of the gas occurs. To compute the magnitude of this restriction, an effective diffusivity can be computed. It is a function of the porosity of the material through which the gas is diffusing, and the tortuosity. The following equation is used to compute the effective diffusivity.

$$D_e = \frac{\epsilon}{\tau} D \quad (\text{Froment and Bishchoff, 1979, p. 167}) \quad (\text{A-2})$$

where D_e = effective diffusivity, cm^2/s
 ϵ = porosity of material through which diffusion occurs
 τ = tortuosity, and
 D = diffusion coefficient, assuming no restriction to diffusion, cm^2/s

The porosity assumed for the drift and shaft fill is 0.3. The value for tortuosity is assumed to be 3 which corresponds to loose random pore structure (Froment and Bischoff, 1979, p. 167).

Figure A-2 illustrates the relationship between the relative concentration of the gas under consideration versus time for a distance of 600 m from the waste disposal area. This distance represents an approximation of the distance from the waste disposal area to the surface entry point of ES-1 or ES-2.

Two sets of curves are presented. The first set assumes no backfilling of the shafts and drift. The second set assumes the drifts and shafts are backfilled with a material that is emplaced loosely. Figure A-2 illustrates that if only binary diffusion occurs, considerable time, 10^5 to 10^6 years, is required to release I_2 or CO_2 at a concentration of ~99 % of the original concentration in the waste disposal areas. Lesser concentrations are released at much shorter times following release of the gas at the disposal area. Also, a substantial reduction in the concentration exiting the shaft can be achieved by emplacing loose shaft and drift fill. For example, 1000 years after gaseous release at the repository horizon, the concentration of gas release at the surface would be approximately 0.1 of the original amount if backfilling occurs. Emplacement of consolidated shaft fill or a single-shaft or drift seal can further reduce the release through the shaft. Because binary gaseous diffusion is a slow process as indicated by Figure 2-1 and because travel times can be reduced substantially by simple backfill, binary-gaseous diffusion is not considered to be a significant release mechanism.

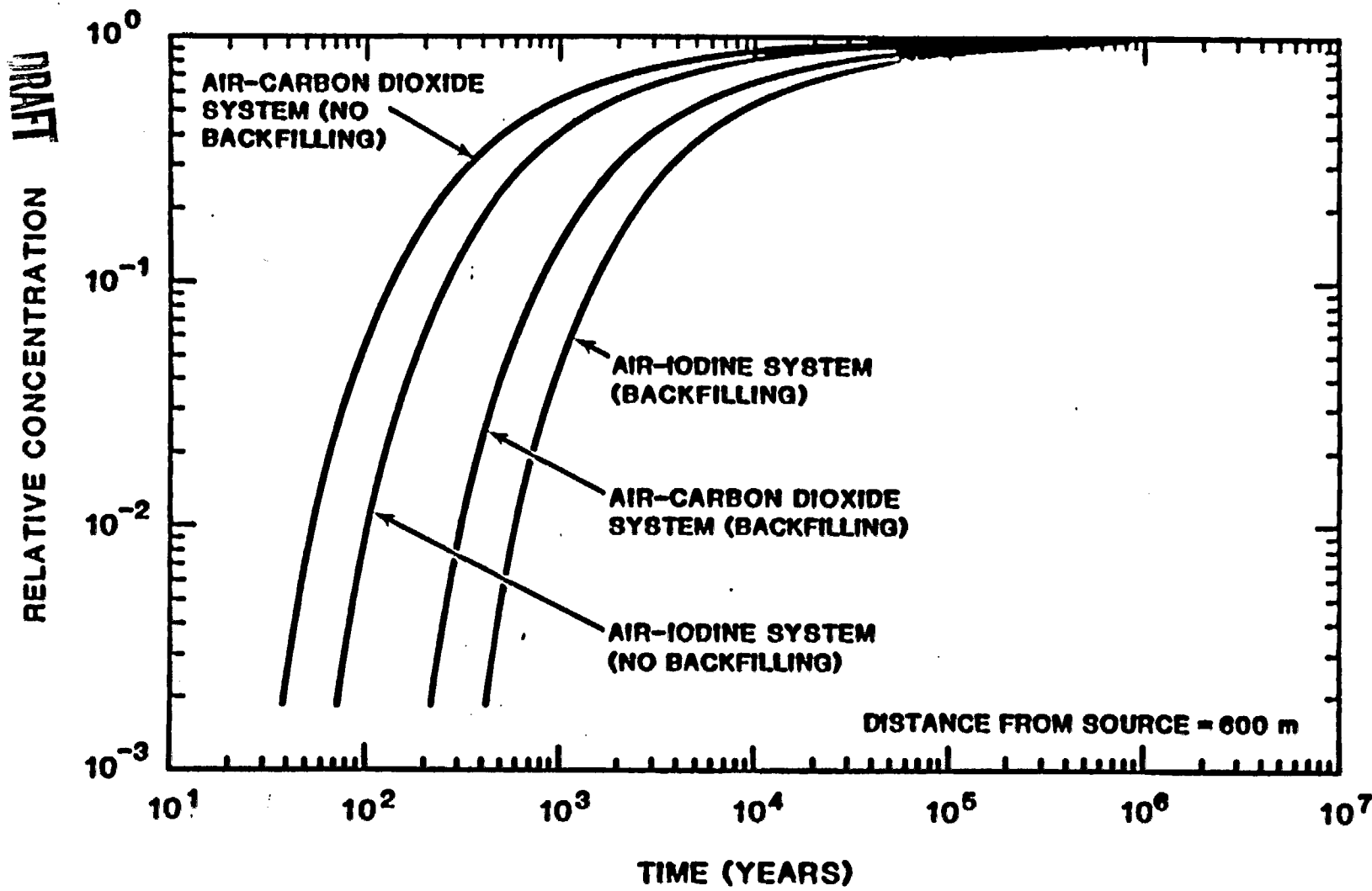


Figure A-2. Concentration of Two Gaseous Systems Due to Binary Gaseous Diffusion (600 m from Point of Release and at Various Times Following Release)

DRAFT

A.5 Gaseous Transport Due to Convective Forces

For a repository located above the water table, there is the possibility of release of radionuclides by air flow out of the repository through the shafts or through the host rock. Air flow may develop as a convective circulation in response to thermal gradient and as a flow from the repository (high pressure zone) to the ground surface (low pressure zone) in response to changes in barometric pressure. These mechanisms are discussed briefly below.

After the emplacement of waste canisters, heat is initially transferred by conduction from the waste canisters to the surrounding rock. Vertical temperature gradients will develop from the repository horizon and potentially affect air and water density. If sufficient energy in the form of heat is imparted to the air or water vapor, convective transport is established.

Two potential convective air flow mechanisms are illustrated in Figure 3-19. Mechanism A assumes that no upward flow occurs through the host rock relative to flow through the shafts, ramps, and drifts. The Exploratory Shaft (ES-1) and adjacent Exploratory Shaft (ES-2) are within the repository boundary, and the temperature is relatively high near the repository horizon. The men-and-materials shaft, the emplacement exhaust shaft, and the ramps are located outside or just inside the repository perimeter, and the temperature gradients are lower. In response to these gradients, air will tend to rise in ES-1 and ES-2 and air will be drawn in through the other entries. This mechanism may occur if the shafts and drifts are open or if the backfill is relatively permeable compared to the host rock. In Mechanism B, convective air circulation is also assumed to occur through the host rock. The waste disposal areas are relatively hot and the heated air tends to rise vertically through the rock as well as through ES-1 and ES-2.

DRAFT

A.6 Gaseous Transport Due to Barometric Forces

Another potential flow mechanism for the transport of radionuclides is the development of a differential air pressure between the repository and

DRAFT

the ground surface. A weather front moving suddenly across the repository site might result in a reduction of barometric pressure, producing a pressure gradient between the repository and the surface. Pressure gradients may also develop more gradually in response changing seasons. Changes in barometric pressure are cyclical or periodic in nature, so that air would eventually move back into the repository. The ease with which air moves in and out of the repository will depend upon the properties of the backfill placed in the shafts and ramps and the surrounding rock. Conceptually, large volumes of air may move through shafts and ramps containing a high-conductivity, coarse backfill. Smaller volumes of air might move through shafts and ramps containing a fine, low-conductivity backfill, although a proportionally greater amount of flow might occur through the damaged zone around the shafts and ramps. In addition, a low conductivity backfill will isolate the repository from large pressure variations at the surface, while a high conductivity backfill will result in a more significant pressure response within the repository.

DRAFT

Explanation of Water Inflows to ES-1

The purpose of this appendix is to describe the shape of the curves in Figure 3-7 of Section 3.2.1 of this report. For ease in explaining the shape of these curves, a single curve is selected for the discussion, i.e., the lines associated with the Tiva Canyon having a hydraulic conductivity of 10^{-2} cm/s (Figure B-1). The features discussed in Figure B-1 are labeled A through E on Figure B-1.

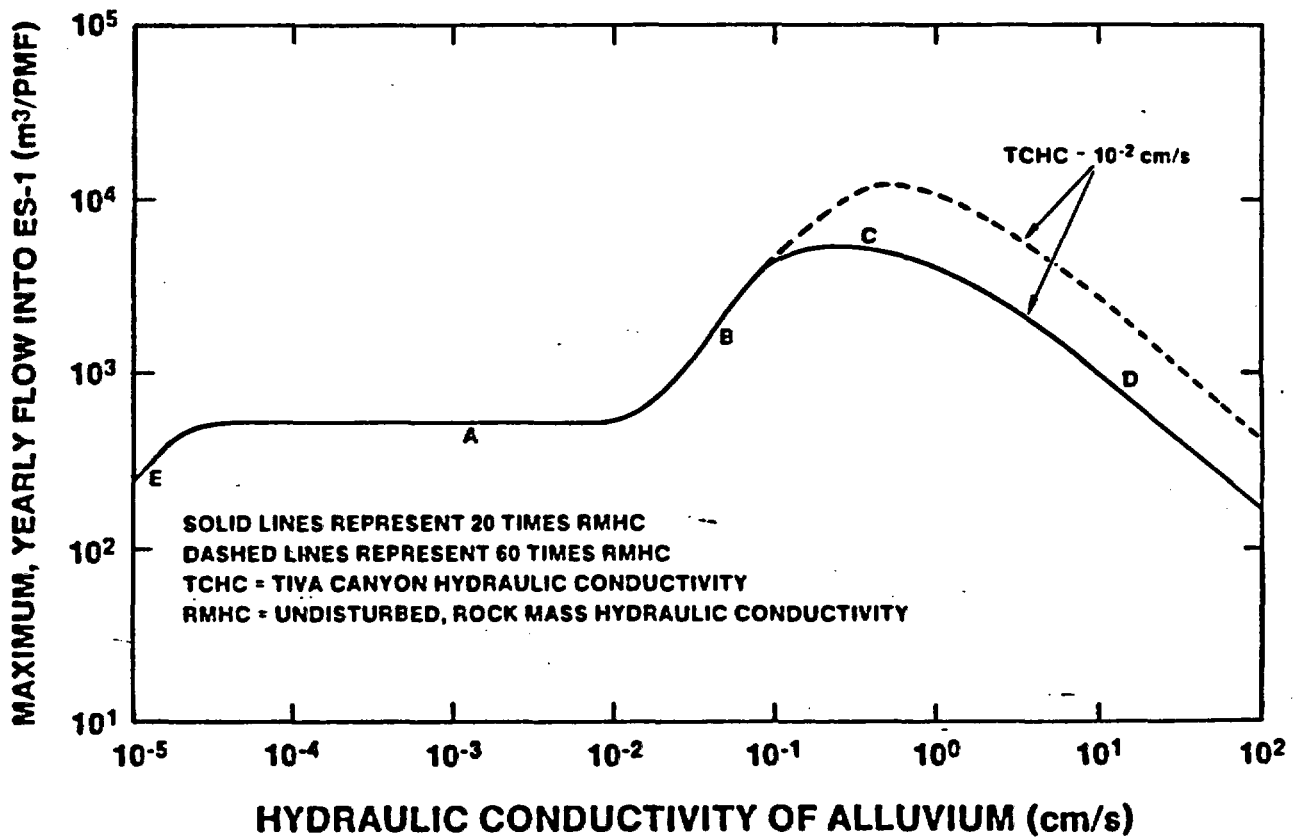
To explain these features of this curve, Figure B-2 is shown below. This curve shows the flow rates for the four flows considered in the model in Section 3.2.1, i.e., alluvial flow, Tiva Canyon flow, Dupuit (or radial) flow, and MPZ model flow. The curves in Figure B-2 that represent the Tiva Canyon and the MPZ model flow rate components used in the calculation of flow into ES-1. When the saturated alluvial hydraulic conductivity is less than the saturated hydraulic conductivity of the underlying Tiva Canyon member, it is assumed that the rate of vertical infiltration into the Tiva Canyon member is equal to the vertical infiltration rate of water leaving the alluvium. When the hydraulic conductivity of the Tiva Canyon is less than the hydraulic conductivity of the alluvium, the vertical infiltration into the Tiva Canyon is equal to the vertical infiltration rate into the Tiva Canyon member. (In both instances the gradient of flow vertically downward in the alluvium and the Tiva Canyon member is conservatively assumed equal to one.)

DRAFT

The flow through the MPZ and the shaft fill is assumed to be dependent on the saturated, hydraulic conductivity of the Tiva Canyon member. Therefore, the MPZ model flow rate is constant for a single value of Tiva Canyon hydraulic conductivity.

The alluvial flow was described in Section 3.2.1 as being parallel or near-parallel to the bedrock-alluvium interface. The alluvial flow rate as computed in this report is dependent on the hydraulic conductivity of the

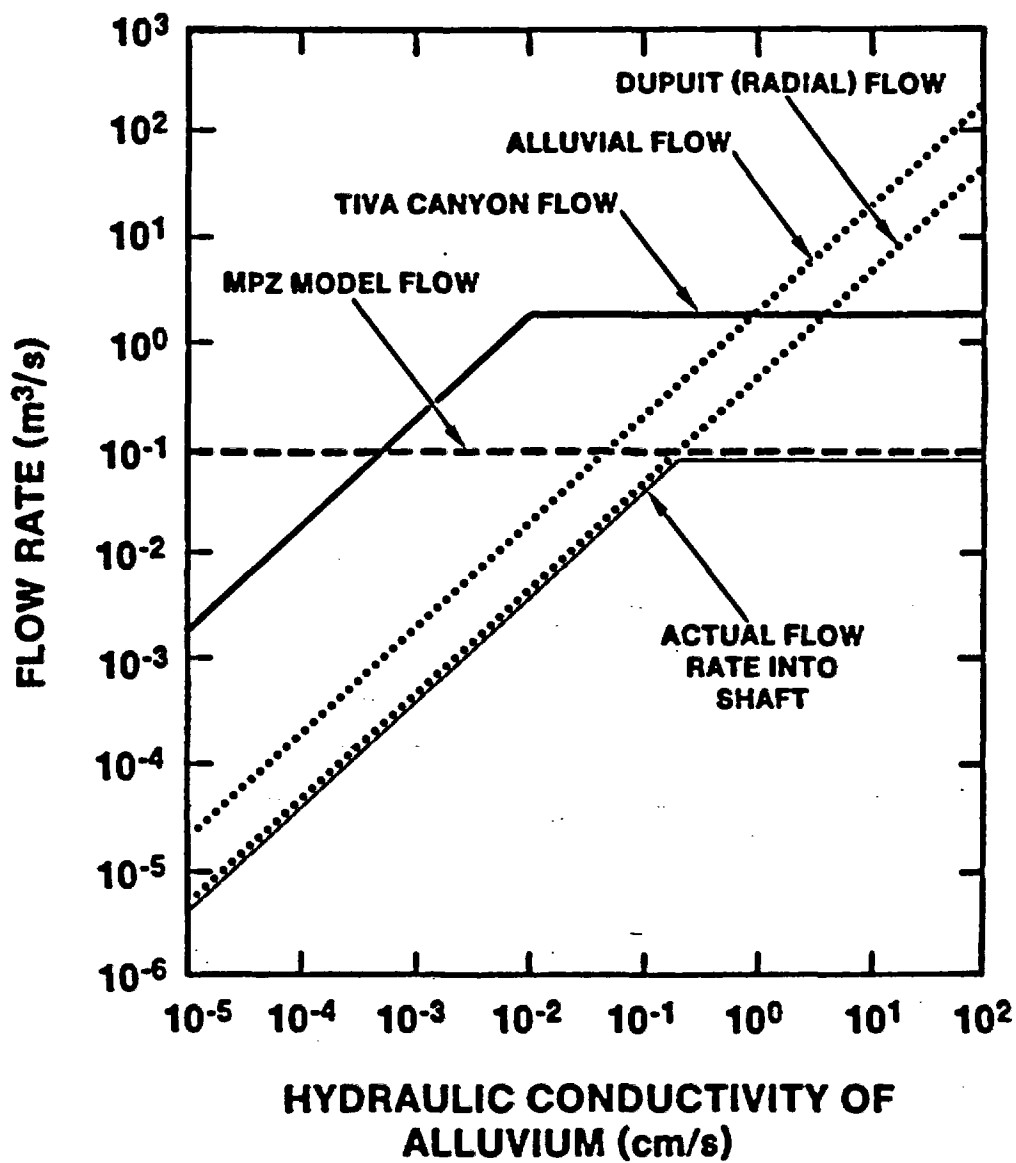
DRAFT



DRAFT

Figure B-1. Estimated Volumes of Water Entering ES-1 (PMF, Shaft Fill Conductivity = 10⁻² cm/s, Excavated Shaft Diameter 4.42 m)

DRAFT



DRAFT

Figure B-2. Approximation of Flow Rates for Flows Used in the Model Presented in Section 3.2 (Saturated, Hydraulic Conductivity Assumed to be 10⁻² cm/s)

DRAFT

alluvium as well as the area of the alluvium that is fully saturated. The radial (Dupuit) flow rate towards the shaft is dependent on the hydraulic conductivity of the alluvium and the height of alluvium above the bedrock alluvium contact that is saturated at any given time. Because the area through which the alluvial flow occurs and the height of saturated alluvium above the bedrock-alluvium contact vary with time, a representative area for alluvial flow and a representative height of saturated alluvium are selected to illustrate how the alluvial flow rate and the radial (Dupuit) flow rate vary with the saturated hydraulic conductivity of the alluvium.

In Figure B-1, the segment of the curve defined as "A" can be explained as follows. The alluvial and Tiva Canyon flows represent flows that do not enter the shaft and MPZ. Therefore, in the "A" portion of Figure B-1, the flow into the shaft and MPZ model is the lesser of the two flows, i.e., the radial (Dupuit) flow and the MPZ model flow (see Section 3.2.1). The nonshaft and MPZ flow is comprised of the Tiva Canyon and the alluvial flow.

The relationship between these various flows and the total flood volume can be described by the following water balance equation:

substituting the equations present in Section 3.2.1.

$$V_{pmf} = V_s + V_{tc} + V_a \quad (B-1)$$

where V_{pmf} = cumulative flow for the PMF
 V_s = cumulative flow down the shaft
 V_{tc} = cumulative infiltration in the Tiva Canyon formation,
 V_a = cumulative alluvial flow.

If the shaft flow is assumed to be governed by the radial Dupuit flow then:

$$V_{pmf} = \frac{\pi K_{all} (H - H_o)^2}{2n \frac{R}{r}} \cdot t + K_{tc} A_{tc} \cdot t + K_{all} i A_{all} \cdot t \quad (B-2)$$

DRAFT

DRAFT

where K_{tc} = Tiva Canyon hydraulic conductivity,
 K_{all} = alluvial hydraulic conductivity
 t = time
 i = alluvial gradient,
 R = outer radius,
 r = inner radius,
 A_{all} = alluvial area, and
 A_{tc} = Tiva Canyon area.

Therefore, if it is assumed that the Tiva Canyon has a saturated hydraulic conductivity value of 10^{-2} cm/s, and the range of alluvial hydraulic conductivity is from 10^{-5} to 10^{-2} cm/s for (segment A) of Figure B-1, then the Tiva Canyon flow will be controlled by the rate of flow vertically through the alluvium. Equation B-3 can then be written as ($10^{-5} \leq K_{all} \leq 10^{-2}$):

$$V_{pmf} = \frac{\pi K_{all} (H - H_o)^2}{\ln \frac{R}{r}} \cdot t + K_{all} A_{tc} t + K_{all} i A_{all} t \quad (B-3)$$

Assuming constant geometry, Equation B-3 can be simplified further to several constant values.

$$C_1 = C_2 t K_{all} + C_3 K_{all} t + C_4 K_{all} t \quad (B-4)$$

where $C_1 = V_{pmf}$
 $C_2 = \frac{\pi (H - H_o)^2}{\ln \left(\frac{R}{r}\right)}$
 $C_3 = A_{tc}$
 $C_4 = i A_{all}$

Because all flows are occurring over the same time period, this equation can be further simplified as:

$$C_1 = C_2 t K_{all} + K_{all} t C_5 \quad (B-5)$$

$$C_1 = K_{all} t (C_2 + C_5) \quad (B-6)$$

DRAFT

DRAFT

where $C_5 = C_3 + C_4$ and $10^{-5} \leq 10^{-2}$.

The term $C_2 t K_{all}$ represents shaft plus MPZ flow and the term $K_{all} t C_5$ represents nonshaft plus MPZ flow. In the equation, there are only two variables, " K_{all} " and " t ." For this relation to be correct, " K_{all} " and " t " are inversely proportional to each other. Further, for any " K_{all} " and " t " combination, the flow into the shaft and MPZ and the nonshaft plus MPZ flow will also be constant. Therefore, the flows between 10^{-5} cm/s and 10^{-2} cm/s for the alluvium is constant. The reason for the lower flow in the range of 10^{-5} to 2×10^{-5} cm/s) is the fact that when the alluvium has a low saturated hydraulic conductivity the time to drain the water from the modelled area is greater than one year. The values plotted on Figure B-1 are yearly inflows.

As the saturated hydraulic conductivity becomes greater than 10^{-2} cm/s the flow rate into the Tiva Canyon can be no greater than the product of the hydraulic conductivity of the Tiva Canyon Member (K_{tc}) or (K_{all}), whichever is lower and the cross-sectional area (A_{tc}). The term in Equation B-4 " $C_3 K_{all} t$ " that describes the Tiva Canyon flow rate no longer applies. The Tiva Canyon flow rate is constant and equal to " $C_3 K_{tc} t$." As the hydraulic conductivity of the alluvium increases between 10^{-2} cm/s to about 2×10^{-1} cm/s on Figure B-1 (Segment B), the Dupuit and alluvial flows will increase but the Tiva Canyon flow remains constant. Therefore, the combined nonshaft plus MPZ flow is constant during a greater and greater proportion as compared to the flow entering the shaft and MPZ. This explains the constantly increasing slope over segment B.

Once the peak "C" is reached on Figure B-1, there is a new factor to consider. The Dupuit flow will no longer dominate the flow into the shaft and MPZ. Rather, the flow rate described by the MPZ model controls flow. This flow rate is constant from 2×10^{-1} cm/s to 100 cm/s as indicated in Figure B-2. However because the nonshaft plus MPZ flow is increasing (due to the increasing alluvial flow) and subsequently the flow nonshaft plus MPZ flow is also increasing, the proportion of total flow going into the shaft and MPZ flow is proportionally decreasing. This phenomena describes the decreasing flow into the shaft and MPZ, or Segment D of Figure B-1. An

DRAFT

DRAFT

additional consideration that contributes to the decreasing flow in Segment D is the fact that the time to drain the PMF volume becomes less and less as the alluvial hydraulic conductivity becomes greater and hence the alluvial flow becomes greater. This effect is very noticeable when the alluvial flow becomes greater than the Tiva Canyon flow, i.e., at about 7×10^{-1} cm/s (alluvial conductivity).

DRAFT

DRAFT

APPENDIX C

The Density Method As Applied To Flow Through A Porous Media

This appendix provides detailed assumptions used in the convective air transport analysis. The assumptions are used to develop a formula for the convective flux rate which may be compared with flux rate relationships for convective transport through a porous media. A discussion of the development of thermal instability and convective air transport is also presented.

In developing the model the following assumptions are made:

1. Darcy's Law is valid

The resistance to air flow through open or backfilled drifts may be characterized as either laminar or turbulent. In turbulent flow, resistance is nonlinearly related to potential. In laminar flow, resistance is linearly related to potential, and flow may be calculated using Darcy's law.

The results of the analyses were used to check the validity of Darcy's law by calculating the Reynolds number from the air velocity or specific discharge, air kinematic viscosity, and characteristic dimension. For laminar flow through backfill, the characteristic dimension is the mean grain diameter, and Darcy's law is valid as long as the Reynolds number does not exceed a value between 1 and 10 (Freeze and Cherry, 1979, p. 73). The calculated Reynolds number was within the specified limits and the assumption of head loss varying linearly with flow rate was found to be justified.

2. Air temperatures in the shaft are the same as in the adjacent rock

Convective air flow through a heated repository will involve a complex coupling of heat transfer from the rock to the air, which will tend to drive air flow, and cooling of the rock by passage of the air, which will tend to reduce the driving mechanism. In the modeling which follows, the effects of cooling of the rock are ignored. The air is assumed to be at the same temperature as the adjacent rock at all points in the repository, including the shafts.

Intuitively, this simplified approach is most valid for the case of a backfilled repository in which air flows relatively slowly and temperatures are able to equilibrate. The faster the air flow, the greater the volume of air moving through the repository, and it is more likely that the rock will be cooled to the extent that convection slows down. A converse effect to rapid air flow

DRAFT

could occur if the air flow is not sufficient to cool the rock in the repository significantly. Flow through the repository would be greater than that calculated using our simplified approach if air in the exit shafts (or rock) is not cooled by heat transfer to the rock. In this case, there is a potential for the repository to act as a heat engine. The driving pressure could then be about three times higher than that calculated with the assumption of equilibrated temperatures. This higher driving pressure occurs, however, because air is expelled at the ground surface at the same temperature as the temperature of the repository rooms, a condition which is intuitively over-conservative.

3. Air flow is incompressible and the air is dry

Since convective transport evolves from air buoyancy effects dependent on temperatures, thermal properties such as air density and air viscosity will change through the circuit. In reality, flow is compressible with the actual resistance to mass flow rate dependent on density and viscosity. In the analyses presented in this report, air compressibility effects on fluid flow are ignored for reasons of simplification. This assumption is considered to be reasonable given that the pressures involved are small (i.e., <0.1 psi). According to Hartman (1982, p. 160), compressibility effects may be ignored for mine static head pressure drops of less than 5 kPa (0.72 psi) or where differences in elevation are less than 430 m.

Convective transport can, in general, involve both the transport of air and water vapor. The development of high temperatures at the repository horizon will result in drying and lowering of moisture content. It is thus assumed that the air may be dry at the time at which peak temperatures are reached. This assumption is conservative because the effect of adding moisture to the convective flow will be to increase the work required to lift the air to the surface and to thus reduce flow rates.

4. Air circulation occurs along specified paths

The model assumes that a particular path for air circulation (Mechanism A or B; Figure 3-19) is established and that flow is one-dimensional through either shaft or ramp backfill, open drifts, or through damaged or undamaged tuff. The model ignores the development of secondary circulation currents that might develop in the host rock above or below the repository away from the waste containers.

The assumptions presented above may be used to derive an expression for flux rate due to convective circulation.

The draft pressure may be calculated by the density method for the circuit (Hartman, 1982):

DRAFT

$$\Delta p = (\gamma_1 - \gamma_0)L \tag{C-1}$$

DRAFT

where

- γ_i - Mean air density of an inlet shaft (pcf),
- γ_o - Mean air density of an outlet shaft (pcf), and
- L - Height of the shaft (ft).

If it is assumed that the mean temperatures T_i and T_o correspond to the densities γ_i and γ_o respectively, then the following relationship may be used to express volumetric thermal expansion effects (Bear, 1976 p. 655):

$$\gamma_i = \gamma_o [1 - \beta(T_o - T_i)] \quad (C-2)$$

where

- β - Coefficient of volumetric thermal expansion ($^{\circ}\text{C}^{-1}$),
- T_i - Mean temperature at density γ_i ($^{\circ}\text{C}$), and
- T_o - Mean temperature at density γ_o ($^{\circ}\text{C}$).

Substituting Equation (C-2) into Equation (C-1), the draft pressure differential is

$$\Delta p = -\beta (T_o - T_i) L \gamma_o \quad (C-3)$$

Expressing the above reaction as a potential difference, the following expression is obtained:

$$\Delta h = \frac{\Delta p}{\gamma_o} = -\beta (T_o - T_i) L \quad (C-4)$$

Substitution of the change in potential (head loss) into Darcy's Law is used to calculate the flux rate. If it is assumed that the resistance to flow occurs in backfilled shafts with the underground repository drifts open, then:

$$v = -K'_e \cdot \frac{\Delta h}{2L} = \frac{-K'_e (T_o - T_i) \beta}{2} \quad (C-5)$$

DRAFT

DRAFT

where K'_e equals the air conductivity and V equals the Darcy flux rate.

The actual velocities through the backfilled shafts are (Freeze and Cherry, 1979 p. 71):

$$V_a = \frac{V}{n} = \frac{-K'_e (T_o - T_i) \beta}{2n} \quad (C-6)$$

where

V_a - Actual velocity, and
 n - Porosity.

The air conductivity K'_e may be expressed as (Freeze and Cherry, 1979 p. 27):

$$K'_e = \frac{\rho g}{\mu} k \quad (C-7)$$

where

k - Intrinsic permeability,
 ρ - Mass density,
 g - Acceleration constant, and
 μ - Absolute viscosity.

Substituting Equation (C-8) into Equation (C-7), the following relationship is obtained:

$$V_a = \frac{-\rho g k \beta (T_o - T_i)}{2n\mu} \quad (C-8)$$

This derived relationship is similar in form to the relationship presented by Bear (1976 p. 655) for convective transport through a porous media. The physical interpretation of the above relationship is that viscous forces just balance buoyant forces for the circulation occurring through the network of underground shafts and entries and surrounding rock. This analysis indicates that calculation of draft pressures by the density

DRAFT

DRAFT

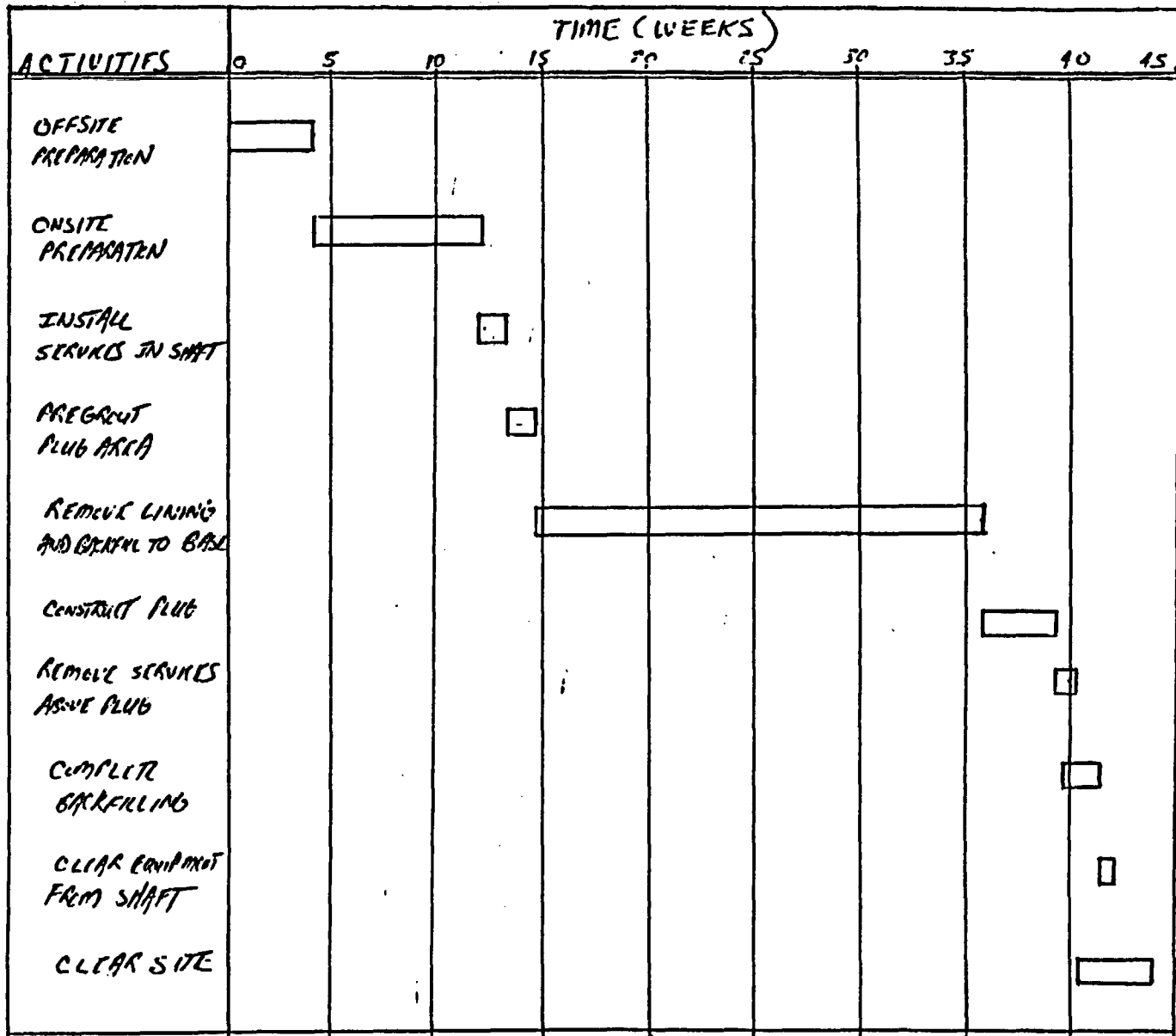
method and head losses over a circuit by Darcy's Law is similar to the evaluation of convective transport through a porous media. Therefore, the density method for calculating air flow rates due to convective transport as presented in Section 3.3 is appropriate.

DRAFT

APPENDIX D

Estimated Construction Schedule and Costs

This appendix presents estimated construction costs and schedule for the complete removal of the liner from the ES and the construction of a single anchor to bedrock plug/seal. The estimated schedule, with a duration of 44 weeks, is presented in Figure D-1. The liner is assumed to be broken by a nonexplosive expansive demolition agent. As discussed in Section 4.3, it is estimated that the use of hydraulic splitters or drilling and blasting would require a similar amount of time, while the use of hand-held pneumatic splitters would require more time. The estimated overall site costs are presented in Table D-1 and assume no existing shaft services at the time of liner removal. It is estimated that \$3.5 million is required for all activities, with approximately 60% of these costs incurred for liner removal and backfilling. The estimated costs for pregrouting and plug construction are \$134,000 and \$380,000, respectively.



DRAFT

FIGURE D-1 CONSTRUCTION SCHEDULE

D-2

**TABLE D-1
OVERALL SITE COST ESTIMATE**

	WEEKS	Offsite 4.0	Onsite 8.0	Shaft Services 1.0	PregROUT Plug 1.5	Remove Lining and Backfill 22.5	Construct Plug 3.5	Shaft Services 0.5	Clear Shaft Top 1.0	Clear Site 2.5	Follow-up Reports 6.0	Total
LABOR		56,800	223,600	52,500	78,800	1,437,000	241,800	14,600	29,100	82,800	46,200	2,263,200
EQUIPMENT												
Common		1,000	177,200	48,600	13,600	57,000	30,500	5,100	7,900	16,200		357,100
Grouting					23,400		10,700					34,100
Drilling					1,900	8,700	4,400					15,000
Mucking						6,500	3,500					10,000
Subtotal		1,000	177,200	48,600	38,900	72,200	49,100	5,100	7,900	16,200		416,200
MATERIALS												
Concrete			10,600				32,500					43,100
Grouting					2,200		300					2,500
Subtotal			10,600		2,200		32,800					45,600
CONSUMABLES												
Common		7,400	26,200	6,600	9,900	182,900	30,400	1,800	3,600	9,000	6,000	283,800
Grouting												
Drilling					900	87,200	4,900					93,000
Mucking						8,400	400					8,800
Subtotal		7,400	26,200	6,600	10,800	278,500	35,700	1,800	3,600	9,000	6,000	385,600

DRAFT

**TABLE D-1
OVERALL SITE COST ESTIMATE (Continued)**

	WEEKS	Offsite 4.0	Onsite 8.0	Shaft Services 1.0	PregROUT Plug 1.5	Remove Lining and Backfill 22.5	Construct Plug 3.5	Shaft Services 0.5	Clear Shaft Top 1.0	Clear Site 2.5	Follow-up Reports 6.0	Total
POWER												
Diesel			3,200	400	600	8,400	1,400	200	400	1,000		15,600
Electrical												
Bristar						306,000	12,000					318,000
Explosives												
Hydraulic Breaker												
Subtotal			3,200	400	600	314,400	13,400	200	400	1,000		333,600
OTHER												
Office		1,700	6,100	1,500	2,300	14,100	7,100	400	800	2,100	1,400	37,400
Freight			35,000							25,000		60,000
Subtotal		1,700	41,100	1,500	2,300	14,100	7,100	400	800	27,100	1,400	97,500
TOTAL		66,900	481,900	109,600	133,600	2,116,200	379,900	22,100	41,800	136,100		3,541,700

DRAFT

D-4

DRAFT

APPENDIX E

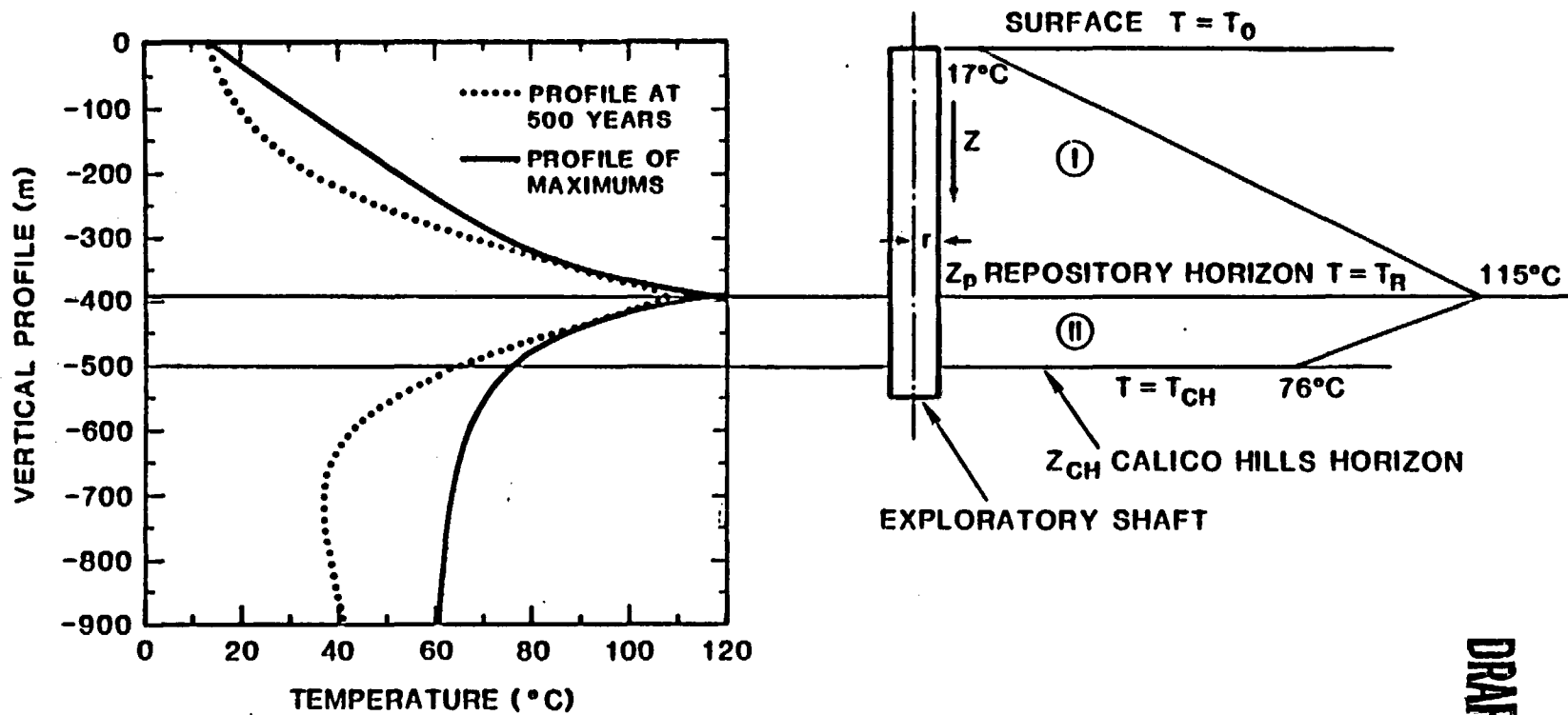
Calculation of Temperature of Water From the Base of the Exploratory Shafts

To estimate temperatures effluent from the base of the ES, calculations presented below were performed to bound the upper limit of water temperature. Since deleterious reactions in the Calico Hills may occur only when the water temperature exceeds some threshold, upper-bound calculations are appropriate in view of the result, to be shown below, that any effluent from the base of the ES is considerably less than the above-mentioned threshold temperature.

In these calculations, we assume that water flow through the ES and its surrounding MPZ is modeled by the flow of water vertically downward through a cylinder whose surface temperature varies to model the maximum global temperature field calculated by Blandford [A. R. Morales, 1985]. Consistent with the bounding nature of these calculations, no local cooling of the cylinder surface is permitted so that maximum effluent temperatures are obtained.

Two separate water flow scenarios have been considered. These are the anticipated yearly influx of $44.2 \text{ m}^3/\text{year}$ and the PMF event of $20,000 \text{ m}^3/\text{year}$. Because the 500-year flood is less severe than the PMF and the PMF results in very small temperature increases, the 500-year flood is not considered here. Consequently, for these calculations, we assume that the rock mass temperature near the ES and hence the cylinder surface temperature increases in a linear fashion from 17°C (average ground-water temperature) to 115°C (average formation temperature at the repository horizon). Below the repository, we assume that the temperature decreases linearly to 76°C at the top margin of the Calico Hills unit. This model is illustrated in Figure E-1.

The thermal response of water flowing through the ES is described by the conservation-of-energy equation, which takes the form



DRAFT

Figure E-1. Model Used to Calculate Water Temperature Elevation of Water Entering Shaft

DRAFT

$$U_Z \frac{\partial T}{\partial Z} - \alpha \frac{1}{r} \frac{\partial}{\partial r} \left(r \frac{\partial T}{\partial r} \right) \quad (E-1)$$

where α is the thermal diffusivity of the combination of water and rock within the ES and the MPZ, U_Z is the average flow velocity, T is the temperature, r is the radial distance from the shaft centerline and Z is vertical distance downward as shown in Figure E-1.

This equation is solved in two regions, I and II, where region I is the zone above the repository and region II is the zone below the repository. The boundary conditions for region I are

$$\begin{aligned} Z_I = 0 & & T_I = T_o \\ r_I = R_o & & Z_I > 0 & & T_I = T_o + (T_R - T_o) \frac{Z_I}{Z_R} \end{aligned} \quad (E-2)$$

and for region II are

$$\begin{aligned} Z_{II} = Z_R & & T_{II} = T_R \text{ for all } r \\ \text{and } r_{II} = R_o, & & Z_{II} > Z_R & & T_{II} = T_R + (T_{CH} - T_R) \frac{(Z_{II} - Z_R)}{(Z_{CH} - Z_R)} \end{aligned} \quad (E-3)$$

These equations may be nondimensionalized, where $\theta_I = \frac{T_I - T_o}{T_R - T_o}$,

$r_I = r'_I R_o$, $Z_I = Z'_I Z_R$ and $K_I = \frac{\alpha}{U_Z} \frac{Z_R}{R_o^2}$ in region I to give

$$\frac{\partial \theta_I}{\partial Z'_I} - \frac{K_I}{r'_I} \frac{\partial}{\partial r'_I} \left(r'_I \frac{\partial \theta_I}{\partial r'_I} \right) \quad (E-4)$$

$$\begin{aligned} Z'_I = 0 & & \theta_I = 0 \\ r'_I = 1 & & \theta_I = Z'_I \end{aligned}$$

In region II, we similarly nondimensionalize, where $\theta_{II} = \frac{T_{II} - T_R}{T_{CH} - T_R}$,

DRAFT

$$r_{II} = r_{II}' R_o, \quad z_{II} = z_{II}' (z_{CH} - z_R) + z_R \text{ and } K_{II} = \frac{\alpha}{U_z} \frac{(z_{CH} - z_R)}{R_o^2}, \text{ to give}$$

$$\frac{\partial \theta_{II}'}{\partial z_{II}'} = \frac{K_{II}'}{r_{II}'} \frac{\partial}{\partial r_{II}'} \left(r_{II}' \frac{\partial \theta_{II}'}{\partial r_{II}'} \right), \quad (E-5)$$

$$\begin{aligned} z_{II}' &= 0 & \theta_{II} &= 0 \\ r_{II}' &= 1 & \theta_{II}' &= z' \end{aligned}$$

Equations E-4 and E-5 are identical except that the nondimensional diffusivities are slightly different. Equations E-4 and E-5 are solved analytically in (Carslaw and Jaeger, 1959, p. 201), and involve a series of Bessel functions that converge very rapidly to their solution.

The solution is

$$\theta = \left(z' - \frac{1-r'^2}{4K} \right) + \frac{2}{K} \sum_{n=1}^{\infty} e^{-K\alpha_n^2 z'} \frac{J_0(r'\alpha_n)}{\alpha_n^3 J_1(\alpha_n)} \quad (E-6)$$

where α_n are the nonzero roots of

$$J_0(\alpha) = 0 \quad (E-7)$$

To solve this equation for the average fluid temperature entering the Calico Hills, we should apply Equation E-6 in both regions I and II. The solution obtained in region I would then be used as a starting temperature for region II. However, since our problem is to estimate the maximum fluid temperature entering the Calico Hills, a convenient simplification is to assume that the fluid temperature exiting region I and entering region II is in thermal equilibrium with the formation at the repository horizon. If lower temperature water were to enter region II, then the water temperature exiting region II would be correspondingly reduced. Hence, we now consider the solution in region II with the assumption that T_R is the rock temperature computed by Blandford. Hence, T_R is taken to be 115°C and T_{CH} is 76°C.

DRAFT

The solution to Equation E-6 for region II is a function of r' , Z' , and K . At the entrance to the Calico Hills, where Z' is 1, we are interested in the average fluid temperature, which is

$$\theta_{AVG} = \frac{\int_0^1 \theta(r') 2\pi r' dr'}{\int_0^1 2\pi r' dr'} = 2 \int_0^1 \theta(r') r' dr' \quad (E-8)$$

The variation in dimensionless fluid temperature with radius is shown in Figure E-2 for K varying between 0.5 and 10.

The fluid temperature profile more closely approaches the formation temperature as the dimensionless thermal diffusivity increases (Figure E-3). Hence, the average fluid temperature at the upper margin of the Calico Hills may be represented solely as a function of K (Figure E-3).

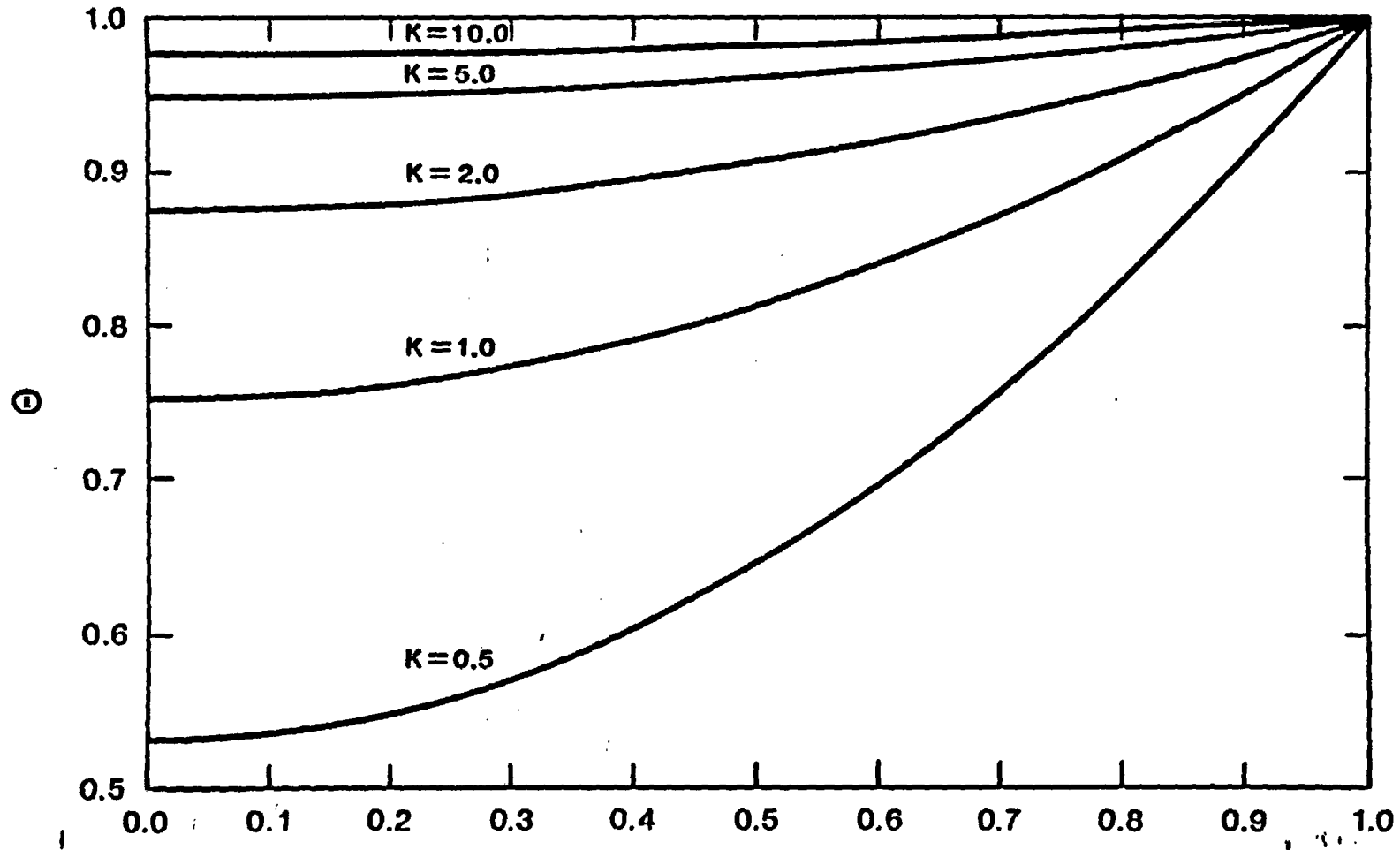
In this figure, the average dimensionless fluid temperature increases as the dimensionless thermal diffusivity increases and the average dimensionless fluid temperature is greater than 0.9 for values of K exceeding 1. When θ_{AVG} is equal to 0.9, the actual fluid temperature is 79.9°C. For the actual fluid temperature to be less than 90°C, θ_{AVG} must exceed 0.64, which occurs for K greater than 0.28.

In the estimation of the dimensionless thermal diffusivity,

$$K = \frac{\alpha}{U_Z} \frac{(Z_{CH} - Z_R)}{R_o^2} \quad (E-9)$$

a range of values are considered for α and U_Z , while R_o , and $Z_{CH} - Z_R$ are defined by the design of the ES. The values of these parameters for two extreme conditions are presented in Table E-1.

DRAFT



DRAFT

Figure E-2. Dimensionless Temperature (Θ) Versus Radius (r) for Different Dimensionless Thermal Diffusivities (K)

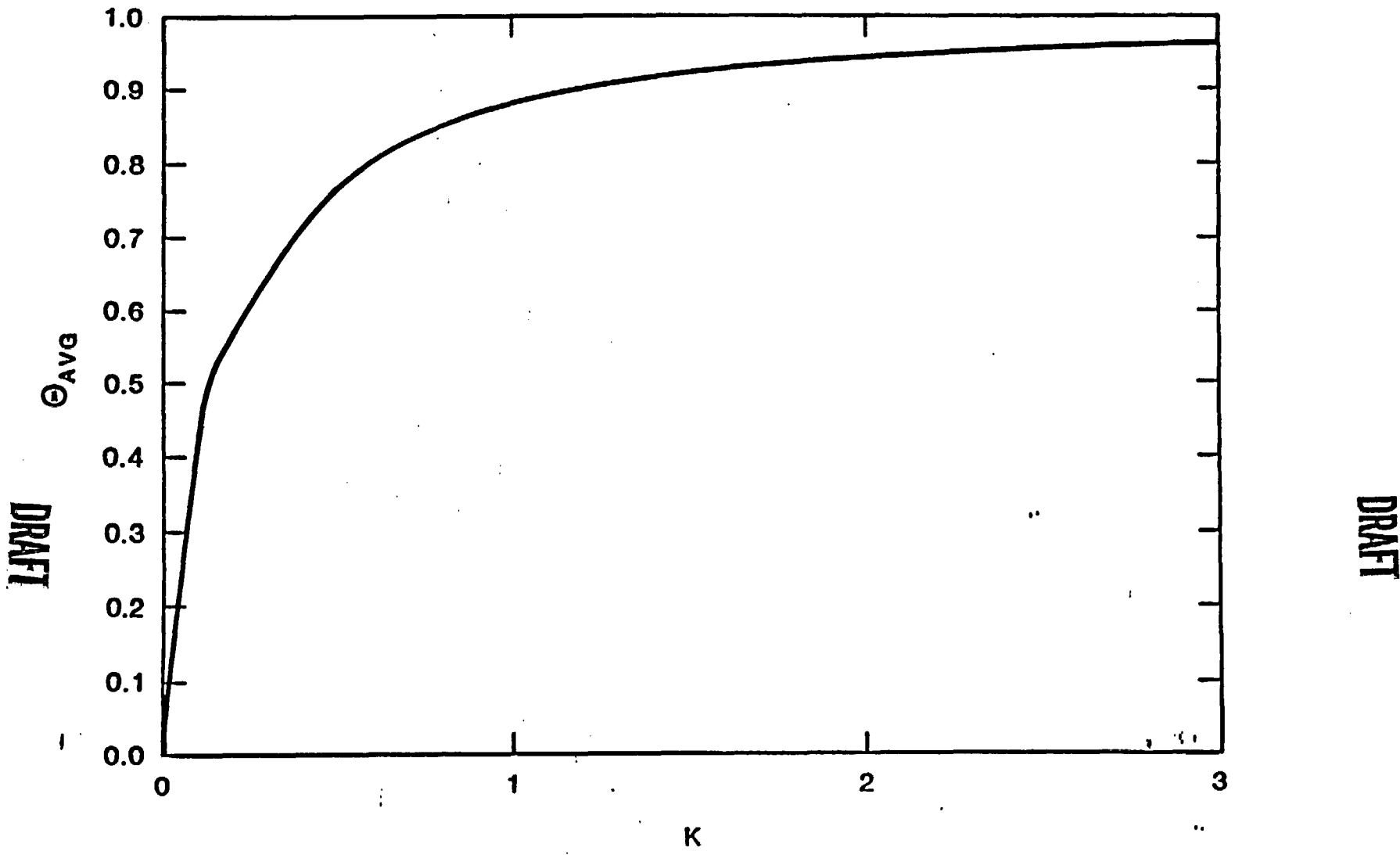


Figure E-3. Average Dimensionless Temperature (Θ_{AVG}) Versus Dimensionless Thermal Diffusivity (K)

DRAFT

Table E-1. Values of Parameters Used to Estimate the Dimensionless Thermal Diffusivity and Resultant Average Dimensionless Temperatures

Case	$Z_{CH} - Z_R$ (m)	R_o (m)	U_z (cm/s)	α (cm ² /s)	K	θ_{AVG}
Expected flow	116.7(383 ft)	4.42(14.5 ft)	2.4×10^{-6}	.0078	192	1.00
Probable maximum flooding	116.7(383 ft)	4.42(14.5 ft)	6×10^{-1}		30	3 .96

For both of these cases, the shaft radius is assumed to encompass the MPZ. By selecting this larger radius, the value of K assumes a conservatively smaller value. In addition, the permeability of the MPZ is assumed to be 60 times the conductivity of the Tiva Canyon. The fluid velocity for the expected flow condition corresponds to 44.2 m³/year, while the maximum fluid velocity is taken to be equivalent to the worst-case hydraulic conductivity assumed for the MPZ. The thermal diffusivity is computed by one of two possible methods. When the fluid velocity is very low, as in the expected flow case, a volumetric average of the thermal diffusivity of the rock and of the intergranular water is computed. At large fluid velocities, the thermal diffusivity is determined by convection processes and is computed by

$$\alpha = \frac{2U_z d_p}{\epsilon} \quad [\text{Levenspiel, 1972, p. 282}] \quad (\text{E-10})$$

where d_p is the effective distance between fractures, and other terms are as defined previously. We assume 16 fractures/meter to give the smallest possible d_p within the MPZ.

As may be seen in Table E-1, the value of K even in the highest flow case of the PMF is large enough so that the average dimensionless temperature is 0.96. In actual temperature units, the maximum fluid temperature is expected to be 77.6°C, while the more normal expected flow condition results in a fluid temperature of 76.03°C.

DRAFT

DRAFT

APPENDIX F

Comparison of Data Used in This Report With The
Reference Information Base (RIB)

The following notes are used throughout this appendix:

- (A) No section found in RIB applicable to these parameters.
- (B) Section identified in the RIB, but values not found.

DRAFT

APPENDIX F
COMPARISON OF DATA USED IN THIS REPORT WITH THE REFERENCE INFORMATION BASE (RIB)

PARAMETER	SECTION	PAGE #	REPORT VALUE	RIB VALUE	RIB SECTION	EXPLANATION
MEN AND MATERIALS SHAFT SUMP	2.0	2-1	24 m	NONE	2.2.7	(B)
EMPLACEMENT EXHAUST SHAFT SUMP	2.0	2-1	3 m	NONE	2.2.7	(B)
EXPLORATORY SHAFT SUMP	2.0	2-1	140 m	NONE	2.2.7	(B)
EXPLORATORY SHAFTS - DEPTH	2.1	2-2	1480 ft (ES-1) and 1020 ft (ES-2)	1480 ft (ES-1) and 1020 ft (ES-2)	2.2.8	
ALUVIAL THICKNESS	2.1	2-4	6.5 TO 10 m	10 m	1.3.1.1	
LOCATIONS OF ES-1 AND ES-2	2.1	2-4	FIGURE 2-2	NONE	2.2.7	(B)
EXCAVATED DIAMETERS OF ES-1 AND ES-2	2.2	2-5	4.3 m AND 4.3 m	14 ft AND 8 ft	2.2.6	EXCAVATED DIAMETER FOR ES-2 CHANGED FROM 8 ft TO 14 ft TO REFLECT RECENT PROJECT GUIDANCE.
FINISHED DIAMETERS OF ES-1 AND ES-2	2.2	2-5	3.7 m AND 3.7 m	3.7 m AND 1.8 m	2.2.6	FINISHED DIAMETER OF ES-2 RECENTLY CHANGED FROM 1.83 m TO 3.7 m
THICKNESS OF ES-1 AND ES-2 LINERS	2.2	2-5	0.3 m AND 0.3 m	1 ft AND 1 ft	2.2.6	
STRENGTH OF CONCRETE LINER	2.2	2-5	35 MPa	NONE		(A)
FRACTURE SPACING IN NONWELDED TUFF	3.1	3-2	80 cm to 200 cm	NONE	1.3.2.4.2.3	(B)
MINIMUM FRACTURE SPACING IN DENSELY, WELDED TUFF	3.1	3-3	6 cm	NONE	1.3.2.4.2.3	(B)

(A) NO SECTION FOUND IN RIB APPLICABLE TO THESE PARAMETERS.

(B) SECTION IDENTIFIED IN THE RIB, BUT VALUES NOT FOUND.

DRAFT

APPENDIX F
COMPARISON OF DATA USED IN THIS REPORT WITH THE REFERENCE INFORMATION BASE (RIB) (Continued)

PARAMETER	SECTION	PAGE #	REPORT VALUE	RIB VALUE	RIB SECTION	EXPLANATION
BLAST-DAMAGE ZONE EXTENT INTO ROCK FROM EDGE OF SHAFT	3.1	3-5	0.5 m TO 1.0 ^m	NONE	2.3	(B)
EXPECTED ENHANCEMENT OF PERMEABILITY OF ROCK MASS AROUND SHAFT	3.1	3-6, 3-8	20 TIMES THE PERMEABILITY OF UNDISTURBED ROCK MASS.	NONE	2.3	(B)
UPPER BOUND ENHANCEMENT OF PERMEABILITY OF ROCK MASS AROUND SHAFT	3.1	3-6, 3-8	40 TO 80 TIMES THE PERMEABILITY OF UNDISTURBED ROCK MASS.	NONE	2.3	(B)
SATURATED, HYDRAULIC CONDUCTIVITY OF SHAFT FILL	3.2.1.1	3-10	10 ⁻² cm/s	NONE	2.3	(B)
PROBABLE MAXIMUM FLOOD (PMF) CLEAR WATER VOLUME	3.2.1.2	3-17	159,000 m ³	NONE	1.17.1	(B)
EXCAVATED DIAMETER ASSUMED IN MPZ MODEL	3.2.1.2	3-14, 3-17	4.42 m	4.27 m	2.2.6	SLIGHT OVERBREAK ASSUMED IN MPZ MODEL.
RANGE OF THE SATURATED, HYDRAULIC CONDUCTIVITY FOR ALLUVIUM	3.2.1.2	3-17	10 ⁻⁵ TO 10 ² cm/s	NONE	—	(A)
RANGE OF THE SATURATED, HYDRAULIC CONDUCTIVITY OF THE BULK ROCK - TIVA CANYON MEMBER	3.2.1.3	3-18	10 ⁻⁵ TO 10 ⁻² cm/s	3.65 x 10 ⁵ mm/yr OR 1.2 x 10 ⁻³ cm/s	1.1.4.3	SINGLE VALUE GIVEN IN THE RIB
AVERAGE GRADE OF THE WATERCOURSE IN COYOTE WASH	3.2.1.2	3-18	0.16	NONE	—	(A)
POROSITY OF ALLUVIUM	3.2.1.2	3-18	0.30	NONE	—	(A)

- (A) NO SECTION FOUND IN RIB APPLICABLE TO THESE PARAMETERS.
(B) SECTION IDENTIFIED IN THE RIB, BUT VALUES NOT FOUND.

DRAFT

APPENDIX F
COMPARISON OF DATA USED IN THIS REPORT WITH THE REFERENCE INFORMATION BASE (RIB) (Continued)

PARAMETER	SECTION	PAGE #	REPORT VALUE	RIB VALUE	RIB SECTION	EXPLANATION
DRIFT LENGTH OF PROPOSED EXPLORATORY DRIFT IN CALICO HILLS UNIT	3.2.2.1	3-29	245 - 300 m	NONE	2.2.7	(B)
BULK, SATURATED HYDRAULIC CONDUCTIVITY OF TOPOPAH SPRING MEMBER AND TUFFACEOUS BEDS OF CALICO HILLS	3.2.2.2	3-31	1.2×10^{-3} cm/s	1.2×10^{-3} cm/s (OR 3.65×10^5 mm/yr) [TOPOPAH SPRING]	1.1.4.3	
	3.2.2.2	3-32	2.4×10^{-4} AND 10^{-3} cm/s	2.4×10^{-4} cm/s (OR 3.5×10^4 mm/yr) [CALICO HILLS]	1.1.4.3	
MANNING'S ROUGHNESS COEFFICIENT	3.2.4	3-39	0.060	NONE	—	(A)
PEAK TEMPERATURE AT THE REPOSITORY HORIZON	3.3.3.1	3-45	115°C	115°C	3.1.1.2	
TEMPERATURE AT THE INLET SHAFTS	3.3.3.1	3-45	13°C	54.9°F (OR 13°C)	1.11.1	
TOTAL CROSS-SECTIONAL ROOF AREA OF REPOSITORY (WASTE ROOMS, SUBMAINS, AND MAINS)	3.3.3.2	3-46	983,700 m ² (VERTICAL EMPLACEMENT) 486,000 m ² (HORIZONTAL EMPLACEMENT)	NONE	—	(A)
TOTAL THICKNESS OF WELDED UNITS ABOVE THE REPOSITORY	3.3.3.2	3-46	260 m	NONE	1.3.1.1.1	(B) VALUES OBTAINED FROM CALMA SYSTEM
TOTAL THICKNESS OF NONWELDED UNITS ABOVE THE REPOSITORY	3.3.3.2	3-46	40 m	NONE	1.3.1.1.1	(B) VALUES OBTAINED FROM CALMA SYSTEM

DRAFT

(A) NO SECTION FOUND IN RIB APPLICABLE TO THESE PARAMETERS.
(B) SECTION IDENTIFIED IN THE RIB, BUT VALUES NOT FOUND.

APPENDIX F
COMPARISON OF DATA USED IN THIS REPORT WITH THE REFERENCE INFORMATION BASE (RIB) (Continued)

PARAMETER	SECTION	PAGE #	REPORT VALUE	RIB VALUE	RIB SECTION	EXPLANATION
ASSUMED AIR CONDUCTIVITY OF NONWELDED PAINTERUSH TUFF UNIT	3.3.3.2	3-46	3×10^{-7} TO 3×10^{-5} m/min.	NONE	—	(A)
ASSUMED AIR CONDUCTIVITY OF TOPOPAH SPRING AND TIVA CANYON MEMBERS	3.3.3.2	3-46	3×10^{-7} TO 3×10^{-4} m/min.	NONE	—	(A)
INTERNAL AREA OF RAMP/SHAFTS						
- WASTE RAMP (HORIZONTAL EMPLACEMENT)	3.3.3.2	3-47	28.3 m ²	28.3 m ² (19-ft DIAMETER)	2.2.1.7 AND 2.2.8	CALCULATED FROM DATA IN RIB
- TUFF RAMP (HORIZONTAL EMPLACEMENT)	3.3.3.2	3-47	30.1 m ²	30.1 m ² (20-ft DIAMETER)	2.2.1.7 AND 2.2.8	CALCULATED FROM DATA IN RIB
- WASTE RAMP (HORIZONTAL EMPLACEMENT)	3.3.3.2	3-47	34.2 m ²	34.2 m ² (22-ft DIAMETER)	2.2.2.7 AND 2.2.8	CALCULATED FROM DATA IN RIB
- TUFF RAMP (VERTICAL EMPLACEMENT)	3.3.3.2	3-47	42.8 m ²	42.8 m ² (24-ft DIAMETER)	2.2.2.7 AND 2.2.8	CALCULATED FROM DATA IN RIB
- MEN-AND-MATERIALS SHAFT	3.3.3.2	3-47	29.2 m ²	29.2 m ² (20-ft DIAMETER)	2.2.8	CALCULATED FROM DATA IN RIB
- EMPLACEMENT EXHAUST SHAFT	3.3.3.2	3-47	29.2 m ²	29.2 m ² (20-ft DIAMETER)	2.2.8	CALCULATED FROM DATA IN RIB
- ES-1	3.3.3.2	3-47	10.5 m ²	10.5 m ² (12-ft DIAMETER)	2.2.8	CALCULATED FROM DATA IN RIB
- ES-2	3.3.3.2	3-47	10.5 m ²	10.5 m ² (6-ft DIAMETER)	2.2.8	CALCULATED FROM DATA IN RIB

- (A) NO SECTION FOUND IN RIB APPLICABLE TO THESE PARAMETERS.
(B) SECTION IDENTIFIED IN THE RIB, BUT VALUES NOT FOUND.

DRAFT

APPENDIX F
COMPARISON OF DATA USED IN THIS REPORT WITH THE REFERENCE INFORMATION BASE (RIB) (Continued)

PARAMETER	SECTION	PAGE #	REPORT VALUE	RIB VALUE	RIB SECTION	EXPLANATION
LENGTH OF RAMP/SHAFTS TO REPOSITORY HORIZON						
- WASTE RAMP	3.3.3.2	3-47	2012 m	6603 ft (OR 2012 m)	2.2.8	—
- TUFF RAMP	3.3.3.2	3-47	1410 m	4627 ft (OR 1410 m)	2.2.8	—
- MEN-AND-MATERIALS SHAFT	3.3.3.2	3-47	314 m	1030 ft (OR 314 m)	2.2.8	—
- EMPLACEMENT EXHAUST SHAFT	3.3.3.2	3-47	314 m	1030 ft (OR 314 m)	2.2.8	—
- ES-1	3.3.3.2	3-47	311 m	1020 ft (OR 311 m)	2.2.8	—
- ES-2	3.3.3.2	3-47	311 m	1020 ft (OR 311 m)	2.2.8	—
HYDRAULIC CONDUCTIVITY OF SHAFT FILL	3.3.3.2	3-48	10^{-4} TO 100 cm/s	NONE	—	(A)
THUNDERSTORM	3.4.2.2	3-62				
- AMPLITUDE			20 mbar	18.96 mbar (MAXIMUM VALUE)	1.11.4	VALUE INFERRED FROM DATA PRESENTED IN RIB
- PERIOD			5 days	NONE		(A)
TORNADO	3.4.2.2	3-62				
- AMPLITUDE			135 mbar	NONE	—	(A)
- PERIOD			1 minute	NONE	—	(A)

(A) NO SECTION FOUND IN RIB APPLICABLE TO THESE PARAMETERS.

(B) SECTION IDENTIFIED IN THE RIB, BUT VALUES NOT FOUND.

DRAFT

APPENDIX F
COMPARISON OF DATA USED IN THIS REPORT WITH THE REFERENCE INFORMATION BASE (RIB) (Continued)

PARAMETER	SECTION	PAGE #	REPORT VALUE	RIB VALUE	RIB SECTION	EXPLANATION
SEASONAL FLUCTUATION	3.4.2.2	3-62				
- AMPLITUDE			3 mbar	3 mbar	1.11.4	—
- PERIOD			365	365	1.11.4	—
POROSITY OF SHAFT FILL	3.4.4	3-70	30 %	NONE	2.3	(B)
UNSATURATED, ROCK POROSITY IN MPZ	3.4.4	3-70	0.042	NONE	1.1.3.1 AND 1.3.1.2	(B) VALUE OBTAINED AS- SUMING AMBIENT SATURA- TION OF 0.65 AND MATRIX POROSITY OF 12 %
MAXIMUM PARTICLE SIZE FOR ORDINARY CEMENTS	3.5.2	3-76	100 μm	NONE	—	(A)
PARTICLE SIZE FOR ULTRAFINE CEMENT	3.5.2	3-76	10 μm	NONE	—	(A)
HYDRAULIC CONDUCTIVITY OF ORDINARY PORTLAND CEMENT-CONCRETE	4.1.	4-2	$10^{-8} - 10^{-6}$ cm/s	NONE	2.3	(B)
HYDRAULIC CONDUCTIVITY OF PENNSYLVANIA STATE UNIVERSITY GROUT, MORTAR, AND CONCRETE	4.1	4-2	1.6×10^{-10} $- 9.5 \times 10^{-10}$ cm/s	NONE	2.3	(B)
HYDRAULIC CONDUCTIVITY OF SHAFT FILL	4.1.1	4-3	10^{-2} cm/s	NONE	2.3	(B)
CEMENT COMPOSITION - ALKALI CONTENT OF ORDINARY PORTLAND CEMENT	4.2.1	4-4	0.05 - 0.15 %	NONE	2.3	(B)

DRAFT

(A) NO SECTION FOUND IN RIB APPLICABLE TO THESE PARAMETERS.
(B) SECTION IDENTIFIED IN THE RIB, BUT VALUES NOT FOUND.

APPENDIX F
COMPARISON OF DATA USED IN THIS REPORT WITH THE REFERENCE INFORMATION BASE (RIB) (Continued)

PARAMETER	SECTION	PAGE #	REPORT VALUE	RIB VALUE	RIB SECTION	EXPLANATION
CEMENT COMPOSITION - pH OF ORDINARY PORTLAND CEMENT PORE FLUID	4.2.1	4-4	13.88	NONE	2.3	(B)
ES CONCRETE LINER THICKNESS	4.2.1	4-5	30.5 cm	30.5 cm	2.2.5.2	—
J-13 WATER COMPOSITION	4.2.1	4-6	TABLE 4-1	NONE	1.2.3.2	(B)
SHAFT LINER SURFACE AREA	4.2.1	4-6	$4.17 \times 10^7 \text{ cm}^2$	COMPUTED VALUE CONSISTENT WITH RIB	2.2.5.2	—
CONCRETE LINER VOID FRACTION	4.2.1	4-6	0.28	NONE	—	(A)
FRACTURE APERIURE IN MODIFIED PERMEABILITY ZONE	4.2.2.1	4-11	50 μm	NONE	1.3.2.4.2.3	(B)
POROSITY OF TS2 MATRIX	4.2.3	4-13	.1062	.1062	1.1.8.1	—
FRACTURE POROSITY IN MODIFIED PERMEABILITY ZONE	4.2.3	4-14	0.0001 - 0.001	NONE	1.3.2.4.2	(B)
THICKNESS OF CALICO HILLS UNIT (ZEOLITIC) AT ES-1	5.2	5-3	100 m	100 m	1.3.1.1.2	IN CALMA SYSTEM
PENETRATION OF ES-1 INTO CALICO HILLS	5.2	5-3	15 m	NONE	—	(A)
FRACTURE APERIURE	A.2	A-4	71 μm and 25 μm	NONE	1.3.4.2	(B)

(A) NO SECTION FOUND IN RIB APPLICABLE TO THESE PARAMETERS.

(B) SECTION IDENTIFIED IN THE RIB, BUT VALUES NOT FOUND.

DRAFT

APPENDIX F
COMPARISON OF DATA USED IN THIS REPORT WITH THE REFERENCE INFORMATION BASE (RIB) (Continued)

PARAMETER	SECTION	PAGE #	REPORT VALUE	RIB VALUE	RIB SECTION	EXPLANATION
SURFACE TENSION OF WATER AGAINST AIR	A.2	A-4	0.07118 kg/s ²	NONE	—	(A)
CONTACT ANGLE BETWEEN WATER IN FRACTURES AND TUFF	A.2	A-4	0°	NONE	—	(A)
DENSITY OF WATER	A.2	A-4	995.67 kg/m ³	NONE	—	(A)
ACCELERATION DUE TO GRAVITY	A.2	A-4	9.80665 m/s ²	NONE	—	(A)
DIFFUSION COEFFICIENT FOR SOLID-SOLID DIFFUSION	A.3	A-5, A-6	10 ⁻¹⁵ cm ² /s and 10 ⁻³⁰ cm ² /s	NONE	—	(A)
BINARY-GAS DIFFUSION COEFFICIENT FOR						
○ AIR-IODINE SYSTEM	A.4	A-6	0.081 cm ² /s	NONE	—	(A)
○ AIR-CARBON DIOXIDE SYSTEM	A.4	A-6	0.156 cm ² /s	NONE	—	(A)
KNUDSEN DIFFUSION COEFFICIENT FOR						
○ IODINE	A.4	A-6	10.6 cm ² /s	NONE	—	(A)
○ CARBON DIOXIDE	A.4	A-6	25.3 cm ² /s	NONE	—	(A)
POROSITY OF DRIFT AND SHAFT FILL	A.4	A-7	0.3	NONE	2.3	(B)
TORTUOSITY OF SHAFT FILL	A.4	A-7	3	NONE	—	(A)
THERMAL DIFFUSIVITY OF WATER	APP. E.	E-3	0.00152 cm ² /s	NONE	—	(A)
THERMAL CONDUCTIVITY OF TS2 - SATURATED	APP. E	E-8	2.34 w/mk	2.34 w/mk	1.3.1.3.1	

(A) NO SECTION FOUND IN RIB APPLICABLE TO THESE PARAMETERS.

(B) SECTION IDENTIFIED IN THE RIB, BUT VALUES NOT FOUND.

DRAFT

APPENDIX F
COMPARISON OF DATA USED IN THIS REPORT WITH THE REFERENCE INFORMATION BASE (RIB) (Continued)

PARAMETER	SECTION	PAGE #	REPORT VALUE	RIB VALUE	RIB SECTION	EXPLANATION
SPECIFIC GRAVITY OF TS2	APP. E.	E-8	2.24 gm/cc	2.24 gm/cc	1.3.1.2.3	
SPECIFIC HEAT OF TS2	APP. E.	E-8	2.38 J/cm ³ K	2.38 J/cm ³ K	1.3.1.3.3	

(A) NO SECTION FOUND IN RIB APPLICABLE TO THESE PARAMETERS.

(B) SECTION IDENTIFIED IN THE RIB, BUT VALUES NOT FOUND.

DRAFT

APPENDIX G

Data Recommended for Inclusion into the Site and
Engineering Properties Data Base (SEPDB)
and Information Proposed for the Inclusion into the
Reference Information Base (RIB)

No data or information contained in this report is recommended for inclusion into the SEPDB or the RIB.

DRAFT